TÉCNICO LISBOA

Torque vectoring control of an electric vehicle with in-wheel motors

Nuno Alexandre de Almeida Salgueiro

Thesis to obtain the Master of Science Degree in

Electrical and Computer Engineering

Supervisor: Prof. João Manuel Lage de Miranda Lemos

Examination Committee

Chairperson: Prof. João Fernando Cardoso Silva Sequeira
Supervisor: Prof. João Manuel Lage de Miranda Lemos
Members of the Committee: Prof. Rita Maria Mendes de Almeida Correia da Cunha

February, 2021

Declaration:

I declare that this document is an original work of my own authorship and that it fulfills all the requirements of the Code of Conduct and Good Practices of the Universidade de Lisboa.

I choose love.
That unbridled liquid emotion that provides you with the kindest empathy,
the purest energy,
to be the change you wish to see,
to better you into a state of harmony,
embracing you in a roaring river of time and wonders.

Acknowledgements

This work could not have been possible without the support of a lot of people. A special thanks to my supervisor, for the opportunity to do this, for his patience and for believing that I could do it, even when I hadn't the faintest idea on how to do it. I'm grateful towards this institution, for being the rock, the obstacle, I needed. Thank you Formula Student, and in particular the team, for accepting me, showing me what a team is all about and ultimately for providing me with the opportunity to give something back. It is my sincere wish that this work is of particular use to you and serve as stepping stone for further work. I would like to extend a formal thank you to the Formula SAE Tire Test Consortium for providing the teams with much needed tire data, and Xsens for their sponsorship through their AHRS unit sensor, that was a major component in verifying and validating the model.

Thank you Naveen for showing me how little I know about math. In the beginning there was a very confused me, afterwards there was a very awed and confused me, hopefully on the right track.

I would like to thank all my friends, of which I will name a few. Thank you Gabriel for telling me that when life throws you lemons, you should throw them back, you don't do lemonade, you do better. Thank you Vanessa for being the best friend I could ever ask for. Your support and unending patience kept me going through the rough patches. To everyone else, for you are many, thank you - in special, those that have been with me forever and are almost like a second family. I hope that my accomplishments and my happiness gives you happiness in turn and that we remain together for another decade.

Last but not least, I would like to thank my family. My uncles for their fatherly advice; my grandmother for her support and providing me with a safe haven; my mother for teaching me that although there is no such thing as magic and superpowers, wanting something badly enough is its own kind of power; my brother for being the friend I will forever have and hope to never take for granted. I would also like to do a special acknowledgement of the example that my mother and grandmother have passed on to me, on resilience and determination. Thank you Mom.

Abstract

Optimal torque distribution of the driving wheels of a vehicle is an open problem. Currently solved with a mechanical differential, nowadays with the electric engine and in particular with an engine per wheel, there is room for other solutions.

We rewrite the problem of "how to turn fast without sliding" taking into account the traction control, developing a system with a starting point and endpoint being the four wheels and the traction with four wheels, and how that model may help estimate and control a vehicle in such a way that you have better performance and handling.

Beyond the mathematical model based on the LuGre tire model, an observer and controller were developed as a Kalman Filter and a Model Predictive controller, as a proof of concept with the observer being validated with real data of a Formula Student car, FST09e.

We therefore conclude that the approach here taken is valid, that the equations within properly represent the dynamics of the vehicle attitude and that a controller capable of taking into account power constraints, traction, lateral stability and desired yaw rate is possible.

Keywords: Torque Vectoring, Kalman Filter, Model Predictive Control, LuGre, State-space

Resumo

A distribuição de torque óptimo pelas rodas motoras de um veículo é um problema aberto. Inicialmente resolvido com o diferencial mecânico, hoje em dia com o motor eléctrico e em particular com um motor por roda, está aberto o caminho para outras soluções.

Este trabalho foca-se em como reescrever o problema - "virar depressa e não derrapar"tendo em conta o controlo de tracção, por forma a obter um sistema cujo o ponto de partida e chegada são as quatro rodas e a tracção às quatro rodas e em como tal modelo pode ajudar na estimação e controlo de um veículo por forma a obter melhor performance e uma melhor condução.

Além da formulação do modelo matemático com base no modelo de pneus LuGre, um observador e controlador foram desenvolvidos, através de um filtro de Kalman e de controlo preditivo baseado em modelo, como prova de conceito e o observador foi validado com dados reais de um carro de competição da equipa de Formula Student, o FST09e, com resultados positivos.

Conclui-se portanto, que a abordagem aqui apresentada é válida, que as equações com o modelo de LuGre descrevem a dinâmica da atitude de um carro e que um controlador capaz de ter em conta restrições de potência, controlo de tracção, de estabilidade lateral e velocidade angular é possível.

Palavras-Chave: Torque Vectoring, Filtro de Kalman, Controlo Preditivo Baseado em Modelo, LuGre, Estado de Espaços

Contents

List of Figures

List of Tables

Glossary

MATLAB Numeric calculation *Software* developed by MathWorks

FSAE TTC The FSAE Tire Test Consortium (FSAE TTC) is a volunteer-managed organization of member schools who pool their financial resources to obtain high quality tire force and moment data targeted for Formula SAE and Formula Student competitions.

FST Lisboa Formula Student Team of Instituto Superior Técnico, Universidade de Lisboa

Acronyms

TV Torque Vectoring

GPS Global Positioning System

IST Instituto Superior Técnico

FST Lisboa Formula Student Lisboa, see Glossary: Formula Student Lisboa

AHRS Attitude and Heading Reference System

FSAE TTC FSAE Tire Test Consortium (FSAE TTC), see Glossary: FSAE TTC

MPC Model Predictive Controller

EKF Extended Kalman Filter

cg Centre of gravity

SAE Society of Automotive Engineers

Nomenculature

g Standard Gravity

ρ Air density

m Mass

I_z Vehicle inertial moment about the z axis

I_ω Wheel inertial moment

ω_z Yaw rate

μ_s Colomb static friction coeficient

μ_k Colomb kinetic friction coeficient, can refer to the x or y axis as μ_{k_x} or μ_{k_y}

α Slip angle, underscript is used to identify the wheel in question, ex α_{rr} for the rear right wheel

κ Slip ratio, underscript is used to identify the wheel in question, ex κ_{rr} for the rear right wheel

β Sideslip angle, can refer to the velocity angle at the center of mass as β_c or at the middle of the rear axis as β_r

ρ_{v_x} Weight for the terminal cost based on the velocity

ρ_{ω_z} Weight for the running cost based on the desired yaw rate

ρ_l Weight for the terminal cost based on the lateral stability

ρ_{slip} Weight for the soft cost based on the wheel slip

ρ_{gforce} Weight for the soft cost based on the yaw rate limit from the lateral g force limit

Chapter 1

Introduction

1.1 Motivation

The torque vectoring problem has been present in the automotive industry for quite some time. The electric car, and the electric engine has brought new avenues of research and problems. With an electric engine per wheel, the usual mechanical differential could no longer be employed but the freedom of actuation brought new opportunities. The work presented here started in the Formula Student Lisboa with a simple controller for torque distribution and the lack of a proper controller for the team provided the motivation for this thesis.

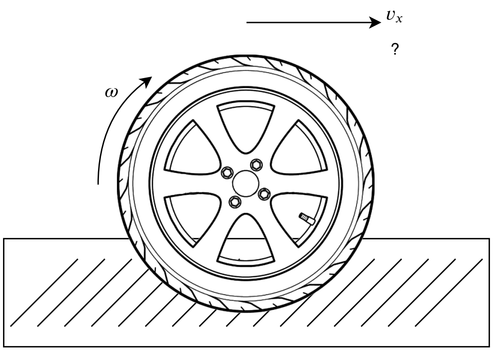

(a)

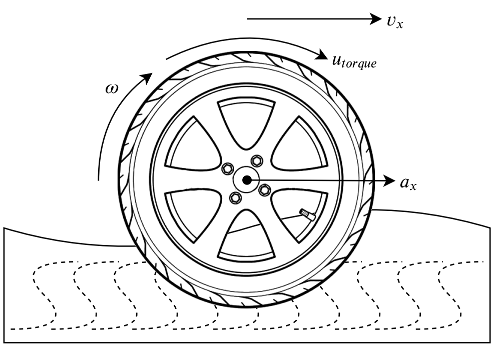

(b)

Figure 1.1: A simple thought experiment that raises some important questions and provided motivation into finding an appropriate tire model. After applying a torque and by looking at the generated force, can we attempt a guess for v_x and for the tire/road interaction (friction, etc.)?

The motivation to estimate the velocity vector without the Global Positioning System came from the fact that the GPS was not always available, and there were some reservations about having your traction control dependant on the GPS. For the team, a robust controller that required as little as possible in way of sensors and could also take into account uncertainty of parameters, normal loads at each tire and steering angles, was a must. There was also a real need to be able to estimate other parameters to evaluate the performance of the car, and thus the observer motivation. All of this on a possibly thigh computational budget. It started as a challenge, seen as in figure 1.1, and a way to apply and learn more about control theory.

1.2 Topic Overview

In short, Torque Vectoring is about finding an answer to the problem of "how fast can I turn without slipping?" by controlling the torque/brake at each wheel. In respect to the electric car it became evident that, with an electric engine, the deadzone of actuation (previously only with brakes) in respect to the roll steer effect could be further reduced when compared to the traditional combustion engine car (Folke 2010) [20]. Yaw rate control was to be the primary aim of this system and a controller was made [20] with feedforward, based on a set-point operation.

The actual impacts of an all electric car, beyond the ecological scope, were surmised (DeNovellis 2012) [40]. Not just the roll stability, but the handling, directional stability, energy consumption, braking/traction (lateral/longitudinal dynamics) and attitude control and road-holding (vertical dynamics) could be affected.

By 2012, the state-of-the art could be said to be the E-VECTOORC [10] project for a 4 wheel(4WD) electric car. Noteworthy is the approach used to estimate the friction conditions with the electric engine, instead of with the hydraulic brake pressure and the slip ratio controller. Beyond that, the main objectives of this project were the extension of the linear region in respect to wheel steer δ and lateral acceleration a_y - more steering angle, more lateral acceleration in a linear relationship, and minimizing the impact of emergency manoeuvres to the vehicle heading.

Since then, other approaches have been made. To name a few: with a focus on the lane changing problem and an explicit objective to replace the ABS and ESC systems [47] by considering the system as a bicycle model with load transfers, for state variables yaw rate ω_z and sideslip angle β, and for inputs the wheel steering angle and yaw moment. They also took into account the engine limitations, in respect to torque rate of change [49]. Robust approaches were also made like in [30] and [1] with the single track equations and an emphasis on the frequency response of the system.

It should be noted that although it seems to be a torque distribution problem, it is in fact a power distribution problem. Often the engines place local constraints on the power available for each wheel, and there are global constraints due to the total available power at the vehicle. The work done on this thesis attempts to write all of these constrains/requirements in such a way that the resulting solution is the torque to be applied at each wheel. The current state of the art is derived from the bicycle model, with the controller outputing a yaw moment that then needs to be translated into a torque for each wheel. This formulation neglects the available power/maximum torque constraint, the traction control problem and the lateral stability.

1.3 Objectives and Deliverables

The objective of this thesis was to develop a mathematical model of the car, diverging from the bicycle model, such that an observer and controller could be implemented.

Ideally the controller must be able to comply with power requirements, both local and global, yaw rate references, be tunable, provide traction control and lateral stability.

Furthermore, the observer should be able to estimate the slip angles and slip ratios of each wheel and the velocity vector of the car, without relying on a GPS system but still allowing it to be added in the future.

The system should be able to handle input noise, and noise/bias to the normal load at each tire and the steering angle.

As a result of this thesis, an observer/controller pair is implemented to showcase the potencial of such an approach.

1.4 Thesis Outline

This thesis consists of two main parts, modelling and developing the observer and controller.

The modelling and system analysis, both for the plant used in the simulations and the controller, is described in the next chapter. The controller and observer design follows, with an emphasis on the controller.

The implementation chapter, describes how the simulation environment and implementation decisions were made.

Chapter 2

System Analysis

In this section we develop the mathematical model for the car dynamics. The car can be thought of as a mass with four points where force is applied to the car as $\mathbf{F}^{Car} = \sum F_i$, and with dynamics taking into account the point of application $\mathbf{r}$ of this force - tire location, and the self-aligning moment of each tire, $\sum M_{z_i} + \sum \mathbf{r}_i \times \mathbf{F}_i$. These four points are at the centre of the tire contact patches. The model that describes the tire-road interaction is called a tire model. We will start at the tire level, from the engine torque and work towards the complete car model. Starting with the single tire, a theoretical one wheeled car, to the full car model. By not taking into account any other forms of friction, we can also derive the "coasting" car and define the equilibrium points of the model.

The approach taken here to model the car behaviour is to consider the car dynamics in a 2D frame, and add the vertical dynamics, such as the load transfer, as variations of the normal load - the normal force generated at the contact patch.

Some assumptions were made about the car model. We assume that there is no camber angle (side tilt of the wheel), the road is flat, the cg is known, yaw rate and wheel turning speed are measurable in the car frame, the normal load at each tyre can be estimated, from a suspension model, and that the measured acceleration is seen from a inertial observer aligned with the car frame. This last one will be achieved with an Attitude and Heading Reference System, that removes the effect of the imaginary forces - euler, coriolis and centrifuge.

2.1 Tire Model

The tire model is the building block from which the car model is derived. In a 2D frame, the tire is reduced to a point that generates a force and a self-aligning torque - due to the rolling motion of the tire. The generated force, depends on the slip and how the tire is aligned in relation to the road plane(e.g. camber angle). The goal of a tire model is not only to accurately model the dynamics of the friction, sliding and the elastic deformations but also take into account how the inputs affect this.

About tire models in general, it is though that a force is generated if there is a slip between the tire and the road, given non-zero friction. This slip is called the slip ratio and is defined as

$$k = \left(\frac{\omega r}{v} - 1\right), \tag{2.1}$$

according to the Society of Automotive Engineers Vehicle Dynamics Standards Committee.

The angle of the velocity vector at the tire contact patch, also called the slip angle, is defined as

$$\alpha = -\arctan\left(\frac{v_y}{|v_x|}\right), \tag{2.2}$$

for each tire.

Most tire models agree that there is a linear relationship between the slip and the generated force, with a saturation zone where the slip is high enough that little to no force is generated at the tire.

2.1.1 Magic Formula Tire Model

In this section, we do a brief overview of the Magic Formula tire model. Tire models can be divided in two groups, the static models, and the dynamic models. The main difference between a static model and a dynamic model, is that the dynamic model has a transient behaviour. Although the Magic Formula (MF) tire model is a static model, it is considered to be the gold standard in tire models.

The slip ratio is related to the longitudinal force F_x and the slip angle with the lateral force F_y generated at the contact patch. In order to describe this phenomenon, Pacejka [42] empirically developed the "Magic Formula" as,

$$y = D\sin\left[C\arctan\left\{Bx - E(Bx - \arctan Bx)\right\}\right] \tag{2.3}$$

with

$$Y(X) = y(x) + S_V \text{ , } Y\text{: output variable } F_x,\ F_y \text{ or } M_z \tag{2.4}$$

$$x = X + S_H \text{ , X: input variable } \tan\alpha \text{ or } k \tag{2.5}$$

$$\tag{2.6}$$

The parameters for this formula are the stiffness B, the shape C, the peak value D, the curvature E and the vertical and horizontal shifts S_V and S_H.

This model is further explained in chapter 4 at [42], where the self-aligning moment M_z is also defined.

While this model has been widely used in control systems, and [45] some have even managed to derive slip dynamics with this model, there are some issues here. Since it relies on a ratio, at low speeds it is not a good approximation. It does not explicitly handle the rolling resistance and relies on an offset for this. The forces generated are not coupled, there is no cross-dependency between longitudinal and lateral forces. Also, the formula is not easily linearised and the parameters are hard to relate to known quantities. As such we selected a different model.

2.1.2 LuGre Tire Model

This work is based on the LuGre dynamic tire model [7], first developed in 1995 by researchers from the universities of Lund and Grenoble and consists on an extension of the Dahl model by adding the Stribeck effect and a variable Coulomb friction force. Since then the LuGre tire model has seen more development by Tsiotras, Velenis and Sorine [56] in 2004 with the development of an exact lumped model. They also derived an approximate tire model assuming uniform load distribution of the weight along the contact patch of the tire. It is this model that is used in this thesis. This assumption results in the loss of the self-aligning torque of the tire. The work of Deur et al [13] in 2005 should also be mentioned since it further extends the model to consider camber, carcass compliance, conicity, ply steer and an additional rolling resistance term.

This model is a dynamic model that attempts to describe the tire-road interaction from a physics point of view. Here the rolling resistance is explained by the hysteresis of the model. While not as explicit as the "Magic Formula" model, this model also has a linear region in respect to the slip and, since it does not rely on an explicit ratio, is well defined at low speeds. However the self-aligning moment is not as accurate.

According to the LuGre tire model, the tire can be seen as a group of bristles that deform as they enter the contact patch of the tire. These imaginary bristles exist both in the longitudinal x and lateral y axis. The deformation z_i, with i being either x or y, is a function of the relative velocity v_{ri} of the bristle elements and the wheel angular velocity ω.

The LuGre tire model [56] is defined as,

$$\frac{dz_i(t,\zeta)}{dt} = \frac{\partial z_i(t,\zeta)}{\partial t} + |\omega r|\frac{\partial z_i(t,\zeta)}{\partial \zeta} \tag{2.7}$$

$$= v_{ri}(t) - C_{0i}(v_r)z_i(t,\zeta) \tag{2.8}$$

$$\mu_i(t,\zeta) = -\sigma_{0i}z_i(t,\zeta) - \sigma_{1i}\frac{\partial z_i(t,\zeta)}{\partial t} - \sigma_{2i}v_{ri}(t) \tag{2.9}$$

$$F_i(t) = \int_0^L \mu_i(t,\zeta)f_n(\zeta)d\zeta \tag{2.10}$$

$$M_z(t) = -\int_0^L \mu_y(t,\zeta)f_n(\zeta)\left(\frac{L}{2} - \zeta\right)d\zeta,\ i = x, y \tag{2.11}$$

with: $z_i(t,\zeta)$ as the internal friction states at time t and position ζ along the contact patch, ω is the wheel angular velocity and r the tire radius, with L the contact patch length of the tire; σ_{0i} the tire bristle stiffness with the corresponding stiction and viscous damping constants σ_{1i} and σ_{2i} of the friction coefficients $\mu_i(t,\zeta)$ and v_{ri} the relative velocity of the contact patch elements in the tire.

Thus equation 2.10 models the longitudinal force F_x, side force F_y and 2.11 the self-aligning moment M_z of the tire.

Deur [12] provided a simplified tire model by assuming a uniform load F_n at the contact patch and making some assumptions about the transient response. It was shown [56] that, with a high enough

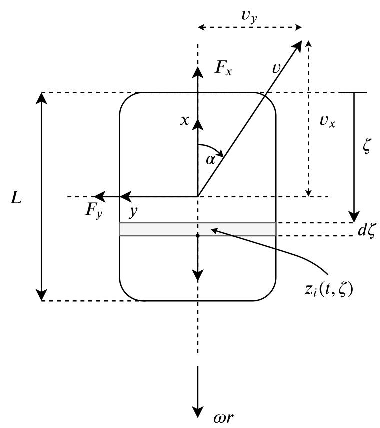

Figure 2.1: Frame of reference for the LuGre tire model, in a top-down view of a tire, in the tire frame.

stiffness, the transient behaviour is a good approximation. This model is defined as,

$$\dot{\tilde{z}}_i(t) = v_{ri} - \left(\frac{||v_r||\sigma_{0i}}{g(v_r)} + \frac{k_i^{ss}}{L}|\omega r| \right) \tilde{z}_i \tag{2.12}$$

$$F_i(t) = F_n \left(\sigma_{0i}\tilde{z}_i + \sigma_{1i}\dot{\tilde{z}}_i + \sigma_{2i} v_{ri} \right) \tag{2.13}$$

with,

$$g(v_r) = \frac{||M_k^2 v_r||}{||M_k v_r||} + \left(\mu_s - \frac{||M_k^2 v_r||}{||M_k v_r||} \right) e^{-\left(\frac{||v_r||}{v_s}\right)^{\gamma}}, g(v_r = [0,0]^T) = \mu_s \tag{2.14}$$

$$M_k = \begin{bmatrix} \mu_{kx} & 0 \\ 0 & \mu_{ky} \end{bmatrix} \tag{2.15}$$

$$k_i^{ss} = \frac{1 - e^{-L/Z_i}}{1 - \frac{L}{Z_i}\left(1 - e^{-L/Z_i}\right)}, Z_i = \frac{|\omega r| g(v_r)}{||v_r||\sigma_{0i}} \tag{2.16}$$

$$v_r = \begin{bmatrix} v_{rx} \\ v_{ry} \end{bmatrix} = \begin{bmatrix} \omega r \\ 0 \end{bmatrix} - \begin{bmatrix} v_x \\ v_y \end{bmatrix} \tag{2.17}$$

$$i = x, y.$$

The trade-off with this approach is that the uniform load assumption results in the loss of the self-aligning moment. Usually the self-aligning moment is very small and thus this loss was deemed acceptable. In 2.12 k_i^{ss} is used to match the steady state behaviour of the tire and $g(v_r)$ is a function that estimates the friction, given the relative velocity of the contact patches, as a value between the static μ_s and kinetic μ_k Coulomb friction coefficients. The Stribeck velocity v_s and the shape parameter are used to model the transition from one coefficient to another in order to achieve the desired steady-state behaviour of the tire friction[12]. With this, $\tilde{z}_i$ becomes the average tire deflection in x and y.

While Velenis [58] started by defining the Coulomb friction coefficient as depending on the direction of the relative velocity vector v_r, and later reformulated the problem using only scalars, here 2.14, we allow for the kinetic friction to depend on the direction of the relative velocity. The only constraint that we placed on his original formulation was that it had to be continuous and the limit at (0,0) be defined.

The only way for the limit,

$$\lim_{(v_{rx},v_{ry})\to(0,0)} g(v_r) = \lim_{(vr_x,vr_y)\to(0,0)} \frac{||M_k^2 v_r||}{||M_k v_r||} + \left(\frac{||M_s^2 v_r||}{||M_s v_r||} - \frac{||M_k^2 v_r||}{||M_k v_r||}\right) e^{-\left(\frac{||v_r||}{v_s}\right)^{\gamma}} \tag{2.18}$$

to be defined and allow for a continuous extension of $g(v_r)$ is for the static friction M_s to be the same along the x and y axis. Otherwise the static friction coefficient would depend on the direction of the measurement.

As such, we took the middle ground between the original definition of [58] and the final form of the LuGre tire model. With $M_s = \begin{bmatrix} \mu_s & 0 \\ 0 & \mu_s \end{bmatrix}$, $g(vr)$ takes the form presented in 2.14 and the limit defined as,

$$\lim_{(v_{rx},v_{ry})\to(0,0)} g(v_r) = \mu_s. \tag{2.19}$$

The level curves of the friction coefficient, as a function of the relative velocity, for the tire configurations in this thesis can be seen in figure 2.2.

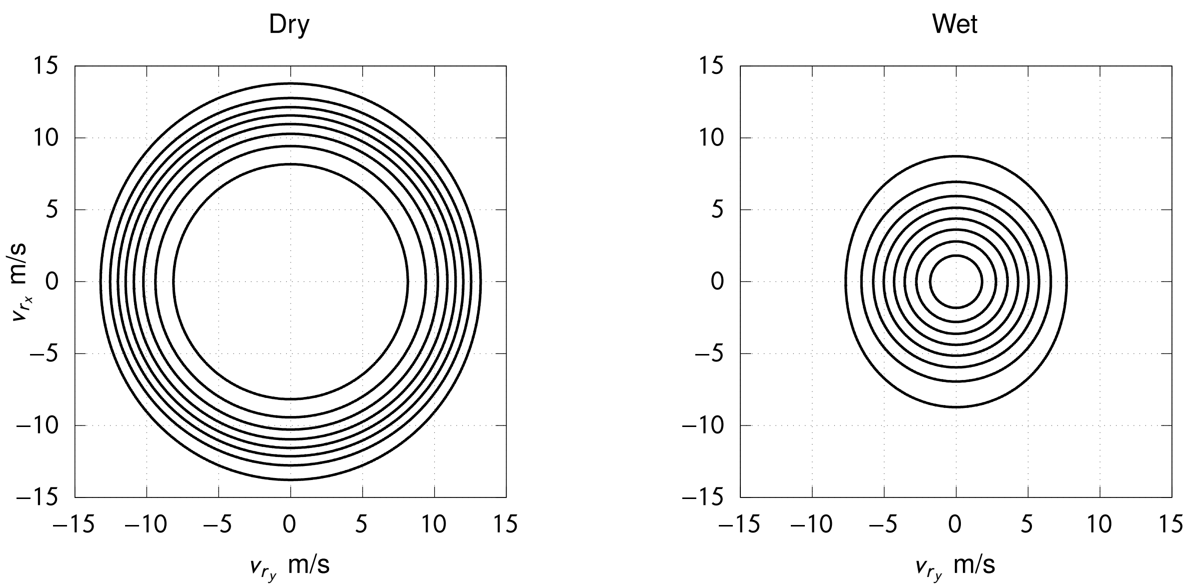

Figure 2.2: $g(v_r)$ level curves as a function of the relative velocity vector v_r.

2.1.3 Linearized Tire Model

Our proposal is to take this model 2.20 and introduce parameters such that,

$$\dot{\tilde{z}}_i(t) = v_{ri} - O_i \tilde{z}_i \tag{2.20}$$

$$F_i(t) = F_n O_{\sigma i} \tilde{z}_i + F_n \sigma_i v_{ri} \tag{2.21}$$

with,

$$O_i = \left(\frac{||v_r|| \sigma_{0i}}{g(v_r)} + \frac{k_i^{ss}}{L} |\omega r| \right) \tag{2.22}$$

$$O_{\sigma i} = \sigma_{0i} - \sigma_{1i} O_i \tag{2.23}$$

$$\sigma_i = \sigma_{1i} + \sigma_{2i}. \tag{2.24}$$

This linearization is done by introducing the parameters O_i and $O_{\sigma i}$, which we will call the rate of bristle restitution s^{-1} and the normalized stiffness in m^{-1}. They are assumed constant for the controller, thus disregarding the partial derivative of these terms, however the plant will have the non-linear behaviour. This approximation is equivalent to assume that we are operating in the linear region, that we are not unduly sliding, which and can be seem in figure 2.3.

This allows for a linear system realization and we can use this in the model predictive part of the controller and to study the dynamics of the car (at steady-state those parameters will be constant). The new damping constant is now σ_i. It can be seen 2.21 that the force is proportional to the load and the bristle deflection. Another way to look at it is by comparing it to a variable stiffness spring.

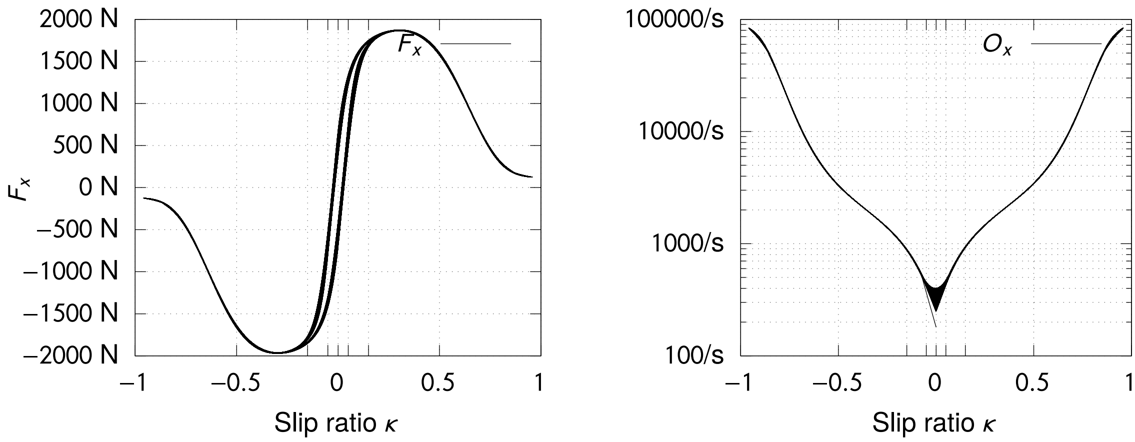

Figure 2.3: Hysteresis and O_x variation with slip. Fixed velocity at 15 m/s, slip angle $\alpha = 0$ and variable wheel angular velocity triangular sweeps at 2Hz.

To the previous model we add the input wheel torque u from the engine, take into account the wheel moment of inertia I_ω and say that the input torque must overcome the corresponding generated force as,

$$I_\omega \dot{\omega} = u - rF_x \tag{2.25}$$

$$= u - rF_n O_{\sigma x} \tilde{z}_x - rF_n \sigma_x v_{rx}. \tag{2.26}$$

The linearised state-space model with states, tire deflection, wheel rotation speed and linear velocity in the tire frame can be written as,

$$\begin{bmatrix} \dot{\tilde{z}}_x \\ \dot{\tilde{z}}_y \\ \dot{\omega} \\ \dot{v}_x \\ \dot{v}_y \end{bmatrix} = \begin{bmatrix} -O_x, & 0, & r, & -1, & 0 \\ 0, & -O_y, & 0, & 0, & -1 \\ -\frac{rF_n}{I_\omega}O_{\sigma x}, & 0, & -\frac{r^2F_n\sigma_x}{I_\omega}, & \frac{rF_n\sigma_x}{I_\omega}, & 0 \\ \frac{F_n}{m}O_{\sigma x}, & 0, & \frac{\sigma_x}{m}r, & -\frac{\sigma_x}{m}, & 0 \\ 0, & \frac{F_n}{m}O_{\sigma y}, & 0, & 0, & -\frac{\sigma_y}{m} \end{bmatrix} \begin{bmatrix} \tilde{z}_x \\ \tilde{z}_y \\ \omega \\ v_x \\ v_y \end{bmatrix} + \begin{bmatrix} 0 \\ 0 \\ \frac{1}{I_\omega} \\ 0 \\ 0 \end{bmatrix} u \tag{2.27}$$

The tire generates a force at the contact patch depending on the tire slip ratio κ and the slip angle α.

We estimated the LuGre tire model from the FSAE TTC data for the Hoosier 18.0 × 7.5 10 R25B tire, and then we modified the values to simulate not so optimum conditions, and called that tire the "wet" tire. The estimated tire is reported in this work as the "dry" tire. Figure 2.4 shows this relationship.

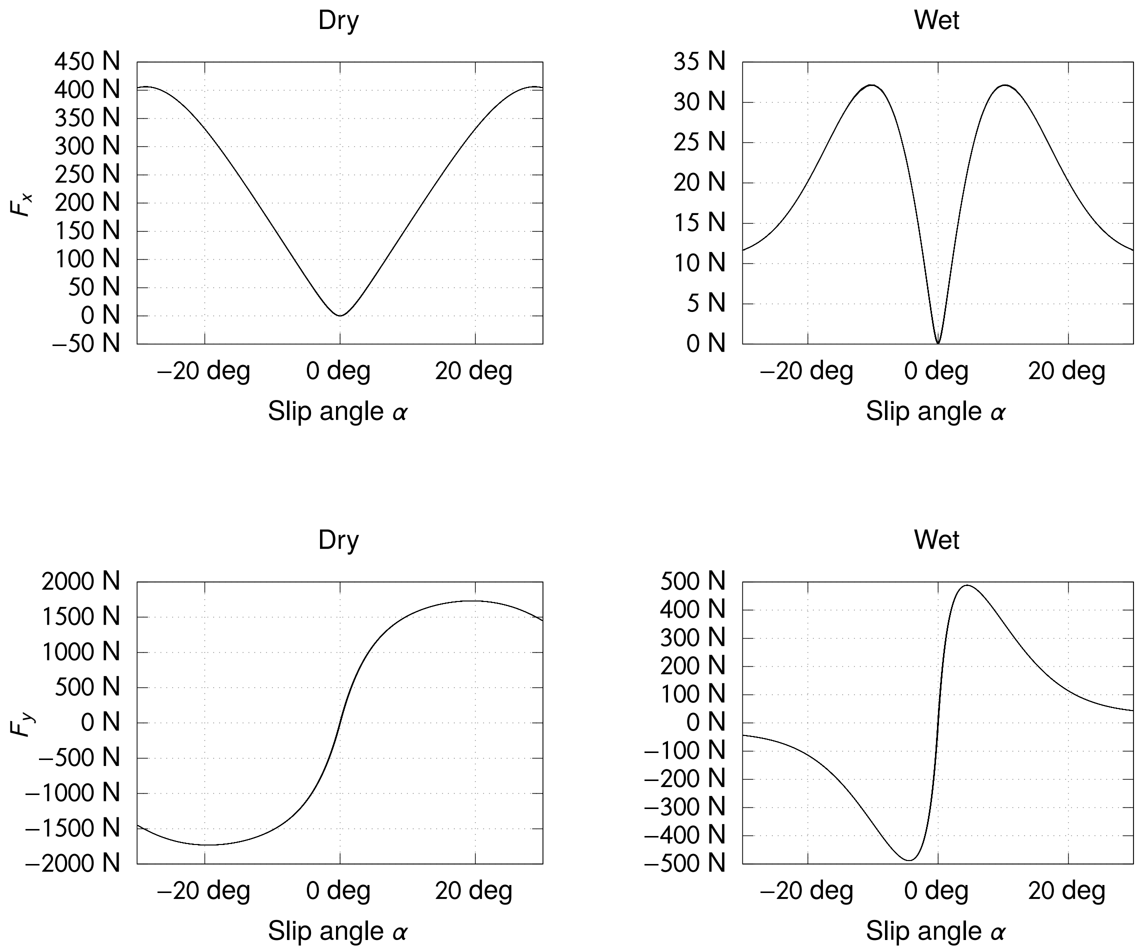

Figure 2.4: Effect of tire velocity angle α on the force generated at the contact patch with fixed velocity at 15 m/s and variable α at 0.1Hz.

Assuming that everything else remains constant, the force along the y axis is most influenced by the slip angle α, while the slip ratio κ affects mostly the x axis. Both have a linear region about the origin that saturates at higher values. Furthermore, these curves can have hysteresis which is the main contributing factor to the rolling resistance.

The normal load F_n or normal force also contributes to the generated force in a linear relationship, as previously seen in the equations.

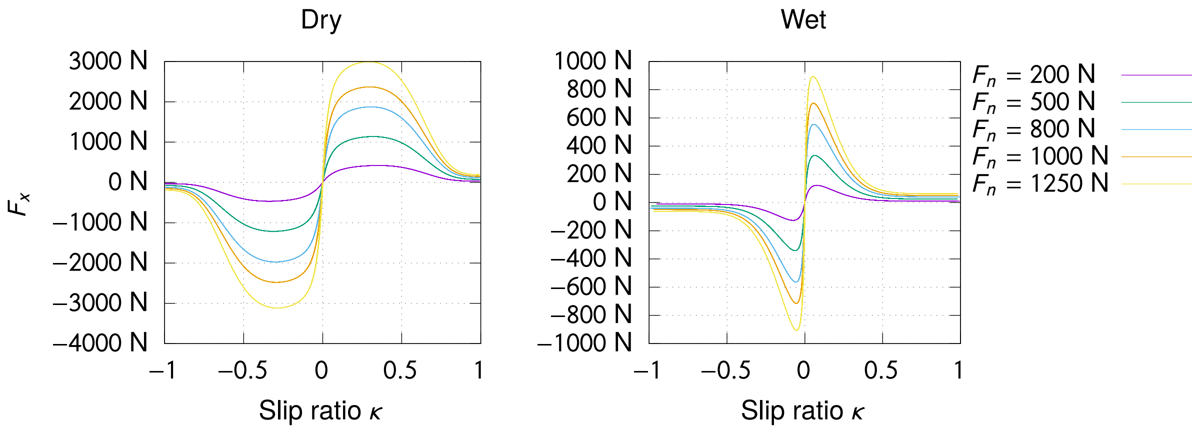

Figure 2.5: Effect of normal load F_n in the force to slip ratio relationship with fixed velocity at 15 m/s, velocity angle α = 0 and variable wheel angular velocity triangular sweeps at 0.1Hz.

There is also another point that needs to be taken into consideration when generating force, and that is the velocity of the moving tire. This is a caracteristic of the LuGre tire model and can be seen in figure

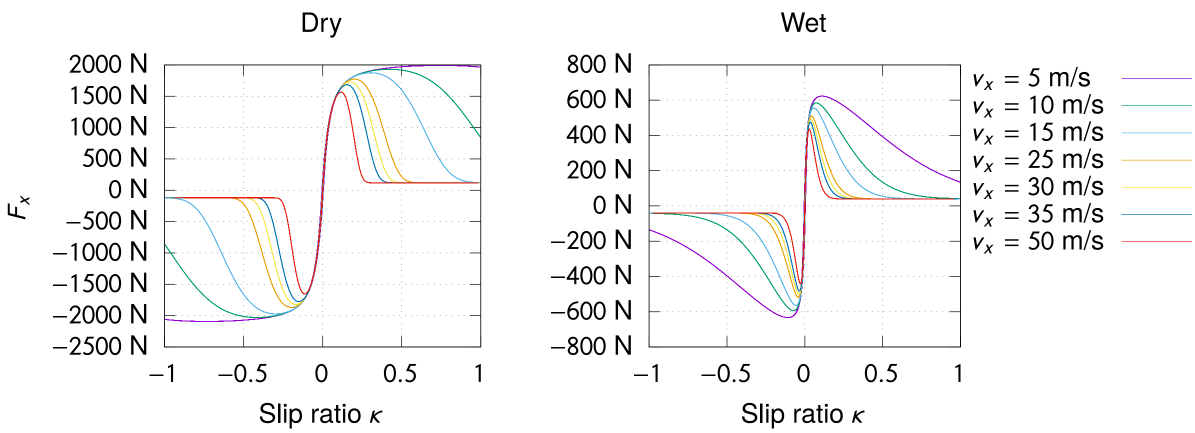

Figure 2.6: Effect of velocity in the force to slip ratio relationship with fixed velocity at 15 m/s, wheel velocity angle α = 0 and variable wheel angular velocity triangular sweeps at 0.1Hz.

2.6. According to the equations, the curve "saturates" faster at higher velocities, while still mantaining the linear region and the overall shape. This phenomena was not seen in the FSAE TTC dataset during the estimation. This can have several reasons: maybe the effect exists and there is some combination of parameters that minimizes this effect; maybe the tire effective radius was not properly estimated; maybe the induced slip in the testbed was not enough to see this. The maximum slip in the dataset is only of 20%.

2.2 Car Model

The car model is derived from the tire model. The current state of the art consists on defining the car model as a bicycle model and defines the states as the yaw rate and the yaw moment. We took a diferent approach and deduced the car dynamics through the previous LuGre tire model for the whole car.

2.2.1 One Wheel Car

We start by studying an hypothetical car with just one wheel. This model will be the basis for the four wheel car model. The challenge here is to derive the equations in respect to the car frame and not the tire frame. To this effect we will define a linear transformation that achieves this.

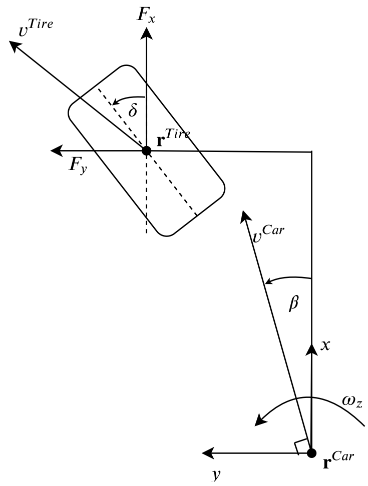

Figure 2.7: Hypothetical single tire car.

Since we are assuming that the car is a rigid body, then by definition the angular velocity must be the same at all points, and beginning by assuming that there is no steering $\delta = 0$, the following must hold,

$$\mathbf{v}^{Tire} = \left[\mathbf{v}^{Car} + \boldsymbol{\omega} \times (\mathbf{r}_{Tire} - \mathbf{r}_{Car})\right]. \tag{2.28}$$

Further assuming that the car centre of gravity is the origin, $\mathbf{r}_{Car} = [0, 0, 0]^T$ and considering only planar motion with yaw rate ω_z then the velocity at the tire can be deduced as,

$$\begin{bmatrix} v_x \\ v_y \end{bmatrix}^{Tire} = \left(\begin{bmatrix} v_x \\ v_y \end{bmatrix}^{Car} + \begin{bmatrix} -r_y\omega_z \\ r_x\omega_z \end{bmatrix} \right). \tag{2.29}$$

To account for the steering $\delta \neq 0$ we simply have to add a rotation matrix R_δ^T to shift the orientation of the projected vector,

$$\begin{bmatrix} v_x \\ v_y \end{bmatrix}^{Tire} = R_\delta^T \left(\begin{bmatrix} v_x \\ v_y \end{bmatrix}^{Car} + \begin{bmatrix} -r_y\omega_z \\ r_x\omega_z \end{bmatrix} \right) \tag{2.30}$$

$$= \begin{bmatrix} \cos\delta, & \sin\delta, & r_x\sin\delta - r_y\cos\delta \\ -\sin\delta, & \cos\delta, & r_x\cos\delta + r_y\sin\delta \end{bmatrix} \begin{bmatrix} v_x^{Car} \\ v_y^{Car} \\ \omega_z \end{bmatrix} \tag{2.31}$$

with,

$$R_\delta = \begin{bmatrix} \cos\delta, & -\sin\delta \\ \sin\delta, & \cos\delta \end{bmatrix},$$

and we have a linear relationship between the two velocity vectors, assuming that the steering is constant.

Writing the autonomous system, using a state vector in respect to the car frame:

$$\begin{bmatrix} \dot{\tilde{z}}_x \\ \dot{\tilde{z}}_y \\ \dot{\omega} \\ \dot{v}_x \\ \dot{v}_y \\ \dot{\omega}_z \end{bmatrix} = A \begin{bmatrix} \tilde{z}_x \\ \tilde{z}_y \\ \omega \\ v_x \\ v_y \\ \omega_z \end{bmatrix}, \; A = \left[\begin{array}{c|c} A_{11} & A_{12} \\ \hline A_{21} & A_{22}, \end{array}\right] \tag{2.32}$$

$$\tag{2.33}$$

with the block matrices $A_{11},\ A_{12}, A_{21}, A_{22}$ defined as,

$$A_{11} = \begin{bmatrix} -O_x, & 0, & r \\ 0, & -O_y, & 0 \\ -\frac{F_n r}{I_\omega} O_{\sigma x}, & 0, & \frac{-F_n r^2}{I_\omega}\sigma_x \end{bmatrix} \tag{2.34}$$

$$A_{12} = \begin{bmatrix} -c, & -s, & r_y c - r_x s \\ s, & -c, & -r_y s - r_x c \\ \frac{F_n r}{I_\omega}\sigma_x c, & \frac{F_n r}{I_\omega}\sigma_x s, & \frac{-F_n r}{I_\omega}\sigma_x \left(r_y c - r_x s\right) \end{bmatrix} \tag{2.35}$$

$$A_{21} = \begin{bmatrix} \frac{F_n}{m} O_{\sigma x} c, & -\frac{F_n}{m} O_{\sigma y} s, & \frac{F_n}{m} r\sigma_x c \\ \frac{F_n}{m} O_{\sigma x} s, & \frac{F_n}{m} O_{\sigma y} c, & \frac{F_n}{m} r\sigma_x s \\ \frac{F_n}{I_z} O_{\sigma y}(r_x s - r_y c), & \frac{F_n}{I_z} O_{\sigma y}(r_x c + r_y s), & \frac{F_n r}{I_z}\sigma_x(r_x s - r_y c) \end{bmatrix} \tag{2.36}$$

$$A_{22} = \begin{bmatrix} -\frac{F_n}{m}(c^2\sigma_x + s^2\sigma_y), & \frac{F_n}{m}(\sigma_y cs - \sigma_x cs), & \frac{F_n}{m}\sigma_x(r_y c^2 - r_x cs) + \frac{F_n}{m}\sigma_y(r_y c^2 + r_x cs) \\ \frac{F_n}{m}(\sigma_y cs - \sigma_x cs), & -\frac{F_n}{m}(c^2\sigma_y + s^2\sigma_x), & \frac{F_n}{m}\sigma_x s(r_y c - r_x s) - \frac{F_n}{m}\sigma_y c(r_x c + r_y s) \\ \frac{F_n}{I_z}\left[\sigma_x(r_y c^2 - r_x cs) + \sigma_y(r_y s^2 + r_x cs)\right], & \frac{F_n}{I_z}\left[\sigma_x(r_y cs - r_x s^2) - \sigma_y(r_x c^2 + r_y cs)\right], & -\frac{F_n}{I_z}\left[\sigma_x(r_y c - r_x s)^2 + \sigma_y(r_y s + r_x c)^2\right] \end{bmatrix} \tag{2.37}$$

$$s = \sin\delta,\ c = \cos\delta, \tag{2.38}$$

we define the building block of the four wheel car model.

This model has six states, three internal states - the deflections $\tilde{z}_x$, $\tilde{z}_y$ and wheel velocity ω, and three external states - car linear velocity and the yaw rate ω_z. The matrix A_{11} describes the dynamics of the internal states, and A_{22} the dynamics of the external states. A_{12} and A_{21} define the dynamics between the external and internal states.

The model outputs are the angular wheel velocity, the velocity derivatives along x and y and the yaw rate ω_z. All of them are assumed to be measurable,

$$\mathbf{y} = C\mathbf{x}, \text{with } C \in \mathbb{R}^{4\times6} \tag{2.39}$$

$$= \left[\omega, \dot{v}_x, \dot{v}_y, \omega_z\right]^T. \tag{2.40}$$

This results in the linear system,

$$\dot{\mathbf{x}} = A(\delta)\mathbf{x} + Bu \tag{2.41}$$

$$\mathbf{y} = C(\delta)\mathbf{x} \tag{2.42}$$

with state,

$$\mathbf{x} = \left[z_x, z_y, \omega, v_x, v_y, \omega_z\right]^T, \tag{2.43}$$

$$\tag{2.44}$$

and u as the input engine torque.

One of the goals of this thesis was to develop an observer for the velocity vector in the car frame. For this model we were able to prove that it is observable with just these outputs.

With the observability matrix as,

$$\text{obsv} = \begin{bmatrix} C \\ CA \\ CA^2 \\ \vdots \\ CA^5 \end{bmatrix}, \tag{2.45}$$

we were able to confirm with the MATLAB symbolic toolbox that the rank of the observability matrix is six, which proves that all states are observable, for any steering angle and damping coefficients (including 0).

It is also worth noting that should the tire be placed at the origin $\mathbf{r} = 0$ then there will be no yaw rate, save for the resulting transient yaw rate from changing the steer angle δ. This is related to the relaxation length of tire tread, which can be seen as a delayed response of the system to a steering change. The steady state of this system would have a yaw rate of zero.

2.2.2 Four wheel Car

Using the previous model to each wheel and taking into account that the external states are shared between wheels, the four wheel car model can be derived.

Let each tire be referenced as rear right (rr), rear left (rl), front right (fr), front left (fl), then the four wheel car is defined as,

$$\dot{\mathbf{x}} = \begin{bmatrix} A(\delta_{rr})^{rr}_{11}, & 0, & 0, & 0, & A(\delta_{rr})^{rr}_{12} \\ 0, & A(\delta_{rl})^{rl}_{11}, & 0, & 0, & A(\delta_{rl})^{rl}_{12} \\ 0, & 0, & A(\delta_{fr})^{fr}_{11}, & 0, & A(\delta_{fr})^{fr}_{12} \\ 0, & 0, & 0, & A(\delta_{fl})^{fl}_{11}, & A(\delta_{fl})^{fl}_{12} \\ A(\delta_{rr})^{rr}_{21}, & A(\delta_{rl})^{rl}_{21}, & A(\delta_{fr})^{fr}_{21}, & A(\delta_{fl})^{fl}_{21}, & \sum A_{22} \end{bmatrix} \mathbf{x} + B\mathbf{u} \tag{2.46}$$

$$= A(\delta_{rr}, \delta_{rl}, \delta_{fr}, \delta_{fl})\mathbf{x} + B\mathbf{u} \tag{2.47}$$

$$\mathbf{y} = C(\delta_{rr}, \delta_{rl}, \delta_{fr}, \delta_{fl})\mathbf{x} = \begin{bmatrix} \omega_{rr} & \omega_{rl} & \omega_{fr} & \omega_{fl} & \dot{v}_x & \dot{v}_y & \omega_z \end{bmatrix}^T \tag{2.48}$$

with state and input,

$$\mathbf{x} = \left[z_x^{rr}, z_y^{rr}, \omega^{rr}, z_x^{rl}, z_y^{rl}, \omega^{rl}, z_x^{fr}, z_y^{fr}, \omega^{fr}, z_x^{fl}, z_y^{fl}, \omega^{fl}, v_x, v_y, \omega_z \right]^T \tag{2.49}$$

$$\mathbf{u} = \left[u^{rr}, u^{rl}, u^{fr}, u^{fl} \right]^T . \tag{2.50}$$

2.2.3 Steering

In this section we describe the steering scheme that is assumed to be adopted. We assume that the car has Ackerman steering.

From figure 2.8 and by assuming a turning point $\mathbf{r} = (r_x, r_y)$ we derive the relationship between each wheel,

$$\begin{bmatrix} \cot \delta_{fr} \\ \cot \delta_{fl} \\ \cot \delta \end{bmatrix} = \begin{bmatrix} \frac{r_y + w_{track}/2}{a - r_x} \\ \frac{r_y - w_{track}/2}{a - r_x} \\ \frac{r_y}{a - r_x} \end{bmatrix} = \begin{bmatrix} \frac{r_y + w_{track}/2}{a + b} \\ \frac{r_y - w_{track}/2}{a + b} \\ \frac{r_y}{a + b}. \end{bmatrix} \tag{2.51}$$

This results in the following identities,

$$\cot \delta_{fr} - \cot \delta = \frac{w_{track}/2}{a + b} \tag{2.52}$$

$$\cot \delta_{fr} - \cot \delta = \frac{-w_{track}/2}{a + b} \tag{2.53}$$

$$\cot \delta_{fr} - \cot \delta_{fl} = \frac{w_{track}}{a + b}. \tag{2.54}$$

The driver is assumed to control the wheel turning angles through δ with 2.52 and 2.53 and requests a corresponding vehicle turning radius,

$$R = w_{base} \cot \delta. \tag{2.55}$$

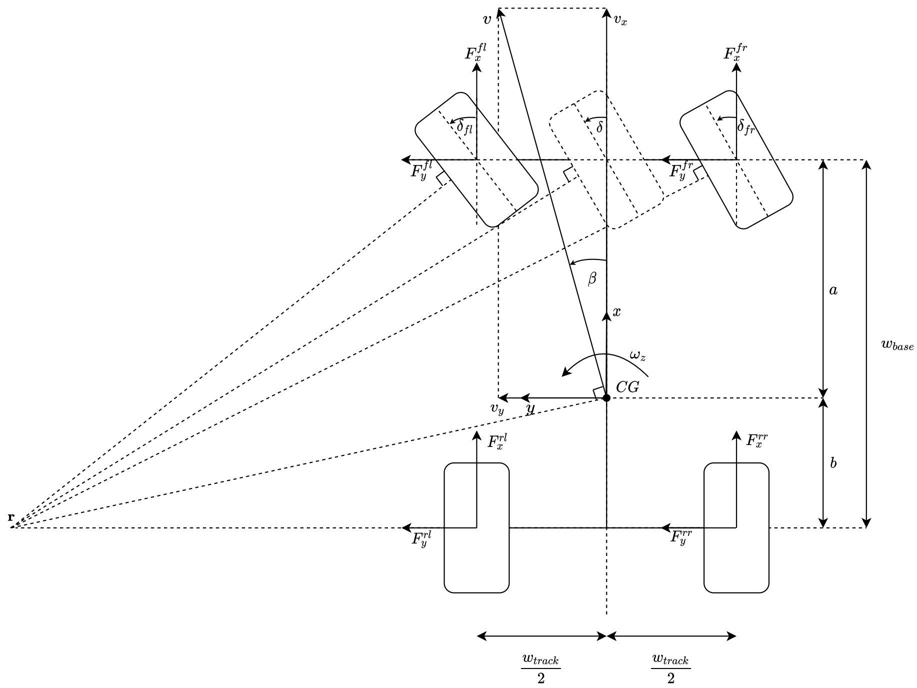

Figure 2.8: Full car model assuming Ackerman steering. An imaginary wheel (equivalent to the bicycle model) turned δ rad is assumed to be controlled by the driver. This corresponds to the front right δ_{fr} and front left δ_{fl} turning angles. The wheelbase w_{base} and wheel track w_{track} are also represented. The car is assumed to have neutral steering when the turning point is on the rear axle axis, as shown in the figure. Different steering schemes can have this point closer or further away from the car.

By assuming that the rear wheels are not steerable, we can write the previous car model only in respect to the steer angle δ as,

$$\dot{\mathbf{x}} = A(\delta)\mathbf{x} + B\mathbf{u} \tag{2.56}$$

$$\mathbf{y} = C(\delta)\mathbf{x}. \tag{2.57}$$

2.2.4 Steady State

The dynamics matrix A has rank 15-1, which means that there is a surface of equilibrium points. Other equilibrium points may be possible, we don't say anything about them, but those belonging to this surface must exist. If we had taken into account the air resistance then the only equilibrium point would be the origin. This is what we call the "coasting" vehicle. The "coasting" vehicle is possible because, so far, no attrition other than the one from the tire-road interaction has been contemplated.

With the aid of MATLAB we were able to define the null space, $\mathcal{N}(A)$, taking into account different rear and front wheel radius r_r, r_f, as the line spanned by the vector $\mathbf{n}$, normalized in respect to the longitudinal speed v_x and parametrized with the steering δ,

$$\mathcal{N}(A) = v_x \mathbf{n}(\delta), \tag{2.58}$$

$$\mathbf{n}(\delta) = \begin{bmatrix} 0 \\ 0 \\ \frac{a+b+\tan\delta \cdot w_{track}/2}{r_r(a+b)} \\ 0 \\ 0 \\ \frac{a+b-\tan\delta \cdot w_{track}/2}{r_r(a+b)} \\ 0 \\ 0 \\ \frac{\sqrt{\left((a+b)\cos\delta + \frac{w_{track}}{2}\sin\delta\right)^2 + (a+b)^2\sin^2\delta}}{r_f(a+b)\cos\delta} \\ 0 \\ 0 \\ \frac{\sqrt{\left((a+b)\cos\delta - \frac{w_{track}}{2}\sin\delta\right)^2 + (a+b)^2\sin^2\delta}}{r_f(a+b)\cos\delta} \\ 1 \\ b\frac{\tan\delta}{a+b} \\ \frac{\tan\delta}{a+b} \end{bmatrix} \text{with, } \mathbf{n}(0) = \begin{bmatrix} 0 \\ 0 \\ 1/r_r \\ 0 \\ 0 \\ 1/r_r \\ 0 \\ 0 \\ 1/r_f \\ 0 \\ 0 \\ 1/r_f \\ 1 \\ 0 \\ 0 \end{bmatrix}. \tag{2.59}$$

The null space 2.59 describes the steady state of the system. It is worth noting that the steady state does not depend on any parameter pertaining to the tire-road interaction, load at each wheel, mass of the vehicle or any other such property. We only require the vehicle dimensions, wheelbase, wheel track, and the tire radius, r_r for the rear tires and r_f for the front tires and the current turning angle δ. Since there is no such dependency, it is not possible to estimate the tire-road interaction if the vehicle is "coasting".

The obtained result for a straight moving vehicle $\mathbf{n}(0)$ is the expected, with the vehicle velocity and each wheel angular velocity depending only on the tire radius. We also derive the relationship between the pairs (ω_z, v_x) and (ω_z, v_y) which shall henceforth be referred as the desired yaw rate and the lateral stability, respectively. From the vector $\mathbf{n}(\delta)$,

$$\frac{v_x}{\omega_z} = \frac{1}{\tan\delta \ / \ (a+b)} \implies \omega_z = \frac{v_x \tan\delta}{a+b} \tag{2.60}$$

$$\frac{v_y}{\omega_z} = \frac{b\tan\delta/(a+b)}{\tan\delta/(a+b)} \implies v_y = b \cdot \omega_z \tag{2.61}$$

we derive the relationships between yaw-rate, longitudinal and lateral velocity.

This is useful in the sense that we can define the desired behaviour, and can also be applied to other problem formulations, such as with the tradicional desired yaw rate equation,

$$\omega_z = \frac{\delta}{a+b+K_u v_x^2} v_x, \tag{2.62}$$

with the understeer coeficient K_u, which can also be used and tuned to achieve more understeer or oversteer. In this case, the v_x^2 term shoud be either fixed to the current estimated or to the propagated expected value from the system dynamics.

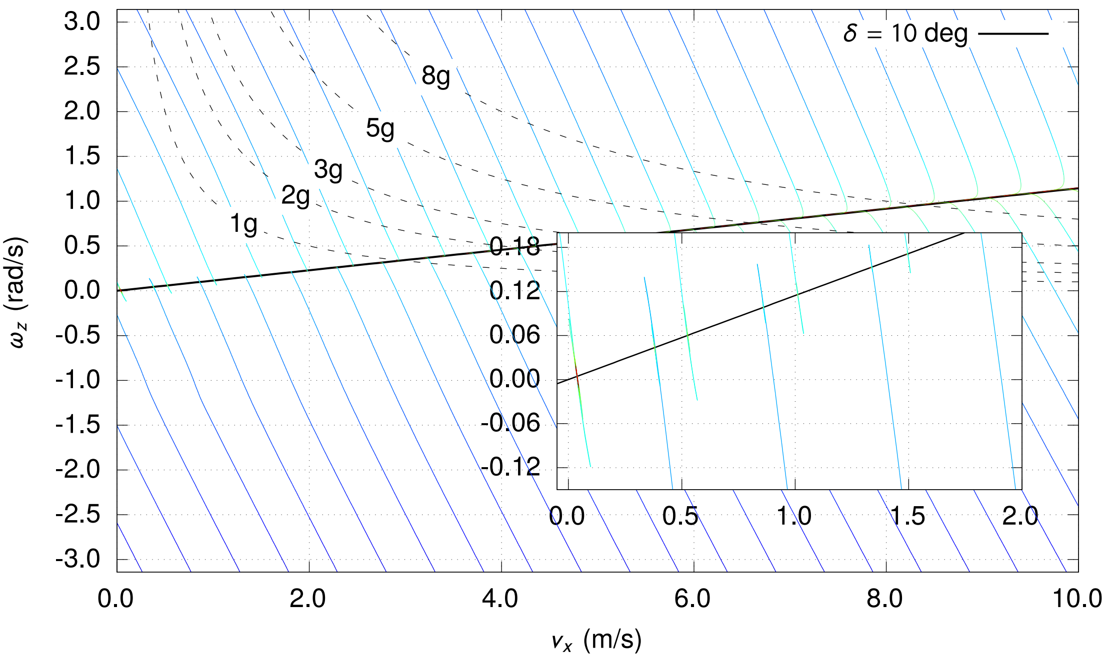

Figure 2.9: Phase trajectories showing the linear relationship between the yaw rate ω_z and the linear velocity along x v_x, in an inertial frame aligned with the car. The starting points at the edges were defined using the null space of the dynamics matrix A, given a vehicle speed and steering angle δ, with the yaw rate being changed to define a point at the edge. A zoom in at the origin is provided. The tire configuration was set to "dry". Lateral g forces represented in dashed black.

Figures (2.9) and (2.10) show the linear relationship at steady state and the convergence of the phase trajectories towards the equilibrium, showing that the system is stable for this range of values and parameters. The air friction drag was taken into account during these simulations, which causes the phase trajectories to slide along the line towards 0. This effect is more visible at higher velocities where the squared dependency on the forward velocity v_x has a greater impact. It can be further seen that at higher velocities the vehicle tends to be asymptotically stable towards the previously defined null space. The phase trajectories were simulated with a very low cg in order to dismiss the load transfer. Ideally we want the state to move along this line and, in the driving case, go towards the specified g force limit.

Other unmodelled dynamics, not just the air drag, where taken into account in the plant simulations.

2.3 Unmodelled Dynamics

There are some dynamics that are not contemplated in the previous model. The normal load is not constant and can change depending on the downforce or the mass transfer between wheels during cornering and/or acceleration [1]. The air friction is another factor that should be taken into account. In this work, the controller will see the air friction as a disturbance to the model. In fact, this disturbance and others, such as transmission losses - not covered in this work - are seen by the tire model as hysteresis.

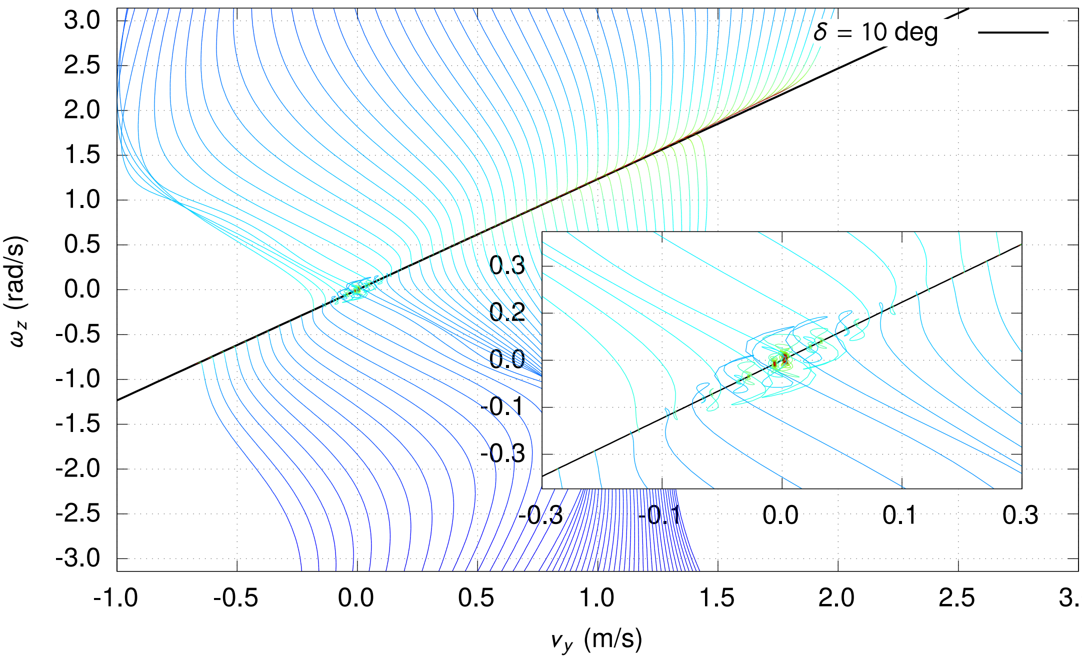

Figure 2.10: Phase trajectories showing the linear relationship between the yaw rate ω_z and the linear velocity along y v_y, in an inertial frame aligned with the car. The starting points at the edges were defined using the null space of the dynamics matrix, given a vehicle speed and steering angle, with the yaw rate being changed to define a point at the edge. A zoom in at the origin is provided. The tire configuration was set to "dry".

This is equivalent to the Pacejka tire model with the offset parameters, allowing the linear region to slide up and down as needed.

2.3.1 Variable Normal Load

The load at each wheel i is not constant. We need to consider the base load, load transfer and the load due to the downforce. The base load F^i_{bn} is the load resulting from the distribution of the weight due to the unsprung mass plus the weight of the wheels,

$$\begin{bmatrix} F^{rr}_{bn} \\ F^{rl}_{bn} \\ F^{fr}_{bn} \\ F^{fl}_{bn} \end{bmatrix} = \begin{bmatrix} \frac{a \cdot g \cdot m}{2(a+b)} \\ \frac{a \cdot g \cdot m}{2(a+b)} \\ \frac{b \cdot g \cdot m}{2(a+b)} \\ \frac{b \cdot g \cdot m}{2(a+b)} \end{bmatrix} + \begin{bmatrix} g \cdot m_{w_r} \\ g \cdot m_{w_r} \\ g \cdot m_{w_f} \\ g \cdot m_{w_f} \end{bmatrix}. \tag{2.63}$$

Next we consider the longitudinal and lateral load transfer due to the vehicle acceleration and the centrifugal forces. Here, we will only consider the load transfer due to the centrifugal force. Not taken into account were the Coriolis and Euler forces. The centrifugal force, due to a rotation about a point **r** is given by

$$\mathbf{F}_c = -m\boldsymbol{\omega} \times (\boldsymbol{\omega} \times \mathbf{r}). \tag{2.64}$$

If we assume that $\mathbf{v}$ is tangent to the force, and take into account only planar motion,

$$\mathbf{F}_c = -m(\boldsymbol{\omega} \times \mathbf{v}) \text{ with, } \mathbf{v} = \boldsymbol{\omega} \times \mathbf{r} \tag{2.65}$$

$$\boldsymbol{\omega} = [0, 0, \omega_z]^T \tag{2.66}$$

$$\mathbf{v} = [v_x, v_y, 0]^T \tag{2.67}$$

$$\implies \begin{bmatrix} F_{cx} \\ F_{cy} \end{bmatrix} = m \begin{bmatrix} -v_y\omega_z \\ v_x\omega_z \end{bmatrix}, \tag{2.68}$$

and use that to write the load transfer F_{tx}, F_{ty}, given in respect to the acceleration and the height h_c of the cg, we have

$$\begin{bmatrix} F_{tx} \\ F_{ty} \end{bmatrix} = m \cdot h_c \begin{bmatrix} \frac{\dot{v}_x - v_y\omega_z}{a+b} \\ \frac{\dot{v}_y + v_x\omega_z}{w_{track}} \end{bmatrix}. \tag{2.69}$$

No distinction was made between the sprung/unsprung mass and no suspension model was assumed.

In addition to this we need to consider the downforce as a result of the air friction and the vehicle aerodynamics. The air friction has a drag component and a downforce component. The downforce is given by the front and back wings, or approximated by an equivalent wing. We assume that the rear wing provides equal downforce to the rear wheels and the front wing provides downforce to the front wheels as,

$$F_{downforce} = \frac{1}{2} W H F \rho v_x^2. \tag{2.70}$$

width W as the wing width, H the chord, and F the lift coefficient.

Adding all of these contributions, the estimated normal load $\mathbf{f}_n(\mathbf{x})$ is given by,

$$\begin{aligned} \begin{bmatrix} F_n^{rr} \\ F_n^{rl} \\ F_n^{fr} \\ F_n^{fl} \end{bmatrix} &= \begin{bmatrix} \frac{a \cdot g \cdot m}{2(a+b)} \\ \frac{a \cdot g \cdot m}{2(a+b)} \\ \frac{b \cdot g \cdot m}{2(a+b)} \\ \frac{b \cdot g \cdot m}{2(a+b)} \end{bmatrix} + \begin{bmatrix} g \cdot m_{w_r} \\ g \cdot m_{w_r} \\ g \cdot m_{w_f} \\ g \cdot m_{w_f} \end{bmatrix} + \begin{bmatrix} W_r H_r F_r \\ W_r H_r F_r \\ W_f H_f F_f \\ W_f H_f F_f \end{bmatrix} \frac{\rho v_x^2}{4} + m \cdot h_c \begin{bmatrix} 1, & 1 \\ 1, & -1 \\ -1, & 1 \\ -1, & -1 \end{bmatrix} \begin{bmatrix} \frac{a_x - v_y\omega_z}{2 \cdot (a+b)} \\ \frac{a_y + v_x\omega_z}{2 \cdot w_{track}} \end{bmatrix} \\ &= \mathbf{f}_n(\mathbf{x}). \end{aligned} \tag{2.71}$$

2.3.2 Wheel radius

The wheel radius is not constant, and even though the variation is small it is still a problem when it comes to tire slip estimations.

We further assume that the tire has a spring like behaviour, with a vertical stiffness k_{stiff}, resulting in the following definition for the loaded radius r_L and contact patch L,

$$r_L = r - \frac{F_n}{k_{stiff}} \tag{2.72}$$

$$L = 2\sqrt{r^2 - r_L^2} \tag{2.73}$$

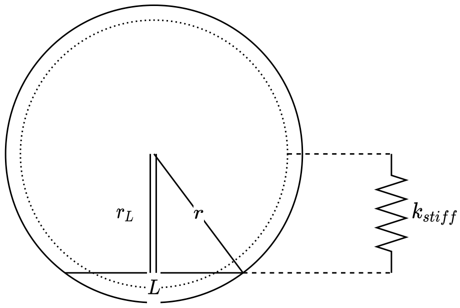

Figure 2.11: The tire is assumed to behave like a spring when loaded, resulting in a loaded tire radius r_L and contact patch length L.

dismissing the transient behaviour of the wheel radius.

See Jazar [25] for a better definition of effective tire radius based on the loaded radius and the unloaded radius (also called geometric radius). In practice the tire radius depends on the type of tire, tire velocity, stiffness, load and inflation pressure. However, in this work, a simplified radius is considered.

2.3.3 Drag

The drag due to the air friction is treated as a disturbance to the model but is modelled in the plant as,

$$F_{drag} = \frac{1}{2}\rho C_D A v_x^2. \tag{2.74}$$

The resulting force from the drag acting on the vehicle is given by the drag equation, with $C_D A$ usually referred as the drag area, ρ the air density and v_x the vehicle speed along the x axis.

This has a negative impact on the vehicle performance because it increases the power required to reach higher velocities and diminishes the resulting acceleration. On the other hand, the downforce has a positive impact on the performance by increasing the normal load.

As a consequence of drag, a theoretical max speed can be derived by saying that the total work done by the forces acting on the vehicle is the result of the consumed power minus the power of the drag force F_{drag}, and setting that to zero,

$$Power = F_{drag} \cdot v_{max} \tag{2.75}$$

$$v_{max} = \sqrt[3]{\frac{Power}{0.5\rho C_D A}}. \tag{2.76}$$

Chapter 3

Observer/Controller Design

The proposed solution consists on a Model Predictive Controller with an EKF observer. The role of the observer is to estimate the state vector, with an emphasis on the velocity vector. The estimated state $\hat{\mathbf{x}}$ and associated covariance matrix $\hat{P}$ are given to the MPC that will minimize a cost function over the prediction horizon, based on the desired behaviour of the system.

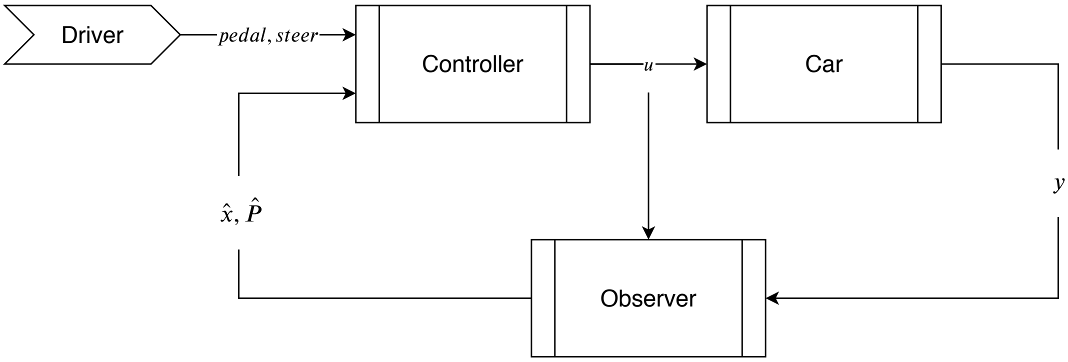

Figure 3.1: High level view of the system with the controller and observer. The driver provides a signal, comprised by the pedal and steer. The controller then actuates on the car, given the driver input and the car state estimation from the observer.

3.1 Observer

The goal of the observer is to provide an accurate estimation of the states, given the plant outputs and the inputs. In order to show if the velocity vector was observable we used an EKF. Should the system be observable, in the simulated conditions, we expect to see a bounded trace of the covariance matrix $trace(\hat{P}_k) < c_{const}, c_{const} > 0$.

Taking the discrete system, see annex A, we consider that,

$$x_{k+1} = A_k \cdot x_k + B_k \cdot u + w_k \text{ with } w_k \sim N(0, Q) \tag{3.1}$$

$$y_k = C_k \cdot x_k + v_k \text{ with } v_k \sim N(0, R). \tag{3.2}$$

The estimation is done through two steps. First we predict what we expect to see. And then, based on the error, we update our estimation.

For the prediction step we take the previous estimation $k-1$, and use he previously linearised model $A_{k-1|k-1}$ to estimate the new state. We use that new estimation to derive a new linearization $A_{k|k-1}$ and calculate the corresponding estimation covariance $\hat{P}_{k|k-1}$.

$$\hat{x}_{k|k-1} = A_{k-1|k-1} \cdot \hat{x}_{k-1|k-1} + B_{k-1|k-1} \cdot u_k \tag{3.3}$$

$$\hat{P}_{k|k-1} = A_{k|k-1} \cdot \hat{P}_{k-1|k-1} \cdot A^T_{k|k-1} + Q \tag{3.4}$$

Then we use the error between the measured outputs y_k and the expected outputs to update our estimation through the optimal Kalman gain K_k,

$$e_k = y_k - C_{k|k-1} \cdot \hat{x}_{k|k-1} \tag{3.5}$$

$$S_k = C_{k|k-1} \cdot P_{k|k-1} \cdot C^T_{k|k-1} + R \tag{3.6}$$

$$K_k = P_{k|k-1} \cdot C^T_{k|k-1} \cdot S_k^{-1} \tag{3.7}$$

$$\hat{x}_{k|k} = x_{k|k-1} + K_k \cdot e_k \tag{3.8}$$

$$\hat{P}_{k|k} = (\mathcal{I} - K_k \cdot C_{k|k}) \cdot \hat{P}_{k|k-1}, \tag{3.9}$$

and make new linearizations $A_{k|k}$ and $C_{k|k}$.

Outside of the observer problem we say that $\hat{x}_k$ is the state estimation at time k and, similarly, that $\hat{P}_k$ is the corresponding covariance matrix. Similarly A_k and C_k correspond to the linearizations.

It is worth noting that proper choice of the expected process noise covariance Q can help with some of the unmodelled dynamics and other disturbances. The sensor noise covariance R must also be adjusted according to the sensors accuracy and noise.

3.2 Controller

The controller used here is a Model Predictive Controller. Implied with this is an optimization problem that must be solved in real-time. To that effect we selected the KWIK algorithm [48]. The KWIK algorithm solves quadratic programming (QP) problems with linear inequality constraints. Some of our constraints are quadratic but can be approximated by linear constraints. In this section we cover the problem definition, the state and input constraints, as well as an alternate cost function with soft constraints, should some constraints prove to be infeasible for a particular horizon.

3.2.1 Model Predictive Controller

MPC is a control strategy under the optimal control umbrella. First developed in the petrochemical industry for process control it has also spread to other areas. It has a strong theoretical basis and its stability, optimality and robustness properties are well known. It is also popular due to it's ability to take into account several constraints, such as in the context of this thesis.

The proposed solution is to transfer the control problem into an optimization problem and solve it through quadratic programming (QP) with a quadratic cost function. This problem is then numerically solved with the KWIK algorithm [48]. Given the discrete piecewise linear system, solve the optimization problem over an horizon window with N time-steps of T_s duration each, with Q and R weight matrices being at least semi-positive definite. Here we will consider only linear constrains, A_u for the inputs and A_x for the state constraints, with the corresponding constraints vectors b_u and b_x. For a time instance m and N k steps, the problem to be solved is to find the inputs $\mathbf{u}_m$ that minimize,

$$\min_{\mathbf{u}_m} J(\mathbf{u}_m) = \sum_{k=1}^{N} x_{m,k}^T \cdot Q \cdot x_{m,k} + u_{m,k}^T \cdot R \cdot u_{m,k} \tag{3.10}$$

$$\begin{aligned}
&\text{s.t.}\\
x_{k+1} &= A_k \cdot x_k + B \cdot u_{k+1}\\
A_u \cdot \mathbf{u}_m &\geq b_u\\
A_x \cdot \mathbf{x}_m &\geq b_x\\
\mathbf{u}_m &= \begin{bmatrix} u_{m,1}^T, & u_{m,2}^T, & \cdots, & u_{m,k}^T, & \cdots, & u_{m,N}^T \end{bmatrix}^T\\
\mathbf{x}_m &= \begin{bmatrix} x_{m,1}^T, & x_{m,2}^T, & \cdots, & x_{m,k}^T, & \cdots, & x_{m,N}^T \end{bmatrix}^T.
\end{aligned}$$

To solve the problem we need to rework the problem formulation. The state can be propagated from the initial state x_0 with the system dynamics and inputs as,

$$x_{m,1} = A_0 x_0 + B u_{m,1} \tag{3.11}$$

$$x_{m,2} = A_1 A_0 x_0 + A_1 B u_{m,1} + B u_{m,2} \tag{3.12}$$

thus,

$$\mathbf{x}_m = \mathcal{M} x_0 + \mathcal{C} \mathbf{u}_m, \tag{3.13}$$

with the auxiliary matrices $\mathcal{C}$

$$\mathcal{C} = \begin{bmatrix} B, & 0, & & \ddots & & 0 \\ A_1 B, & B, & 0, & & \ddots & \vdots \\ A_2 A_1 B, & A_1 B, & B, & 0, & & \vdots \\ \vdots & \vdots & \vdots & \vdots & 0 & \vdots \\ (\Pi_{i=N}^{1} A_i) B, & (\Pi_{i=N-1}^{1} A_i) B, & \cdots, & A_2 A_1 B, & A_1 B, & B \end{bmatrix}, \tag{3.14}$$

and $\mathcal{M}$

$$\mathcal{M} = \begin{bmatrix} A_0 \\ A_1 A_0 \\ A_2 A_1 A_0 \\ \vdots \\ \Pi_{i=N-1}^{0} A_i \end{bmatrix} \tag{3.15}$$

which allows us to write the the state constraints as inputs constraints,

$$A_x \mathbf{x}_m \geq b_x \tag{3.16}$$

$$A_x \mathcal{M} x_0 + A_x \mathcal{C} \mathbf{u}_m \geq b_x \tag{3.17}$$

$$A_x \mathcal{C} \mathbf{u}_m \geq b_x - A_x \mathcal{M} x_0 \tag{3.18}$$

and adding the previous input constraints we arrive at the more compact form,

$$A_c \mathbf{u}_m \geq b_c \tag{3.19}$$

$$A_c = \begin{bmatrix} A_x \mathcal{C} \\ A_u \end{bmatrix} \tag{3.20}$$

$$b_c = \begin{bmatrix} b_x - A_x \mathcal{M} x_0 \\ b_u \end{bmatrix}. \tag{3.21}$$

We then rewrite the problem,

$$\min_{\mathbf{u}_m} J = \mathbf{u}_m^T H \mathbf{u}_m + 2 \cdot (F \cdot x_0)^T \mathbf{u}_m \tag{3.22}$$

$$\text{s.t.}$$

$$A_c \mathbf{u} \geq b_c$$

$$H = \mathcal{C}^T Q \mathcal{C} + R \tag{3.23}$$

$$F = \mathcal{C}^T Q \mathcal{M}, \tag{3.24}$$

which can be solved with the KWIK algorithm [48] if the Hessian matrix H is positive definite $H > 0$ and Hermitian $H = H^H$.

Lastly, taking into account that if the car is at rest $x_0 = 0$ and if $H \geq 0$, then the only possible solution is $\mathbf{u}_m = 0$. To address this, when x_0 is small, it is set to some other slightly higher value. There is a range of values for transitioning, both from rest - driving, and to rest - braking.

3.2.2 Input Constraints

The input constraints have to do with the engine curve and the overall available power. We assume that the electric engine will be functioning as an engine, while accelerating, or as a brake, consuming power to brake and not as a generator, consuming mechanical power and generating electric power. However, this section can be revisited for a more in depth power management. We feel that the example provided here is enough for a proof of concept. We could also factor in some constraint/cost to reduce uneven engine wear, like the one proposed in [27] and/or to take into account heat generation.

For the engine curve, we assume that there is some maximum and negative torque, and power constraints when braking and accelerating that define the engine curve. Other engine curves can be considered. The maximum driving and braking torque constraint is trivial to enforce over the horizon, and is considered in the input constraints. For the power constraint we can write it by propagating the wheel speed state and multiplying it by the input torque,

$$P^i_{engine} = \omega^i \cdot u^i, \tag{3.25}$$

with e_s as the wheel speed selector matrix, such that,

$$\mathbf{P}^{rr,rl,fr,fl}_{engine_m} = \operatorname{diag}(\mathbf{u}_m) \cdot (e_s \mathcal{M} x_0 + e_s \mathcal{C} \mathbf{u}_m) = \begin{bmatrix} P^{rr}_{engine_{m,1}} \\ P^{rl}_{engine_{m,1}} \\ P^{fr}_{engine_{m,1}} \\ P^{fl}_{engine_{m,1}} \\ \cdots \\ P^{rr}_{engine_{m,N}} \\ P^{rl}_{engine_{m,N}} \\ P^{fr}_{engine_{m,N}} \\ P^{fl}_{engine_{m,N}} \end{bmatrix}, \tag{3.26}$$

we arrive at a quadratic constraint in respect to $\mathbf{u}_m$. This can be avoided if we assume that, besides the one directly connected, the contribution from one engine to some other wheel is negligible. Which amounts to say that the product $e_s\mathcal{C}$ can be approximated through a diagonal matrix. This decouples the problem into constraints to be satisfied by each engine i, since the power at each engine can be approximated by,

$$P^i_{engine_{m,k}} = u^i_{m,k} \cdot m_{aux} + {u^i_{m,k}}^2 \cdot c_{aux}, \tag{3.27}$$

with m_{aux} and c_{aux} as the corresponding entries of $e^i_s \cdot \mathcal{M} \cdot x_0$ and $e^i_s \cdot \mathcal{C}$. With this, we can solve

$$P^i_{engine_{m,k}} \leq \text{max driving/braking engine power}, \tag{3.28}$$

in respect to the input torque $u^i_{m,k}$ and find the equivalent driving/braking torque constraint as a linear inequality constraint, such that the local power constraints can be written as

$$\mathbf{u}_m \geq b_{\text{equivalent engine torque constraint}}. \tag{3.29}$$

The equivalent engine torque constraint can be determined by finding the roots of equation 3.27.

For the overall available power, the previous approximation is not as useful. But we can propagate the wheel turning speed across the horizon with only the autonomous system dynamics and the previous input solution, getting ${}^{*}\omega^{i}_{m,k}$ from $\mathcal{M}x_0 + \mathcal{C}\mathbf{u}_{m-1}$, and say that the power generated at each wheel is approximately given by 3.25. We then say that the total power consumption must be less than a given limit,

$$P_{\text{total}_{m,k}} \approx \sum_{i}^{rr,rl,fr,fl} {}^{*}\omega^{i}_{m,k} \cdot u^{i}_{m,k}, \tag{3.30}$$

and use it to make a linear inequality constraint in respect to the inputs.

All of the above was also used to do the braking power constraints, both local and global.

3.2.3 State Constraints

The state constraints ensure that there are tip-over safeguards and that the wheel slip ratio does not exceed a predetermined value. The tip-over safeguards can be made to enforce a minimum load at each tire or to limit the lateral g forces. The wheel slip constraint can be turned into a linear constraint if we rewrite 2.1 into,

$$v^{i}_{x}(k+1) - \omega r = 0, \tag{3.31}$$

with v^{i}_{x} as the longitudinal speed at a tire i in the tire frame. Which results in the following linear constraints,

$$v^{i}_{x}(1+k^{+}) - \omega^{i} r \geq 0 \tag{3.32}$$

$$v^{i}_{x}(1-k^{-}) + \omega^{i} r \geq 0. \tag{3.33}$$

The velocities at each tire can then be mapped into velocities at the centre of mass with the linear transformation 2.30, thus ensuring we can have this constraint as a linear constraint in our optimization problem 3.10,

$$\begin{bmatrix} -r & \begin{bmatrix} (1+k^{+}) & 0 \\ (1-k^{-}) & 0 \end{bmatrix} \begin{bmatrix} \cos\delta & \sin\delta & r_x \sin\delta - r_y \cos\delta \\ -\sin\delta & \cos\delta & r_x \cos\delta + r_y \sin\delta \end{bmatrix} \\ r & \end{bmatrix} \begin{bmatrix} \omega^{i} \\ v_x \\ v_y \\ \omega_z \end{bmatrix} \geq 0 \tag{3.34}$$

$$\implies \begin{bmatrix} -r & (1+k^{+})\cos\delta & (1+k^{+})\sin\delta & (1+k^{+})(r_x \sin\delta - r_y \cos\delta) \\ r & (1-k^{-})\cos\delta & (1-k^{-})\sin\delta & (1-k^{-})(r_x \sin\delta - r_y \cos\delta) \end{bmatrix} \begin{bmatrix} \omega^{i} \\ v_x \\ v_y \\ \omega_z \end{bmatrix} \geq 0. \tag{3.35}$$

For the tip-over problem we can define a limit for the g forces. This means that if a turning radius is requested that can't satisfy this constraint at the initial velocity, the controller will brake the car in such a way that it does the tightest turn with, at most, the specified g force until the requested turning radius is achieved. It will then only expend energy in maintaining that velocity. Similarly, the controller will allow the car to accelerate until the maximum gforce is achieved.

The lateral g forces are considered to be only due to the centrifugal force, which is also responsible for the lateral load transfer, disregarding the contribution from $\dot{v}_y$,

$$g_{force_y} = \mathrm{sign}(\omega_z)\frac{v_x \cdot \omega_z}{g} \tag{3.36}$$

Any constraint done here in respect to both the longitudinal velocity and the yaw rate results in a non-linear constraint. Since we can directly measure the yaw rate, the approach taken here was to propagate the longitudinal velocity and use that value has a constant,

$$\frac{g \cdot g_{force\ limit_y}}{{}^{*}v_x} \geq |\omega_z| \tag{3.37}$$

which can be turned into two linear constraints, one for the lower bound and another for the upper bound of ω_z, for each time step.

The tip-over prevention can also be ensured by placing steering constraints on the input steer from the driver and limiting the maximum steer angle as in stated by Kang [28]. Or by making constraint similar to the g force constraint, based on the minimum acceptable normal load at each tire.

3.2.4 Cost Function

According to the system dynamics, the cost function must minimize the lateral stabilization error and ensure the yaw rate - linear velocity relationship. At thrust, we want a compromise between the highest longitudinal speed at the end of the horizon $v_{x|N}$ and the minimum error during the horizon. With some positive weight factors ρ we devised the following cost function,

$$\min_{\mathbf{u}_m} J = -\rho_{v_x} v_{x,N}^2 + \sum_{k=1}^{N}\left[\rho_{\omega_z}\left(\omega_{z,k} - \frac{v_{x,k}\tan\delta}{a+b}\right)^2 + \rho_l(v_{y,k} - b\omega_{z,k})^2\right], \tag{3.38}$$

$$\tag{3.39}$$

that happens to result in a symmetric positive definite matrix H 3.22. Should H not be positive definite at some point, it can be reconstructed to provide a convex hull by decomposing it and enforcing positive eigenvalues. In practice, only least energetic component was negative. For the most part H is at least semi-positive definite $H \geq 0$. Whether or not H is full rank is tied to whether or not the system is over-actuated. In those cases we can't ensure that the solution is the most optimum solution, in the sense of optimum control.

Should the MPC problem be infeasible, we need to known why. One possibility is when the slip constraints for a given wheel can't be met. In such a case a quadratic cost J_{slip} for those wheels is added to the cost function in order to bring it back to feasibility,

$$J_{slip} = \rho_{slip} \sum \left(v_x^i - \omega^i r \right)^2 \tag{3.40}$$

with ρ_{slip} as a weight and the sum being only about those wheels.

The other possibility for an infeasible problem is if the g force can't be within bounds over the horizon. In which case we also add a very high quadratic cost to the yaw rate ω_z in order to reduce the g force.

With this we can ensure that even when the problem is infeasible, we can move towards a feasible operation point without dismissing the original problem formulation.

Chapter 4

Implementation

The end goal of this thesis is to implement the observer/controller pair in the FST Lisboa team cars, serving as the control basis for further algorithms. This chapter covers the Matlab implementation work, from a configuration and design point of view. The used and developed simulink models are shown and the implementation details of the observer, controller and plant are covered.

The implementation of this thesis was made entirely in Matlab. A LuGre library was developed to generate the state space matrices. The plant, observer and controller were made in level-2 s-functions. These s-functions make use of the developed library and are parametrized accordingly and can be latter developed in C code. The s-functions were developed due to the ease of implementation of non linear systems, debugging and the ability to set a sampling time for the discrete blocks (observer & controller) or continuous (plant) as needed.

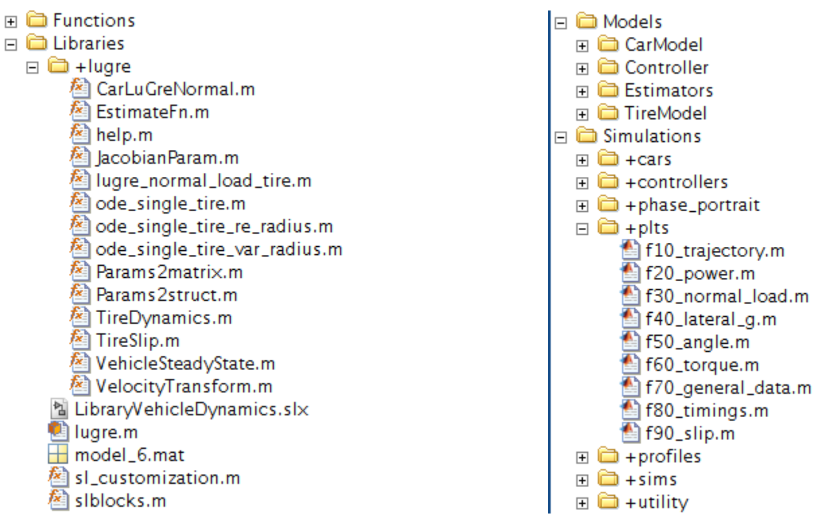

Figure 4.1: Broad overview of the structure of the Matlab implementation.

Notable functions developed are the s-functions "msfcn_extended_kalman", "msfcn_full_car_normal_load" and the "c_msfcn_linear_mpc_KWIK". These are respectively the observer, plant and the controller. They make use of the function "CarLuGreNormal" in the library. That is the main function in the library since it returns the state space matrices of the car. The next most important is the "TireDynamics" that returns the state space matrices of the single tire model, and is used by the "CarLuGreNormal" to assemble the full car system, with a similar approach as the developed model equations in chapter 2. The "TireDynamics" function also allows for fixed O_i parameters, variable tire radius and contact patch length (based on the normal load).

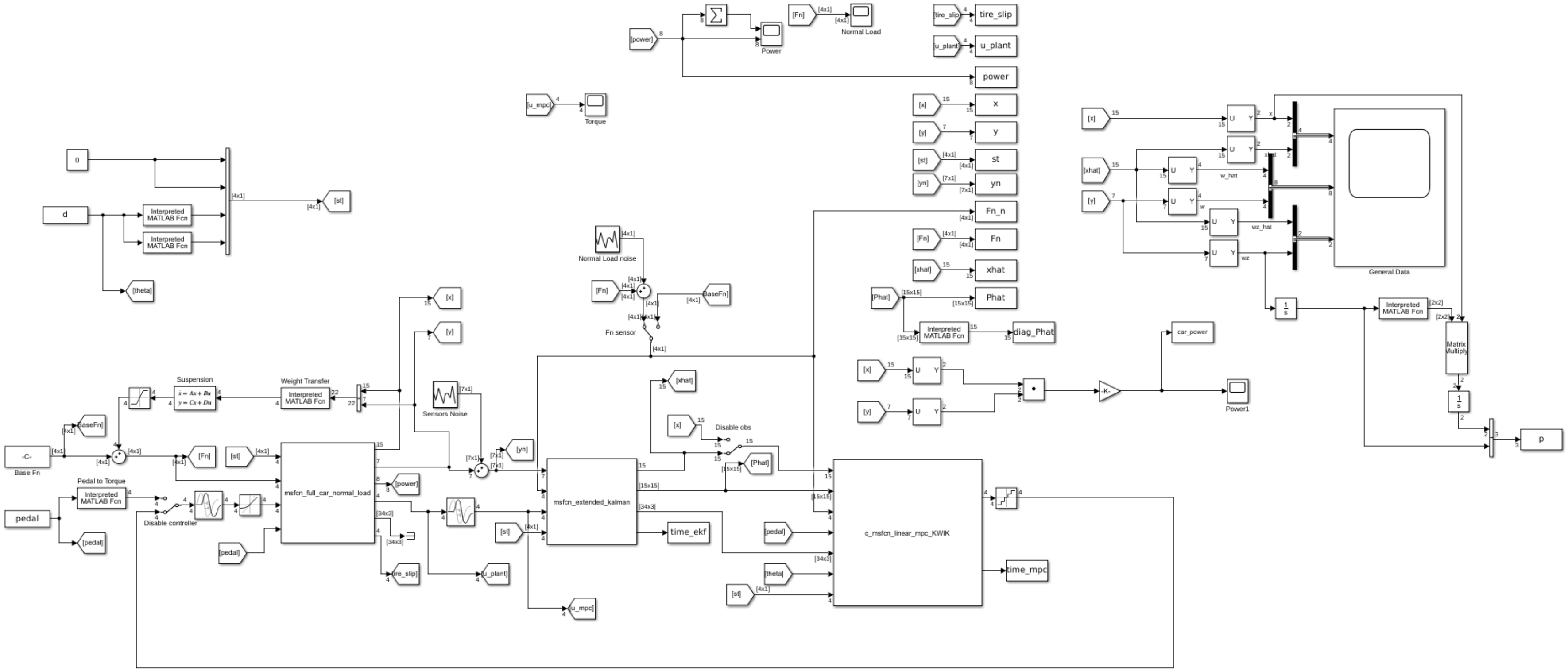

Figure 4.2: Simulink developed for simulating the car, observer and controller. Used to test the observer/controller pair in several configurations.

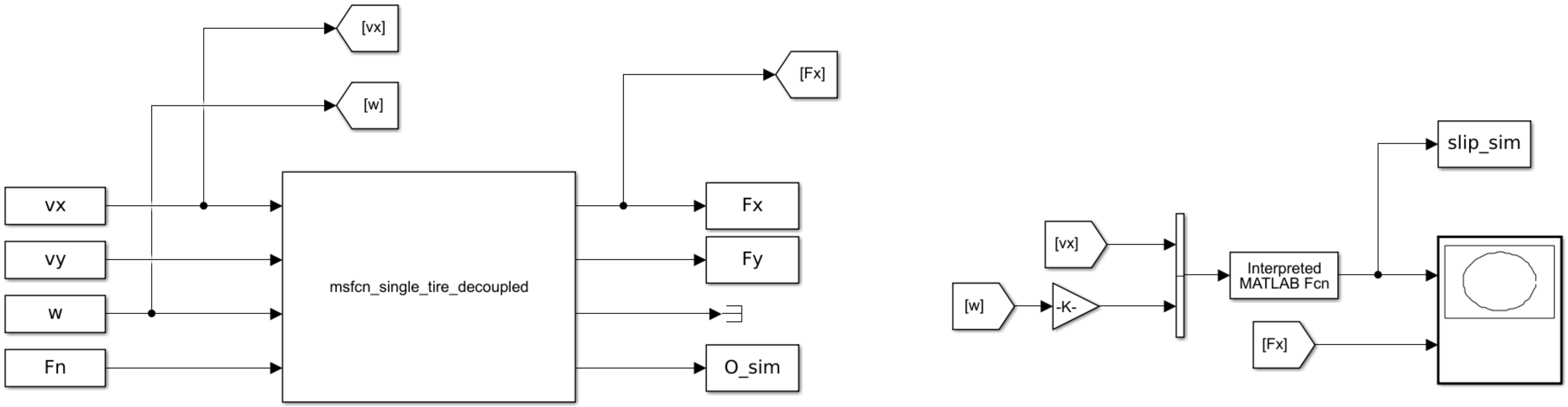

Figure 4.3: Simulink developed to simulate a single tire. Used to study tire hysteresis and the effect of the slip angle, slip ratio, normal load and constant O_i parameters.

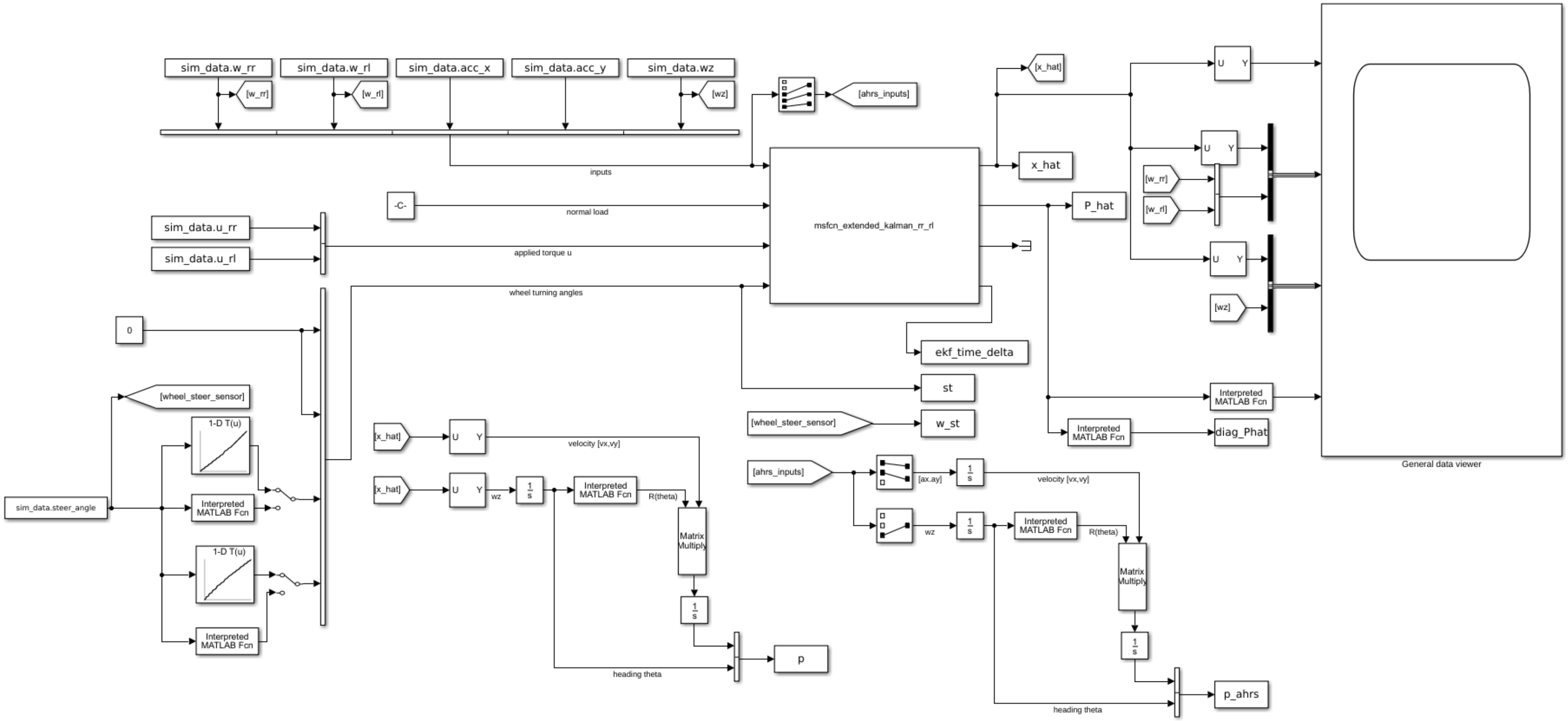

Figure 4.4: Simulink developed for simulating the kalman filter, given a dataset.

The main simulink, show in figure 4.2, features mass transfers in a very simplified way ,the suspension is simply a lowpass filter on the mass transfers, the communication transport delay, engine slew rate, noise in the sensors and in the normal load - including bias in the normal load; allows disabling the controller/observer for individual component testing. It was used extensively in the course of this project in order to better understand the vehicle dynamics and limits of the controller/observer.

Next, by order of importance is the simulink of the decoupled tire 4.3. It allowed for proper hysteresis analysis, slips and the parameter effects on the tire behaviour.

The tire parameters were estimated with the MATLAB non linear grey box estimation, from the System Identification Toolbox, and the FSAE TTC dataset.

Lastly the observer only simulink 4.4, was developed to test datasets collected in one of the FST Lisboa team's run and allowed to finally see the quality of the estimations and provide the team with a useful tool to further validate design choices, and better understand the car. As a side note, from the data we were able to find steering wheel issues and an issue in the left rear wheel, both validated in the workshop.

The following sections deal with the more in-depth parameters and implementation details of each component.

4.1 Observer

The observer is implemented using the previous Kalman equations. However, in practice the observer provides the controller with the $x_{k\hat{+}1|k}$ and $P_{k\hat{+}1|k}$ estimates. This allows for a single discretization per cycle, reducing the computational cost and minimizing the impact of the transport delay.

For the process noise covariance matrix Q and sensor noise covariance R, we chose based on a qualitative performance analysis and sensor data.

By analysing the periodogram in figure 4.5, obtained with MATLAB, and assuming that there is white noise in the signal (seen as a flat line in dB), we took the high frequency noise as the noise power N_0 and chose a diagonal R matrix compatible with these values.

The process covariance noise matrix Q was chosen based on the perceived performance of the observer and also set as a diagonal matrix.

	Sensor R	Process Q
$\sigma^2_{\omega_i}$	0.05	10^{-2}
$\sigma^2_{a_x}$	0.5	10^{-3}
$\sigma^2_{a_y}$	0.5	10^{-3}
$\sigma^2_{\omega_z}$	0.0001	10^{-3}
$\sigma^2_{z_x}$		10^{-7}
$\sigma^2_{z_y}$		10^{-7}
Sampling Time $T_{s_{EKF}}$	10 ms	
PreWarp Frequency	$\frac{2\pi}{3T_{s_{EKF}}}$ rad/s	

Table 4.1: EKF covariance parameters, sampling time, PreWarp frequency (for the bilinear transform) used for the observer.

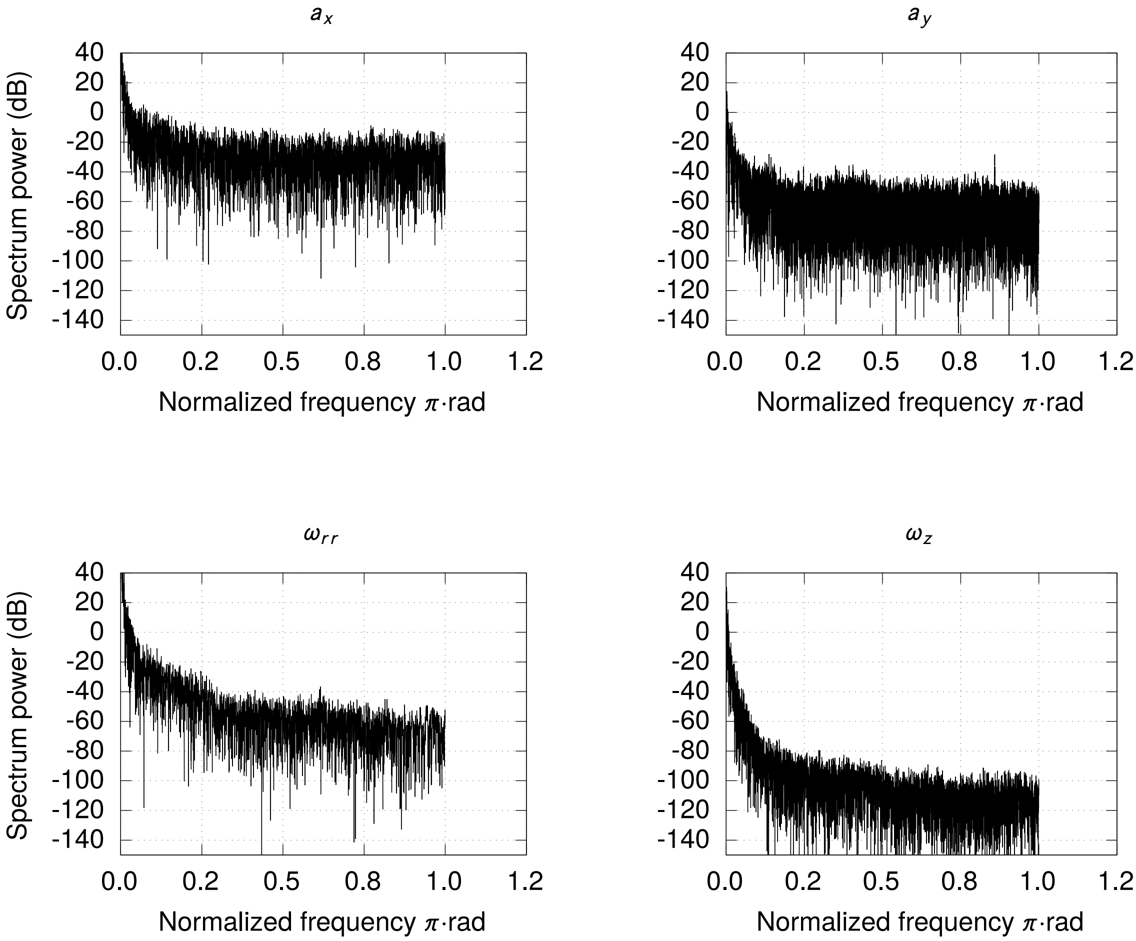

Figure 4.5: Estimated power spectral density: periodogram of the directly observable states from sensor readings. The periodogram of the left rear wheel was not included, since the type of signal is the same as the rear right wheel.

Table 4.1 surmises the EKF settings used in this work.

4.2 Controller

The controller is implemented with the KWIK algorithm provided by MATLAB in "mpcqpsolver". Therefore the implementation effort was mostly in constructing the optimization problem, such that it met all requirements, and in tuning the controller.

Due to noise, the controller can attempt to correct the heading of the vehicle by braking or accelerating. It just so happens that braking and accelerating some wheels is the fastest way to achieve the required yaw moment. This is not always desirable, specially in the presence of noise. Thus a deadzone was implemented to limit the braking solutions only when the yaw rate error e_{ω_z} and/or the lateral stability error e_l was outside of this deadzone.

Since we have the covariance matrix $\hat{P}$ from the observer, we can use a linear transformation T as,

$$T_l = \begin{bmatrix} 0 & \cdots & 0 & 1 & -b \end{bmatrix} \tag{4.1}$$

$$T_{\omega_z} = \begin{bmatrix} 0 & \cdots & 0 & 1 & 0 & -\frac{\tan\delta}{a+b} \end{bmatrix} \tag{4.2}$$

to find the associated covariance

$$\sigma^2_{e_{\omega_z}} = T_{\omega_z} \cdot P \cdot T^T_{\omega_z} \tag{4.3}$$

$$\sigma^2_{e_l} = T_l \cdot P \cdot T_l^T. \tag{4.4}$$

The same was also used to place an upper limit on the global braking/driving power when propagating the state over the horizon.

For the H matrix of the MPC problem, we ensure that it is positive definite by reconstructing it. First we take the Schur decomposition as

$$H = V \cdot D \cdot V^T \tag{4.5}$$

with V as a unitary matrix as $V^{-1} = V^T$ and the diagonal entries of D as the eigenvalues. If there is a negative eigenvalue we use that value to add a weight to the diagonal entries of H plus some small ϵ to ensure full rank. In the worst case scenario, multiple negative eigenvalues, or if the eigenvalue with the highest energy is negative, we set $D = \mathrm{abs}(D)$ and reconstruct H adding a diagonal matrix composed of ϵ entries, should the resulting matrix be only semipositive definite.

Table 4.2 surmises the MPC settings.

MPC parameters		Description
ρ_{v_x}	1	end velocity cost weight
ρ_{ω_z}	10^4	desired yaw rate running cost weight
ρ_l	10^3	lateral stability running cost weight
ρ_{gforce}	10^8	yaw rate soft running cost weight
ρ_{slip}	10^{18}	slip soft running cost weight
Maximum driving engine Power	35kW	
Maximum braking engine Power	30kW	
Maximum vehicle driving Power	80kW	
Maximum vehicle braking Power	30kW	
$T_{s_{MPC}}$	100 ms	
Maximum slip ratio	± 0.05	
Prewarp Frequency	$\frac{2\pi}{4T_{s_{MPC}}}$ rad/s	PreWarp Frequency for the bilinear transform

Table 4.2: Table with the MPC settings.

4.3 Plant

The modelled vehicle is the FST09e, with two configurations: 2 rear driving wheels (FST09e 2w) and 4 driving wheels (FST09e 4w). Taking into account figure 2.8, the car dimensions and parameters are detailed in table 4.3.

Vehicle parameters		Description
m	325 Kg	mass with driver
a	0.73 m	distance between the front wheel axis an the cg
b	0.81 m	distance between the rear wheel axis an the cg
w_{track}	1.2 m	wheel track
I_z	600 kg/m^2	inertia moment about the z axis
I_ω	4 kg/m^2	non driving wheel moment of inertia
I_{ω_d}	10 kg/m^2	driving wheel moment of inertia
r	0.2286 m	unloaded tire radius
$C_D A$	1.33	drag coefficient
gear ratio	16.25	
communications delay	10 ms	
WHF_{front}	0.9330	front downforce coefficient
WHF_{rear}	2.1770	rear downforce coefficient

Table 4.3: Simulated vehicle parameters.

The estimated parameters for the LuGre tire are described in table 4.4.

	Tire parameters		Description
	k_{stiff}	96.865 kN/m	vertical tire stiffness
	σ_{0x}	911.2273 m^{-1}	bristle stiffness
	σ_{0y}	429.4989 m^{-1}	
	$\sigma_{1x,1y,2x,2y}$	0 s/m	stiction and viscous damping coefficients
Dry	μ_s	2.6564	static friction coefficient
	μ_{kx}	0.1500	kinetic friction coefficient
	μ_{ky}	0.1201	
	v_s	10 m/s	stribeck velocity
	γ	4.9299	shape coeficient
Wet	μ_s	0.8855	static friction coefficient
	μ_{kx}	0.050	kinetic friction coefficient
	μ_{ky}	0.040	
	v_s	3.3333 m/s	stribeck velocity
	γ	1.6433	shape coeficient

Table 4.4: Tire parameters used in the simulations. The dry parameters were the estimated parameters from the FSAE TTC dataset.

4.4 Verification and Validation

The verification and validation of the model was done through the state estimations from the EKF on a run with the FST09e. The car had two engines on a rear wheel configuration, and only those angular velocities were available, since those measurements are tied to the engines. Figure 4.6 shows the result of the integration of the velocity and yaw rate estimations. The line colour is such that green means that the instant center of rotation is on the line that passes through the rear axle, red that is bellow it, and blue that it is above. Ideally we want the sideslip angle at the rear axle β_r to be 0.

As it can be seen, even though we don't have data about all the wheels, only the driving ones, and in spite of parameter uncertainty - many of the parameters could not be validated, the estimation shows a

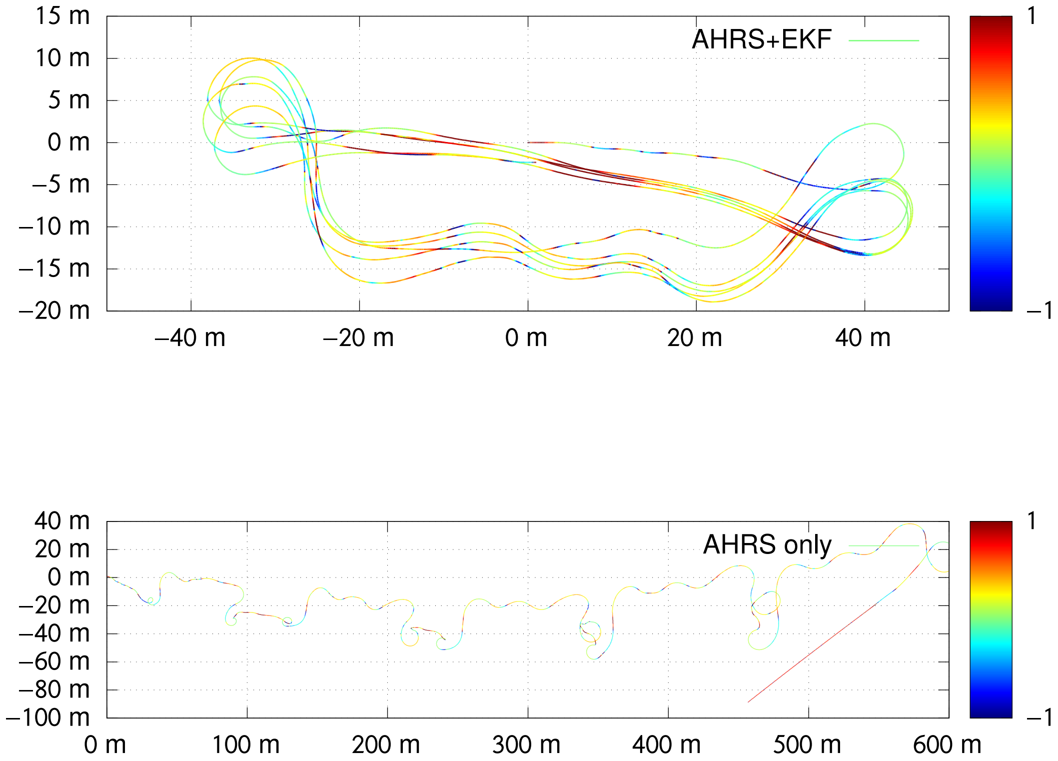

Figure 4.6: Trajectory estimation by integrating the velocity and yaw rate estimations from the EKF at 100Hz. The car starts at the origin and first moves along the positive x axis, to the right. The line color shows racio of the sideslip angle at the rear axle and at the cg $\frac{\beta_r}{\beta_c}$.

trajectory that has the shape of the test track and it "closes the circle" of more than 600m in a $\approx$ 3 min test run on a vehicle that at some points reached almost 2g of lateral force. While this is a qualitative measure, the comparison with the sensor data serves to show how much of an improvement the estimation made.

Figure 4.7 also shows the estimated velocities alongside the trace of the covariance matrix. The trace of the covariance matrix is used as a qualitative measure of the uncertainty and serves to see whether or not the uncertainty is bounded, thus proving that these results can be used to supply the controller with state estimations in a stable manner. Furthermore it also hints at the possibility of the system being locally observable. Figure 4.8 shows some quantities computed from the state estimation. It can be seen that during a turn, the estimation improves and that the slip ratio follows the expected braking/driving manouvers even though the mechanical braking was not taken into account in the observer estimations. As a side note, normal loads were assumed to be constant which can be the reason why the slip ratio of the left wheel remains so low. Another reason could be that the transmission of the left wheel offers more resistantance than the right one. The torque measurements were done applying a constant factor to the measured current at the engines, and are likely to be lower than reported due to current saturation and the engine wear.

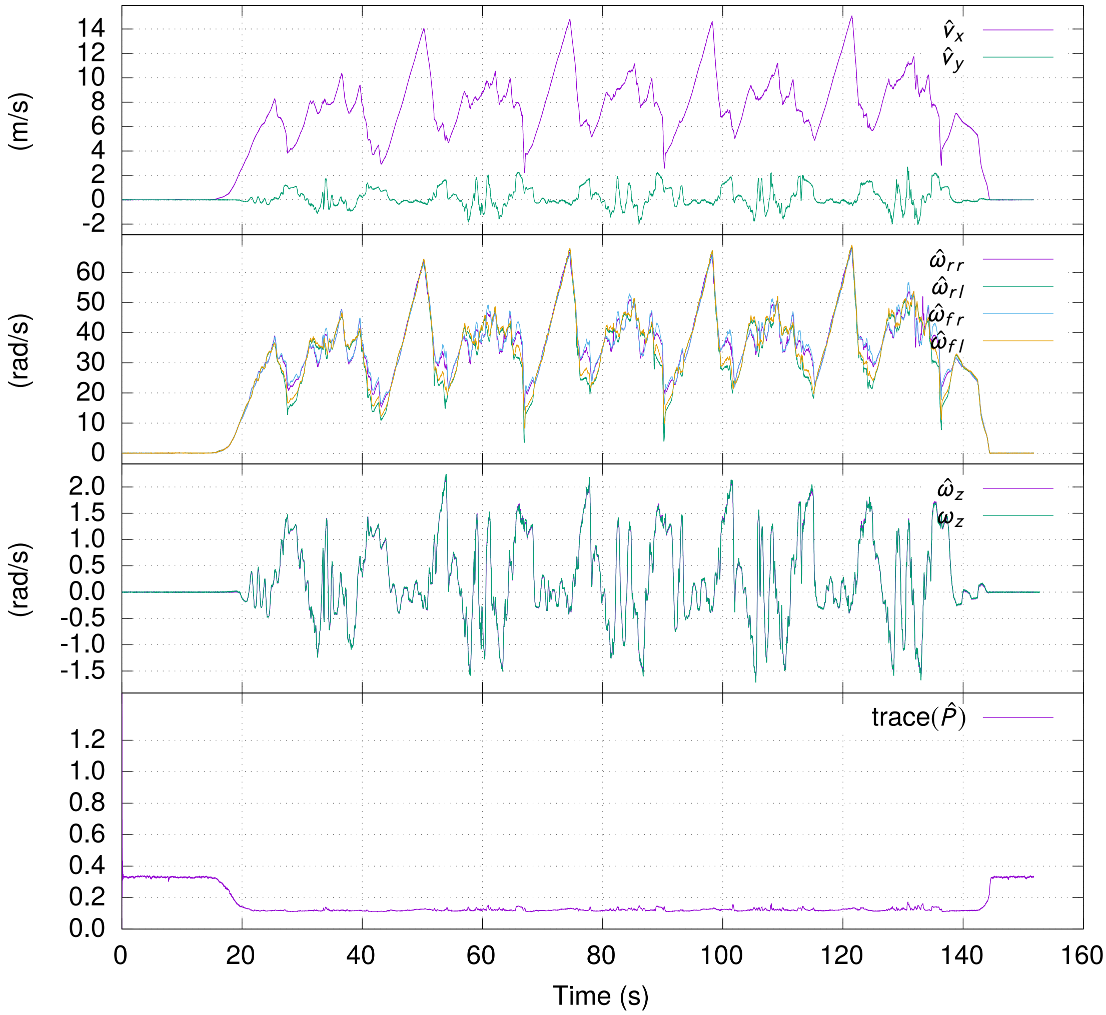

Figure 4.7: Estimations from the kalman filter applied to the dataset run. From top to bottom: linear velocities estimations; wheel angular velocities; yaw rate estimation $\hat{\omega}_z$ and sensor reading ω_z; trace of the covariance matrix $\hat{P}$ of the state estimation.

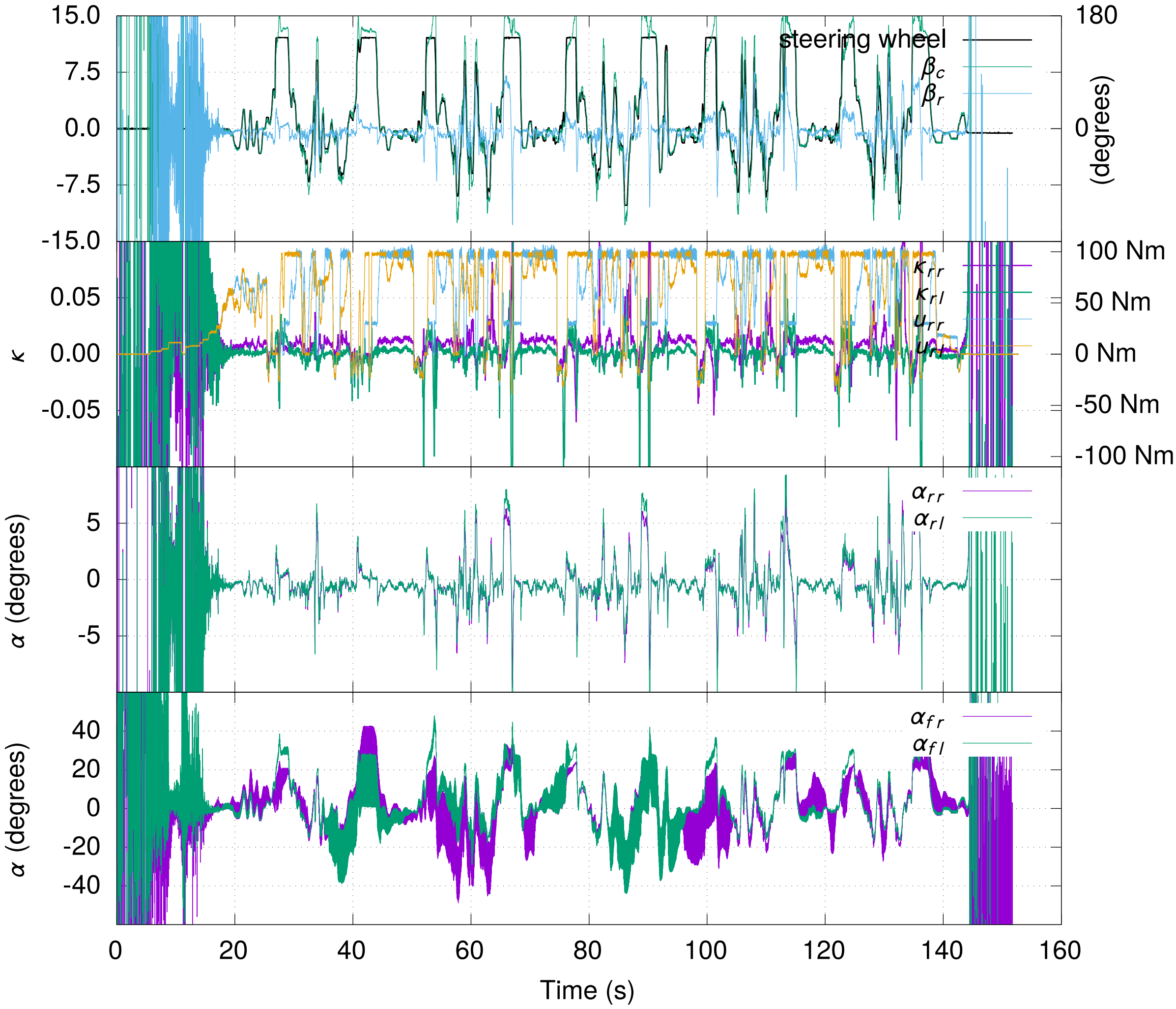

Figure 4.8: Slip ratios and slip angles, estimated from the attitude values and known vehicle dimensions. The front slip angles are estimated taking into account the wheel turning angle, which may be inaccurate. From the top to bottom: The steering wheel signal, with scale axis at the right, and the velocity angles at the rear axis β_r and at the center of mass β_c; the slip ratios of the driving wheels κ_{rr} κ_{rl}, with the corresponding applied torque to the wheel u_{rr} and u_{rl}, torque scale to the right; rear wheels slip angle α_{rr}, α_{rl}; front wheels slip angle α_{fr}, α_{fl}.

Chapter 5

Results

In order to better understand and measure the performance of the observer/controller pair, 3 simulation tests were done, with noise. The simulations were done on a personal computer, with a Intel i7-4700HQ processor.

The turning test, to evaluate the attitude of the vehicle, stability of the response, the g force limit and the settling time of the yaw rate as well the acceleration during the turn, should vehicle be short of the the g force limit.

The acceleration test, in order to measure the traction control, how fast the total available power was applied to the car and how straight the car went by measuring the side drift. Last, the braking test, also with similar objectives.

The annex, contains the plots for some of the simulations.

5.1 Simulations

5.1.1 Turning

The turning test consists on a short acceleration run followed by a steep wheel steer angle change, requesting a 17.5 m turning radius and continuing to accelerate. Table 5.1 shows how fast the car is set into the curve, by looking at the settling time of β_r, and the effect of such a sharp turn has on the attitude of the car, by looking at the peak β_r value. Further, timmings for the observer and controller are provided in order to validate the chosen sampling times for the controller and observer. The settling time for the wet four wheel simulation was not provided since β_r was not sufficiently impacted, which is a good result.

		Turning				
		1st arc radius	Max β_r	β_r Settling(15%)	$T_{95\%\ EKF}$	$T_{95\%\ MPC}$
Dry	FST09e 2w	17.49 m	0.93 deg	0.20 s	9.78 ms	89.74 ms
	FST09e 4w	17.71 m	0.82 deg	0.35 s	9.08 ms	81.73 ms
Wet	FST09e 2w	17.46 m	0.68 deg	0.19 s	9.88 ms	97.78 ms
	FST09e 4w	17.78 m	0.39 deg		$8.77 ms$	80.26 ms

Table 5.1: General data on the turning simulation test.

Table 5.2 surmizes the yaw rate values. Take into account that for the two wheel configuration, the car had to accelerate on the curve, thus a longer rise time is reported. The speed at the start and end of the turning maneuver is surmized in 5.3.

		Yaw rate ω_z				
		Settling Min	Settling Max	Rise (5%-95%)	Settling (2%)	Overshoot
Dry	FST09e 2w	0.9590 rad/s	1.0195 rad/s	1.7694 s	2.1943 s	1.0967%
	FST09e 4w	0.9544 rad/s	1.0223 rad/s	0.3961 s	0.5092 s	2.0063%
Wet	FST09e 2w	0.9596 rad/s	1.0204 rad/s	5.1181 s	6.6460 s	1.1446%
	FST09e 4w	0.9477 rad/s	1.0250 rad/s	0.3789 s	11.5633 s	3.1584%

Table 5.2: Yaw rate summary of the turning simulation test.

		Turning		
		Velocity before turn	Terminal velocity	Deviation before turning
Dry	FST09e 2w	13.1507 m/s	17.5368 m/s	0.0422 m
	FST09e 4w	17.8495 m/s	17.6853 m/s	0.0015 m
Wet	FST09e 2w	11.4939 m/s	17.5194 m/s	0.0348 m
	FST09e 4w	17.1954 m/s	17.9041 m/s	0.0000 m

Table 5.3: Velocity conditions for the turning simulation.

It can be seen that the car is properly set into the curve, quickly achieving the proper attack angle, seen through β_c, table 5.4, and in β_c. This was achieved by braking the inner rear wheel and then achieving and mantaining the maximum speed, defined from the requested arc and lateral g force limit. See annex B.2.1 for an example of this.

		Turning β_c				
		Settling Min	Settling Max	Rise (5%-95%)	Settling (2%)	Overshoot
Dry	FST09e 2w	2.5200 deg	2.6547 deg	0.2028 s	0.3308 s	0.0847%
	FST09e 4w	2.5209 deg	2.6646 deg	0.2697 s	0.3168 s	0.4436%
Wet	FST09e 2w	2.5537 deg	2.6903 deg	0.2488 s	0.2733 s	1.4506%
	FST09e 4w	2.5212 deg	2.6675 deg	0.4026 s	0.4512 s	0.6118%

Table 5.4: Sideslip angle β_c summary, from the turning simulation.

5.1.2 Acceleration

The goal of the accelaration test is to see how well the car goes straight and how fast the whole power is used. Table 5.5 surmises how fast the car reaches the 100m mark, 100kmh, the drift, max speed and the computacional timings.

		Acceleration					
		100m	100 kmh	Drift (100m)	Max Speed	$T_{95\%\ EKF}$	$T_{95\%\ MPC}$
Dry	FST09e 2w	9.67 s	11.64 s	−0.2060 m	43.4826 m/s	10.93 ms	86.78 ms
	FST09e 4w	6.89 s	7.97 s	−0.1329 m	45.5187 m/s	9.69 ms	67.57 ms
Wet	FST09e 2w	10.25 s	13.02 s	−0.1745 m	43.3595 m/s	9.71 ms	66.74 ms
	FST09e 4w	7.06 s	8.16 s	−0.1550 m	45.4958 m/s	9.06 ms	63.96 ms

Table 5.5: General data on the acceleration simulation test.

Table 5.6 shows the results from a power point of view. Keep in mind that the two rear wheel configuration can only use 70kW worth of power, since there are only two engines.

		Power				
		SettlingMin	SettlingMax	Rise(5%-98%)	SettlingTime(2%)	Overshoot
Dry	FST09e 2w	59264.8491 W	70721.5090 W	7.6685 s		1.3694%
	FST09e 4w	76667.3081 W	79874.0087 W	2.8217 s	4.5142 s	0.2194%
Wet	FST09e 2w	50547.0315 W	70653.5099 W	8.4064 s		0.8121%
	FST09e 4w	76567.2365 W	79948.2199 W	2.8648 s	4.2117 s	0.7763%

Table 5.6: Power summary on the acceleration simulation test.

In general the four wheel configuration can more easily place the full power on the ground, since it does not need as high slip ratios to achieve this, and the performance difference between the wet and dry scenarios is negletable. The settling times for the two wheel configuration where not estimated but the plots are available in the annex. See annex B.2.2 for more details.

5.1.3 Braking

The braking in the simulation test does not take into account the mechanical braking, and was done only to evaluate drift, and the power constraints. It can be seen in table 5.7 that they were achieved.

		Braking					
		Time	Distance	Drift	Max Power	$T_{95\%\ EKF}$	$T_{95\%\ MPC}$
Dry	FST09e 2w	4.2945 s	30.5424 m	0.0103 m	30794.9704 W	7.95 ms	86.15 ms
	FST09e 4w	3.8360 s	31.1629 m	0.0058 m	32900.1087 W	10.14 ms	89.63 ms
Wet	FST09e 2w	5.8024 s	39.9180 m	0.0586 m	30535.7724 W	9.69 ms	104.19 ms
	FST09e 4w	3.8559 s	31.7787 m	0.0309 m	32563.9473 W	9.88 ms	78.95 ms

Table 5.7: General data on the braking simulation test.

Chapter 6

Conclusions

To conclude this work, there are several points that we would like to make.

6.1 Achievements

Looking at the work developed, the results, and taking into account what we set up to do, we can say that we met all the proposed objectives. The only thing we could not verify was the performance of the controller in the car, although the observer alone is sufficient to justify this and further work. Should the attitude estimations be correct, in spite of the parameter uncertainties, then we managed to do with a common sensor and some current measurements, what dedicated and expensive sensors do, and we could implement this observer into virtually any electric car.

We managed to develop a vehicle model, an observer, a robust controller, agnostic to the number of driving wheels, capable of enforcing power constraints, attitude constraints, achieving desired yaw rates and slip ratios, tunable and customizable for other needs and objectives while being computacionaly viable.

6.2 Future Work

After the conclusion of this work, we believe that an online parameter estimation for the tire/road interaction and some car parameters should be developed and the state estimation problem should be incorporated into the model predictive controller since the observation and control problems are not completely separable. The solver should also be independently implemented and natively support the switching of hard constraints into soft constraints. In line with this, more work on the observability and detectability of the system should be done.

Another point that could be better explored is how the pedal interacts with the controller. Currently the pedal is assumed to control the total available power, but also having it as a factor in the velocity weight of the MPC might be a better approach, or even in the slip ratio limit.

An electric engine state space model, if linear, could also be incorporated into the controller, changing the problem from a torque input into an engine current input. Should the resulting model also be observable, this could be a factor for the engine temperature and wear estimation. The engine wear leveling could then be achieved with input weights in the controller. This could also be the foundation for cooling strategies, even wear and temperature control by placing weights/limits on the actuation, based on these measures.

Lastly, the suspension model should be incorporated in order to have better normal load estimations and, consequently tire slip estimations. And maybe in the future, we could also develop active suspension models that could further improve handling and weight distribution.

Even the tire model could be improved by taking into account the non-linearities that were not fully explored in this work, such as conicity and temperature to name a few.

But all of this can only be accomplished with proper state estimation and known vehicle dynamics. We hope that more work can be done as a result of this thesis and problem formulation.

6.3 Closing Remarks

I would like to conclude this work by thanking everyone involved in the Formula Student Lisboa team, past and current members. The competition provides an opportunity to improve teamwork, soft skills, hard skills, and a number of problems that span several disciplines in what is often a major undertaking each year. A better place where we can fail, learn from it, and explore our limits would be hard to get. More acknowledgement and support from this institution would go a long way in what is first and foremost a student initiative with far reaching potential in our future as engineers, individuals, and ultimately in the image of this learning institution.

Bibliography

[1] Hasan Alipour, Mehran Sabahi, and Mohammad Bagher Bannae Sharifian. "Lateral stabilization of a four wheel independent drive electric vehicle on slippery roads". In: *Mechatronics* 30 (2015), pp. 275–285. ISSN: 09574158. DOI: 10.1016/j.mechatronics.2014.08.006. URL: http://dx.doi.org/10.1016/j.mechatronics.2014.08.006.

[2] Pierre Apkarian, Pascal Gahinet, and Greg Becker. "Self-scheduled H∞ control of linear parameter-varying systems: a design example". In: *Automatica* 31.9 (1995), pp. 1251–1261. ISSN: 00051098. DOI: 10.1016/0005-1098(95)00038-X.

[3] G Arun. "Fractional PID and Sliding-Mode-Controller for Active Vehicle Suspension System". In: (2015), pp. 1428–1434.

[4] Jakob Bechtoff, Lars Koenig, and Rolf Isermann. "Cornering Stiffness and Sideslip Angle Estimation for Integrated Vehicle Dynamics Control". In: *IFAC-PapersOnLine* 49.11 (2016), pp. 297–304. ISSN: 24058963. DOI: 10.1016/j.ifacol.2016.08.045. URL: http://dx.doi.org/10.1016/j.ifacol.2016.08.045.

[5] Thomas Besselmann, Johan Löfberg, and Manfred Morari. "Explicit MPC for LPV systems: Stability and optimality". In: *IEEE Transactions on Automatic Control* 57.9 (2012), pp. 2322–2332. ISSN: 00189286. DOI: 10.1109/TAC.2012.2187400.

[6] Stephen Boyd et al. "Distributed optimization and statistical learning via the alternating direction method of multipliers". In: *Foundations and Trends in Machine Learning* 3.1 (2010), pp. 1–122. ISSN: 19358237. DOI: 10.1561/2200000016.

[7] C. Canudas de Wit et al. "A new model for control of systems with friction". In: *IEEE Transactions on Automatic Control* 40.3 (Mar. 1995), pp. 419–425. ISSN: 00189286. DOI: 10.1109/9.376053. URL: http://ieeexplore.ieee.org/document/376053/.

[8] Yu Cao et al. "Straight Running Stability Control Based on Optimal Torque Distribution for a Four in-wheel Motor Drive Electric Vehicle". In: *Energy Procedia* 105 (2017), pp. 2825–2830. ISSN: 18766102. DOI: 10.1016/j.egypro.2017.03.616.

[9] Christoforos Chatzikomis et al. "Comparison of Path Tracking and Torque-Vectoring Controllers for Autonomous Electric Vehicles". In: *IEEE Transactions on Intelligent Vehicles* 3.4 (2018), pp. 559–570. ISSN: 2379-8858. DOI: 10.1109/tiv.2018.2874529.

[10] David A. Crolla and Dongpu Cao. “The impact of hybrid and electric powertrains on vehicle dynamics, control systems and energy regeneration”. In: *Vehicle System Dynamics* 50.sup1 (Jan. 2012), pp. 95–109. ISSN: 0042-3114. DOI: 10.1080/00423114.2012.676651. URL: http://www.tandfonline.com/doi/abs/10.1080/00423114.2012.676651.

[11] Joško Deur. “Modeling and Analysis of Longitudinal Tire Dynamics Based on the Lugre Friction Model”. In: *IFAC Proceedings Volumes* 34.1 (2001), pp. 91–96. ISSN: 14746670. DOI: 10.1016/s1474-6670(17)34383-5.

[12] Josko Deur, Jahan Asgari, and Davor Hrovat. “A 3D brush-type dynamic tire friction model”. In: *Vehicle System Dynamics* 42.3 (2004), pp. 133–173. ISSN: 00423114. DOI: 10.1080/00423110412331282887.

[13] Joško Deur et al. “Extensions of the LuGre tyre friction model related to variable slip speed along the contact patch length”. In: *Vehicle System Dynamics* 43.SUPPL. (Jan. 2005), pp. 508–524. ISSN: 00423114. DOI: 10.1080/00423110500229808. URL: http://www.tandfonline.com/doi/abs/10.1080/00423110500229808.

[14] S.V. Drakunov. “Sliding-mode observers based on equivalent control method”. In: 9 (2005), pp. 2368–2369. DOI: 10.1109/cdc.1992.371368.

[15] K. El Majdoub et al. “Vehicle longitudinal motion modeling for nonlinear control”. In: *Control Engineering Practice* 20.1 (2012), pp. 69–81. ISSN: 09670661. DOI: 10.1016/j.conengprac.2011.09.005.

[16] Gurkan Erdogan. “Why Tires are important for Vehicle Control Systems ?” In: (2009), pp. 2–28.

[17] Marcello Farina, Giancarlo Ferrari-Trecate, and Riccardo Scattolini. “Distributed Moving Horizon Estimation for Linear Constrained Systems”. In: *IEEE Transactions on Automatic Control* 55.11 (Nov. 2010), pp. 2462–2475. ISSN: 0018-9286. DOI: 10.1109/TAC.2010.2046058. URL: http://doi.wiley.com/10.1002/rnc.1676%20http://ieeexplore.ieee.org/document/5437313/.

[18] Yuan Feng et al. “Torque Vectoring Control for Distributed Drive Electric Vehicle Based on State Variable Feedback”. In: *SAE International Journal of Passenger Cars - Electronic and Electrical Systems* 7.2 (2014), pp. 328–336. ISSN: 19464622. DOI: 10.4271/2014-01-0155.

[19] Michel Fliess, Cédric Join, and Hebertt Sira-Ramírez. “Non-linear estimation is easy”. In: *International Journal of Modelling, Identification and Control* 4.1 (2008), pp. 12–27. ISSN: 17466180. DOI: 10.1504/IJMIC.2008.020996. arXiv: 0710.4486.

[20] Reiner Folke et al. “Torque vectoring a new level of freedom for electric vehicles”. In: *ATZ worldwide* 112.6 (2010), pp. 8–12. DOI: 10.1007/bf03225125.

[21] Jyotishman Ghosh, Andrea Tonoli, and Nicola Amati. “A Torque Vectoring Strategy for Improving the Performance of a Rear Wheel Drive Electric Vehicle”. In: *2015 IEEE Vehicle Power and Propulsion Conference, VPPC 2015 - Proceedings* (2015). DOI: 10.1109/VPPC.2015.7352887.

[22] Supratim Ghosh and Justin Ruths. “On structural controllability of a class of bilinear systems”. In: *Proceedings of the IEEE Conference on Decision and Control* 2015-Febru.February (2014), pp. 3137–3142. ISSN: 07431546. DOI: 10.1109/CDC.2014.7039873.

[23] Alf J. Isaksson et al. “Using horizon estimation and nonlinear optimization for grey-box identification”. In: *Journal of Process Control* 30 (2015), pp. 69–79. ISSN: 09591524. DOI: 10.1016/j.jprocont.2014.12.008. URL: http://dx.doi.org/10.1016/j.jprocont.2014.12.008.

[24] Valentin Ivanov et al. “Electric vehicles with individually controlled on-board motors: Revisiting the ABS design”. In: *Proceedings - 2015 IEEE International Conference on Mechatronics, ICM 2015*. 2015, pp. 323–328. ISBN: 9781479936335. DOI: 10.1109/ICMECH.2015.7083996.

[25] Reza N Jazar. *Vehicle Dynamics*. Cham: Springer International Publishing, 2017. ISBN: 978-3-319-53440-4. DOI: 10.1007/978-3-319-53441-1. URL: http://link.springer.com/10.1007/978-3-319-53441-1.

[26] Chi Jin et al. “Vehicle Side Slip Angle Observation with Road Friction Adaptation”. In: *IFAC-PapersOnLine* 50.1 (2017), pp. 3406–3411. ISSN: 24058963. DOI: 10.1016/j.ifacol.2017.08.593. URL: https://doi.org/10.1016/j.ifacol.2017.08.593.

[27] Angelos Kampanakis et al. “A Torque Vectoring Optimal Control Strategy for Combined Vehicle Dynamics Performance Enhancement and Electric Motor Ageing Minimisation”. In: *IFAC-PapersOnLine* 49.11 (2016), pp. 412–417. ISSN: 24058963. DOI: 10.1016/j.ifacol.2016.08.061. URL: http://dx.doi.org/10.1016/j.ifacol.2016.08.061.

[28] Juyong Kang, Jinho Yoo, and Kyongsu Yi. “Driving Control Algorithm for Maneuverability, Lateral Stability, and Rollover Prevention of 4WD Electric Vehicles With Independently Driven Front and Rear Wheels”. In: *IEEE Transactions on Vehicular Technology* 60.7 (Sept. 2011), pp. 2987–3001. ISSN: 0018-9545. DOI: 10.1109/TVT.2011.2155105. URL: http://ieeexplore.ieee.org/document/5770244/.

[29] Dhanaraja Kasinathan et al. “An Optimal Torque Vectoring Control for Vehicle Applications via Real-Time Constraints”. In: *IEEE Transactions on Vehicular Technology* 65.6 (2016), pp. 4368–4378. ISSN: 00189545. DOI: 10.1109/TVT.2015.2467374.

[30] S. Kaspar et al. “Robust torque vectoring control”. In: *IFAC Proceedings Volumes (IFAC-PapersOnline)* 19 (2014), pp. 12023–12028. ISSN: 14746670. DOI: 10.3182/20140824-6-za-1003.02359.

[31] Edward M. Kasprzak and David Gentz. “The formula sae tire test consortium-tire testing and data handling”. In: *SAE Technical Papers* (2006). ISSN: 26883627. DOI: 10.4271/2006-01-3606.

[32] Nikolaos Kazantzis and Costas Kravaris. “Nonlinear observer design using Lyapunov’s auxiliary theorem”. In: *Proceedings of the IEEE Conference on Decision and Control* 5.June 1997 (1997), pp. 4802–4807. ISSN: 01912216. DOI: 10.1016/S0167-6911(98)00017-6.

[33] Matthias Korte et al. “Design of a robust adaptive vehicle observer towards delayed and missing Vehicle Dynamics sensor signals by usage of Markov Chains”. In: *Proceedings of the American Control Conference* June (2013), pp. 6798–6803. ISSN: 07431619. DOI: 10.1109/acc.2013.6580907.

[34] Arthur J. Krener and Alberto Isidori. “Linearization by output injection and nonlinear observers”. In: *Systems and Control Letters* 3.1 (1983), pp. 47–52. ISSN: 01676911. DOI: 10.1016/0167-6911(83)90037-3.

[35] Seung Hi Lee et al. *Slip angle estimation: Development and experimental evaluation*. Vol. 8. PART 1. IFAC, 2013, pp. 286–291. ISBN: 9783902823366. DOI: 10.3182/20130626-3-AU-2035.00071. URL: http://dx.doi.org/10.3182/20130626-3-AU-2035.00071.

[36] Jingliang Li, Yizhai Zhang, and Jingang Yi. "A hybrid physical-dynamic tire/road friction model". In: *Journal of Dynamic Systems, Measurement and Control, Transactions of the ASME* 135.1 (2013). ISSN: 00220434. DOI: 10.1115/1.4006887.

[37] Qian Lu et al. "H∞ loop shaping for the torque-vectoring control of electric vehicles: Theoretical design and experimental assessment". In: *Mechatronics* 35 (2016), pp. 32–43. ISSN: 09574158. DOI: 10.1016/j.mechatronics.2015.12.005. URL: http://dx.doi.org/10.1016/j.mechatronics.2015.12.005.

[38] L. Menini and A. Tornamb?? "Feedback linearization of impulsive nonlinear control systems". In: *AIP Conference Proceedings* 1479.1 (2012), pp. 1447–1449. ISSN: 0094243X. DOI: 10.1063/1.4756433.

[39] Asal Nahidi et al. "Modular integrated longitudinal and lateral vehicle stability control for electric vehicles". In: *Mechatronics* 44 (2017), pp. 60–70. ISSN: 09574158. DOI: 10.1016/j.mechatronics.2017.04.001.

[40] Leonardo de Novellis et al. "Torque vectoring for electric vehicles with individually controlled motors: State-of-the-art and future developments". In: *World Electric Vehicle Journal* 5.2 (2012), pp. 617–628. ISSN: 20326653. DOI: 10.3390/wevj5020617.

[41] Hans B. Pacejka. *Tire and Vehicle Dynamics*. Elsevier, 2006. ISBN: 9780750669184. DOI: 10.1016/B978-0-7506-6918-4.X5000-X. URL: http://www.engineering108.com/Data/Engineering/Automobile/tyre-and-vehicle-dynamics.pdf%20https://linkinghub.elsevier.com/retrieve/pii/B9780750669184X5000X.

[42] Hans B. Pacejka and Egbert Bakker. "THE MAGIC FORMULA TYRE MODEL". In: *Vehicle System Dynamics* 21.sup001 (Jan. 1992), pp. 1–18. ISSN: 0042-3114. DOI: 10.1080/00423119208969994. URL: http://www.tandfonline.com/doi/abs/10.1080/00423119208969994.

[43] Alberto Parra et al. "Intelligent Torque Vectoring Approach for Electric Vehicles with Per-Wheel Motors". In: *Complexity* 2018 (2018). ISSN: 10990526. DOI: 10.1155/2018/7030184.

[44] Karmvir Singh Phogat, Debasish Chatterjee, and Ravi N. Banavar. "A discrete-time Pontryagin maximum principle on matrix Lie groups". In: *Automatica* 97 (2018), pp. 376–391. ISSN: 00051098. DOI: 10.1016/j.automatica.2018.08.026. arXiv: 1612.08022. URL: https://doi.org/10.1016/j.automatica.2018.08.026.

[45] Bingtao Ren et al. "MPC-based yaw stability control in in-wheel-motored EV via active front steering and motor torque distribution". In: *Mechatronics* 38 (2016), pp. 103–114. ISSN: 09574158. DOI: 10.1016/j.mechatronics.2015.10.002. URL: http://dx.doi.org/10.1016/j.mechatronics.2015.10.002.

[46] I. Michael Ross et al. "Riemann-Stieltjes optimal control problems for uncertain dynamic systems". In: *Journal of Guidance, Control, and Dynamics* 38.7 (2015), pp. 1251–1263. ISSN: 07315090. DOI: 10.2514/1.G000505.

[47] Volker Scheuch et al. "A safe Torque Vectoring function for an electric vehicle". In: *World Electric Vehicle Journal* 6.3 (2013), pp. 731–740. ISSN: 20326653. DOI: 10.1109/EVS.2013.6915027.

[48] C. Schmid and L.T. Biegler. "Quadratic programming methods for reduced hessian SQP". In: *Computers & Chemical Engineering* 18.9 (Sept. 1994), pp. 817–832. ISSN: 00981354. DOI: 10.1016/0098-1354(94)E0001-4. URL: https://linkinghub.elsevier.com/retrieve/pii/0098135494E00014.

[49] Zhibin Shuai et al. "Lateral motion control for four-wheel-independent-drive electric vehicles using optimal torque allocation and dynamic message priority scheduling". In: *Control Engineering Practice* 24.1 (2014), pp. 55–66. ISSN: 09670661. DOI: 10.1016/j.conengprac.2013.11.012. URL: http://dx.doi.org/10.1016/j.conengprac.2013.11.012.

[50] Efstathios Siampis, Efstathios Velenis, and Stefano Longo. "Torque Vectoring Model Predictive Control with Velocity Regulation Near the Limits of Handling". In: *Vehicle System Dynamics* (2015), pp. 2553–2558. ISSN: 17445159. DOI: 10.1080/00423114.2015.1064972. URL: http://www.tandfonline.com/doi/pdf/10.1080/00423114.2015.1064972.

[51] J Slotine and W Li. *Applied Nonlinear Control*. 1990. ISBN: 0130408905.

[52] Jacob Svendenius and Magnus Gäfvert. "A semi-empirical dynamic tire model for combined-slip forces". In: *Vehicle System Dynamics* 44.2 (2006), pp. 189–208. ISSN: 00423114. DOI: 10.1080/00423110500385659.

[53] Discrete-time Control Systems. "Discretization of Continuous-Time Systems". In: *Journal of The Society of Instrument and Control Engineers* 32.2 (1993), pp. 120–127. ISSN: 1883-8170. DOI: 10.11499/sicejl1962.32.120.

[54] Zhiqiang Tang. "Modeling and Estimation of Dynamic Tire Properties". In: *Electrical Engineering* 54.1 (2010), pp. 13–34. URL: http://www.vehicular.isy.liu.se/Publications/MSc/09%7B%5C_%7DEX%7B%5C_%7D4227%7B%5C_%7DJL.pdf.

[55] B. Tibken and E. P. Hofer. "Systematic observer design for bilinear systems". In: *Proceedings - IEEE International Symposium on Circuits and Systems* 3.9 (1989), pp. 1611–1616. ISSN: 02714310. DOI: 10.1109/iscas.1989.100671.

[56] Panagiotis Tsiotras, Efstathios Velenis, and Michel Sorine. "A LuGre tire friction model with exact aggregate dynamics". In: *Proceedings of the American Control Conference* 2 (2004), pp. 1457–1462. ISSN: 07431619. DOI: 10.1109/ACC.2004.182988.

[57] J. Velazquez Alcantar and F. Assadian. "Vehicle dynamics control of an electric-all-wheel-drive hybrid electric vehicle using tyre force optimisation and allocation". In: *Vehicle System Dynamics* 57.12 (Dec. 2019), pp. 1897–1923. ISSN: 0042-3114. DOI: 10.1080/00423114.2019.1585556. URL: https://www.tandfonline.com/doi/full/10.1080/00423114.2019.1585556.

[58] E. Velenis et al. “Dynamic tyre friction models for combined longitudinal and lateral vehicle motion”. In: *Vehicle System Dynamics* 43.1 (Jan. 2005), pp. 3–29. ISSN: 0042-3114. DOI: 10.1080/00423110412331290464. URL: http://www.tandfonline.com/doi/abs/10.1080/00423110412331290464.

[59] X. D. Wu et al. “Parameter identification for a LuGre model based on steady-state tire conditions”. In: *International Journal of Automotive Technology* 12.5 (Oct. 2011), pp. 671–677. ISSN: 1229-9138. DOI: 10.1007/s12239-011-0078-9. URL: http://link.springer.com/10.1007/s12239-011-0078-9.

[60] M. Zeitz. “The extended Luenberger observer for nonlinear systems”. In: *Systems and Control Letters* 9.2 (1987), pp. 149–156. ISSN: 01676911. DOI: 10.1016/0167-6911(87)90021-1.

Part I

Appendix

Appendix A

Bilinear transform for State-Space Models

Taking a continuous linear state-space system as,

$$\dot{\mathbf{x}} = A\mathbf{x} + B\mathbf{u} \tag{A.1}$$

$$\mathbf{y} = C\mathbf{x} \tag{A.2}$$

a discretization of the system can be obtained as

$$A_d = e^{AT_s} \tag{A.3}$$

$$B_d = (e^{AT_s} - I)BA^{-1} \tag{A.4}$$

and keeping C from the continuous system. However, this requires A to be invertible. In this work the A matrix is not full rank and we used the bilinear transform instead.

The billinear transform (also known as Tustin transform) with frequency ω_0 match (sometimes called frequency pre-wrap) and sampling time T_s, corresponding to $\omega_s = 2\pi/T_s$ was used. We can adjust the response by specifying a frequency to match against, and the observability properties of the pair (A, C) are kept in (A_d, C_d).

Taking the Laplace transform, assuming (A, C) constant and disregarding the initial conditions,

$$\mathcal{L}\begin{cases} \dot{\mathbf{x}} = & A\mathbf{x} + B\mathbf{u} \\ \mathbf{y} = & C\mathbf{x} \end{cases} \rightarrow \begin{cases} s\mathbf{X}(s) = & A\mathbf{X}(s) + B\mathbf{U}(s) \\ \mathbf{Y}(s) = & C\mathbf{X}(s) \end{cases} \tag{A.5}$$

$$\Rightarrow \begin{cases} \mathbf{X}(s) = & (s\mathbf{I} - A)^{-1}B\mathbf{U}(s) \\ \mathbf{Y}(s) = & C(s\mathbf{I} - A)^{-1}B\mathbf{U}(s), \end{cases} \tag{A.6}$$

we define $\mathbf{G}(s)$ as the transfer function,

$$\mathbf{G}(s)\mathbf{U}(s) = \mathbf{Y}(s) \tag{A.7}$$

$$\mathbf{G}(s) = C(s\mathbf{I} - A)^{-1}B. \tag{A.8}$$

The bilinear transform is an aproximate map from s to $z = e^{sT_s}$. We apply the bilinear transform and define the frequency match to ω_0 with the gain K,

$$s \approx K\frac{z-1}{z+1} \text{ with, } K = \frac{\omega_0}{\tan(\omega_0 T_s/2)} \text{ and } \lim_{\omega_0 \to 0} K = \frac{2}{T_s}, \tag{A.9}$$

which results in,

$$\begin{aligned}
H(z) = G\left(K\frac{z-1}{z+1}\right) &= D_d + C_d(z\mathbf{I} - A_d)^{-1}B_d && \text{(A.10)}\\
&= C\left(K\frac{z-1}{z+1}\mathbf{I} - A\right)^{-1} B && \text{(A.11)}\\
&= \frac{z+1}{K}C\left((z-1)\mathbf{I} - \frac{z+1}{K}A\right)^{-1} B && \text{(A.12)}\\
&= (z+1)C\left(z(K\mathbf{I} - A) - (K\mathbf{I} + A)\right)^{-1} B && \text{(A.13)}\\
&= (z+1)C\left(zP - Q\right)^{-1} B \text{ with, } P = K\mathbf{I} - A, Q = K\mathbf{I} + A && \text{(A.14)}\\
&= (z+1)C\left(z\mathbf{I} - P^{-1}Q\right)^{-1} P^{-1}B, \text{ with, } A_d = P^{-1}Q \text{ and } B_d = \sqrt{2K}P^{-1}B, && \text{(A.15)}
\end{aligned}$$

by considering that,

$$\begin{aligned}
(z+1)C &= C(z+1) && \text{(A.16)}\\
&= C(z\mathbf{I} + \mathbf{I} + A_d - A_d) && \text{(A.17)}\\
&= C((z\mathbf{I} - A_d) + (\mathbf{I} + A_d)) && \text{(A.18)}\\
&= C((z\mathbf{I} - A_d) + P^{-1}(P + Q)) && \text{(A.19)}\\
&= C((z\mathbf{I} - A_d) + 2KP^{-1}) && \text{(A.20)}
\end{aligned}$$

we can rewrite $H(z)$,

$$\begin{aligned}
H(z) &= \frac{z+1}{\sqrt{2K}}C\left(z\mathbf{I} - A_d\right)^{-1} B_d && \text{(A.21)}\\
&= \frac{1}{\sqrt{2K}}C((z\mathbf{I} - A_d) + 2KP^{-1})\left(z\mathbf{I} - A_d\right)^{-1} B_d && \text{(A.22)}\\
&= \frac{1}{\sqrt{2K}}C(\mathbf{I} + 2KP^{-1}\left(z\mathbf{I} - A_d\right)^{-1})B_d && \text{(A.23)}\\
&= \frac{1}{\sqrt{2K}}CB_d + \sqrt{2K}CP^{-1}\left(z\mathbf{I} - A_d\right)^{-1} B_d && \text{(A.24)}\\
&= CP^{-1}B + \sqrt{2K}CP^{-1}\left(z\mathbf{I} - A_d\right)^{-1} B_d && \text{(A.25)}\\
&= D_d + C_d(z\mathbf{I} - A_d)^{-1}B_d && \text{(A.26)}
\end{aligned}$$

and write the discretized system matrices as,

$$A_d = (K\mathbf{I} - A)^{-1}(K\mathbf{I} + A) \tag{A.27}$$

$$B_d = \sqrt{2K}(K\mathbf{I} - A)^{-1}B \tag{A.28}$$

$$C_d = \sqrt{2K}C(K\mathbf{I} - A)^{-1} \tag{A.29}$$

$$D_d = C(K\mathbf{I} - A)^{-1}B \tag{A.30}$$

Appendix B

Simulations

B.1 FST09e 4w

B.1.1 Turning

Turning Dry FST09e 4w

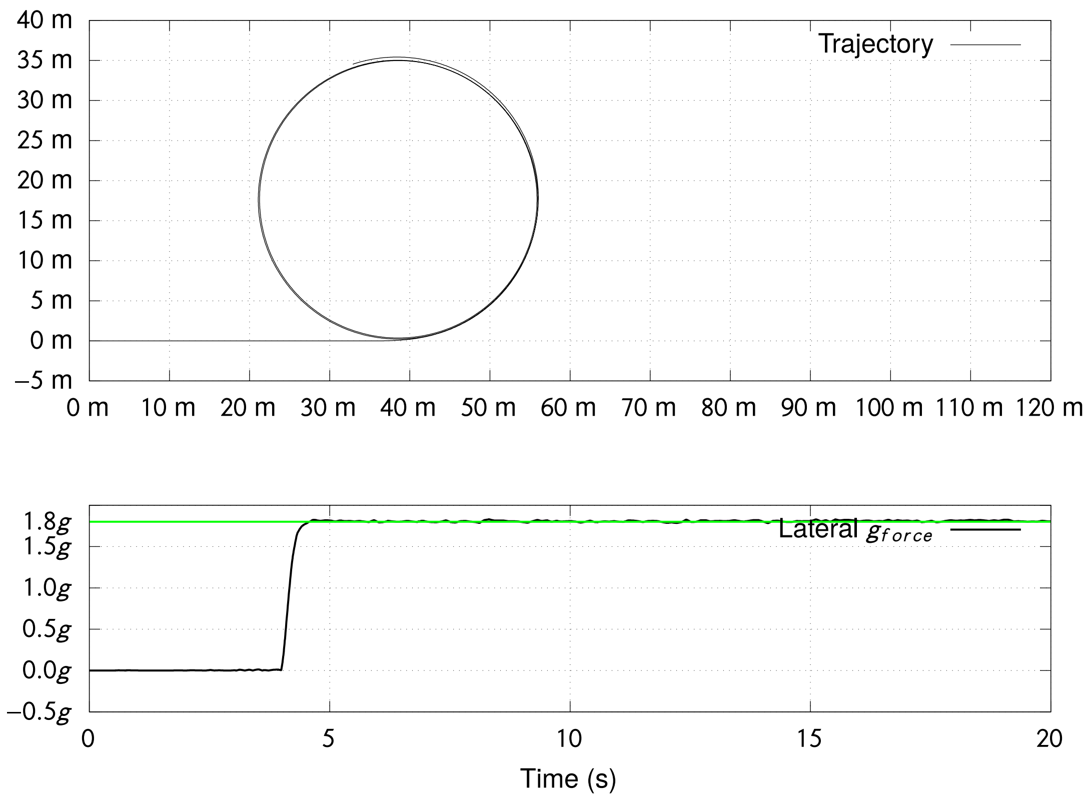

Figure B.1: Vehicle trajectory and lateral g force for a simulation of an acceleration followed by turning with expected radius of 35m, with four wheel traction configuration on dry terrain.

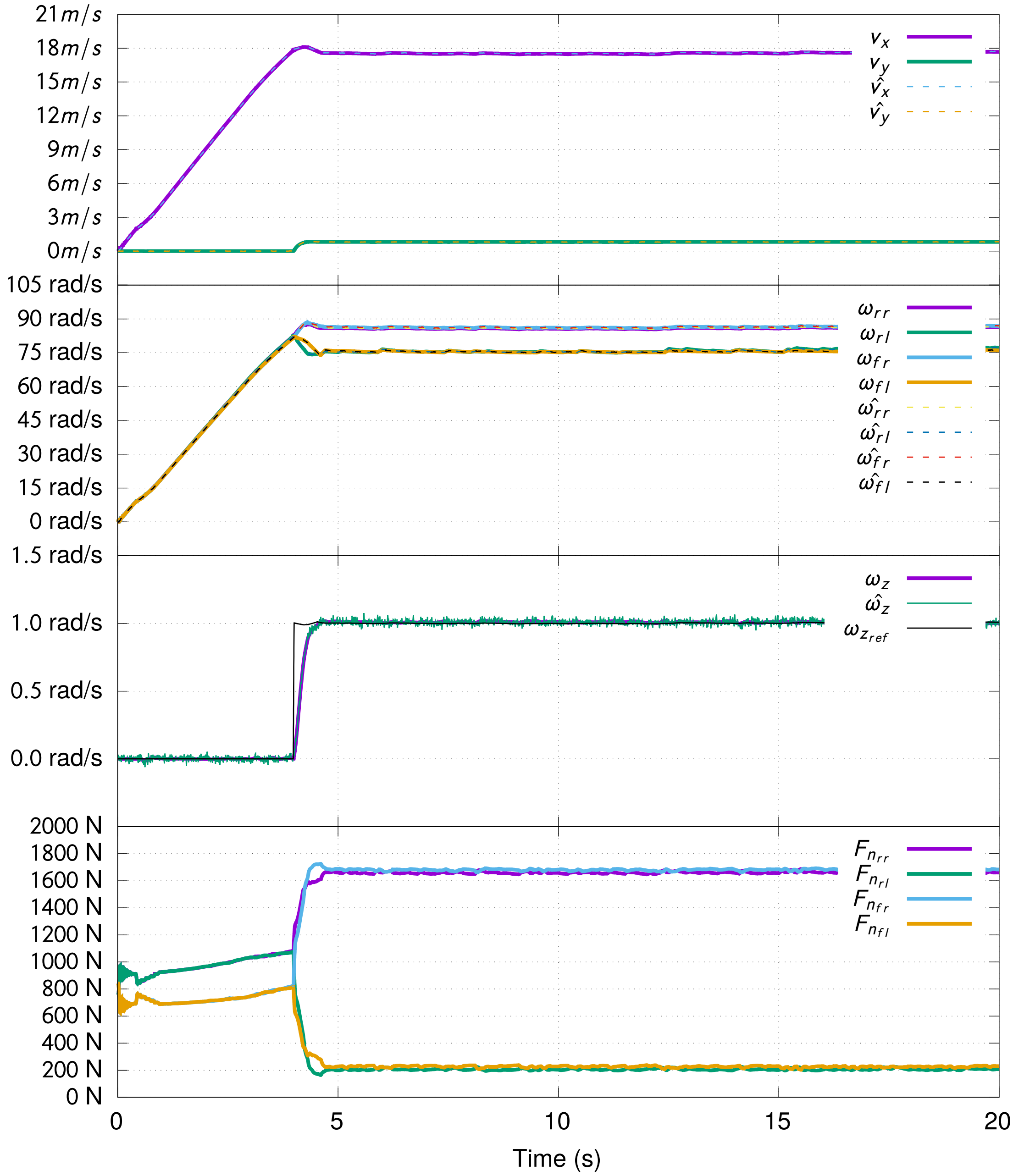

Figure B.2: Vehicle velocity, wheel angular velocity and yaw rate estimation, ground truth and reference yaw rate, for a simulation of an acceleration followed by turning with expected radius of 35m, with four wheel traction configuration on dry terrain.

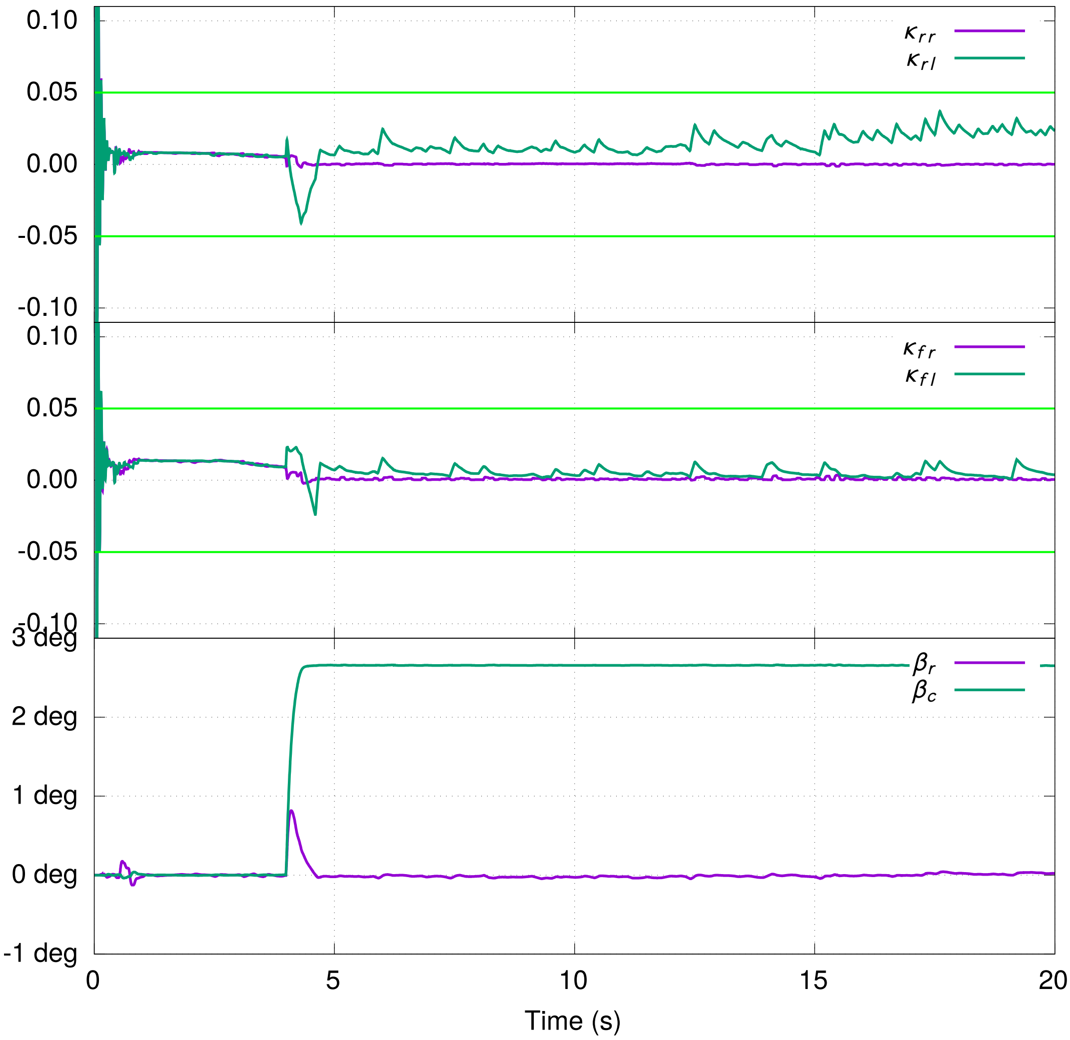

Figure B.3: Front, rear slip ratios and sideslip angles for a simulation of an acceleration followed by turning with expected radius of 35m, with four wheel traction configuration on dry terrain.

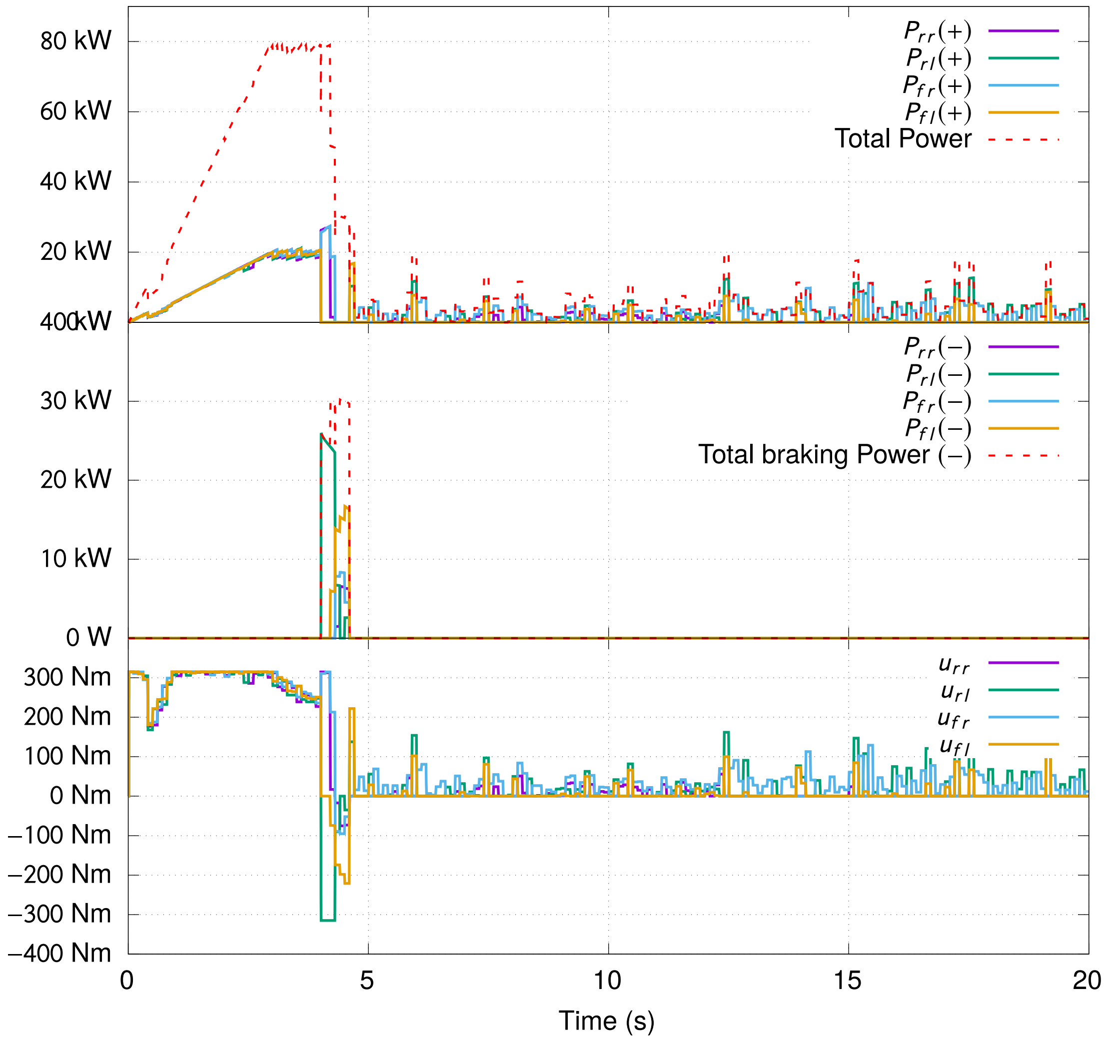

Figure B.4: Total and braking power, as well as the engine torque for a simulation of an acceleration followed by turning with expected radius of 35m, with four wheel traction configuration on dry terrain.

Turning Wet FST09e 4w

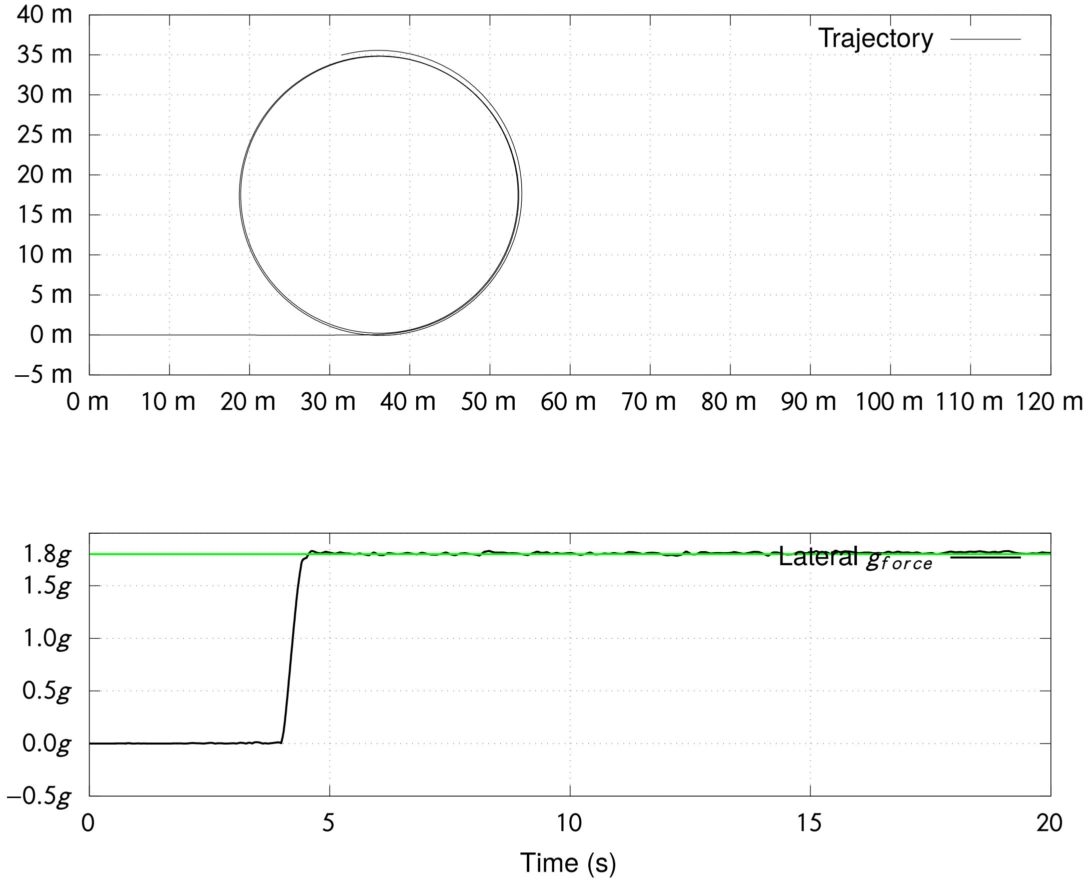

Figure B.5: Vehicle trajectory and lateral g force for a simulation of an acceleration followed by turning with expected radius of 35m, with four wheel traction configuration on wet terrain.

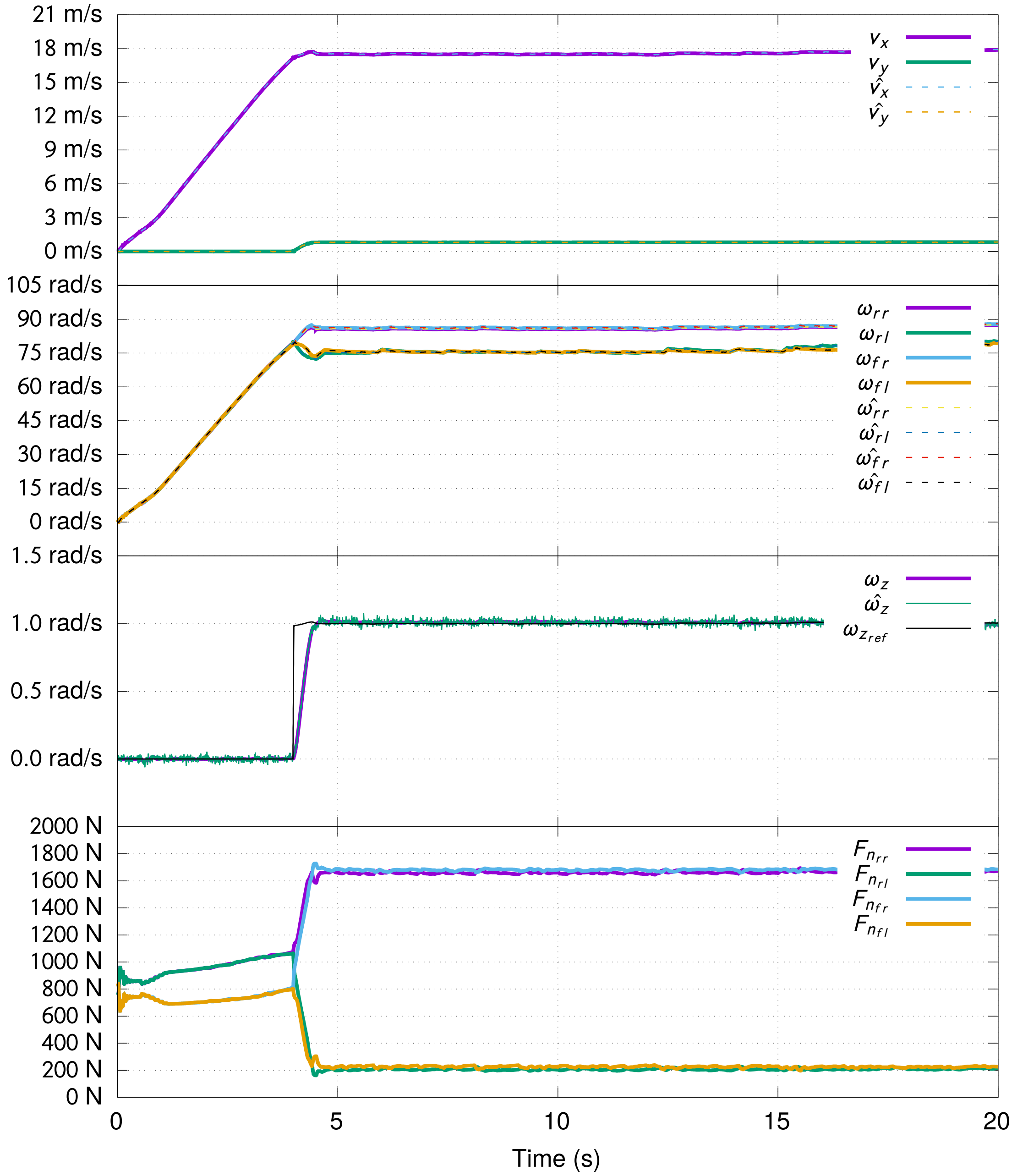

Figure B.6: Vehicle velocity, wheel angular velocity and yaw rate estimation, ground truth and reference yaw rate, for a simulation of an acceleration followed by turning with expected radius of 35m, with four wheel traction configuration on wet terrain.

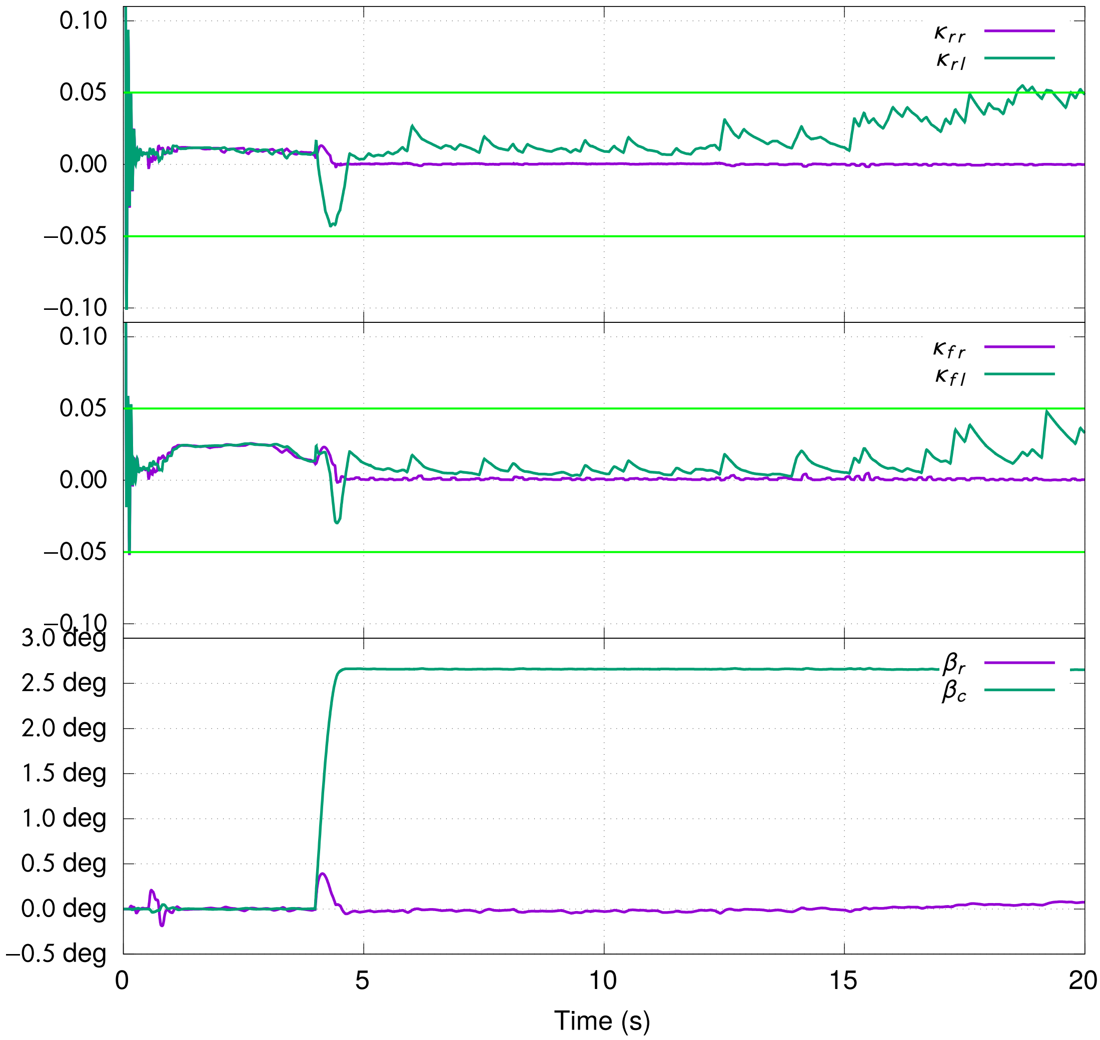

Figure B.7: Front, rear slip ratios and sideslip angles for a simulation of an acceleration followed by turning with expected radius of 35m, with four wheel traction configuration on wet terrain.

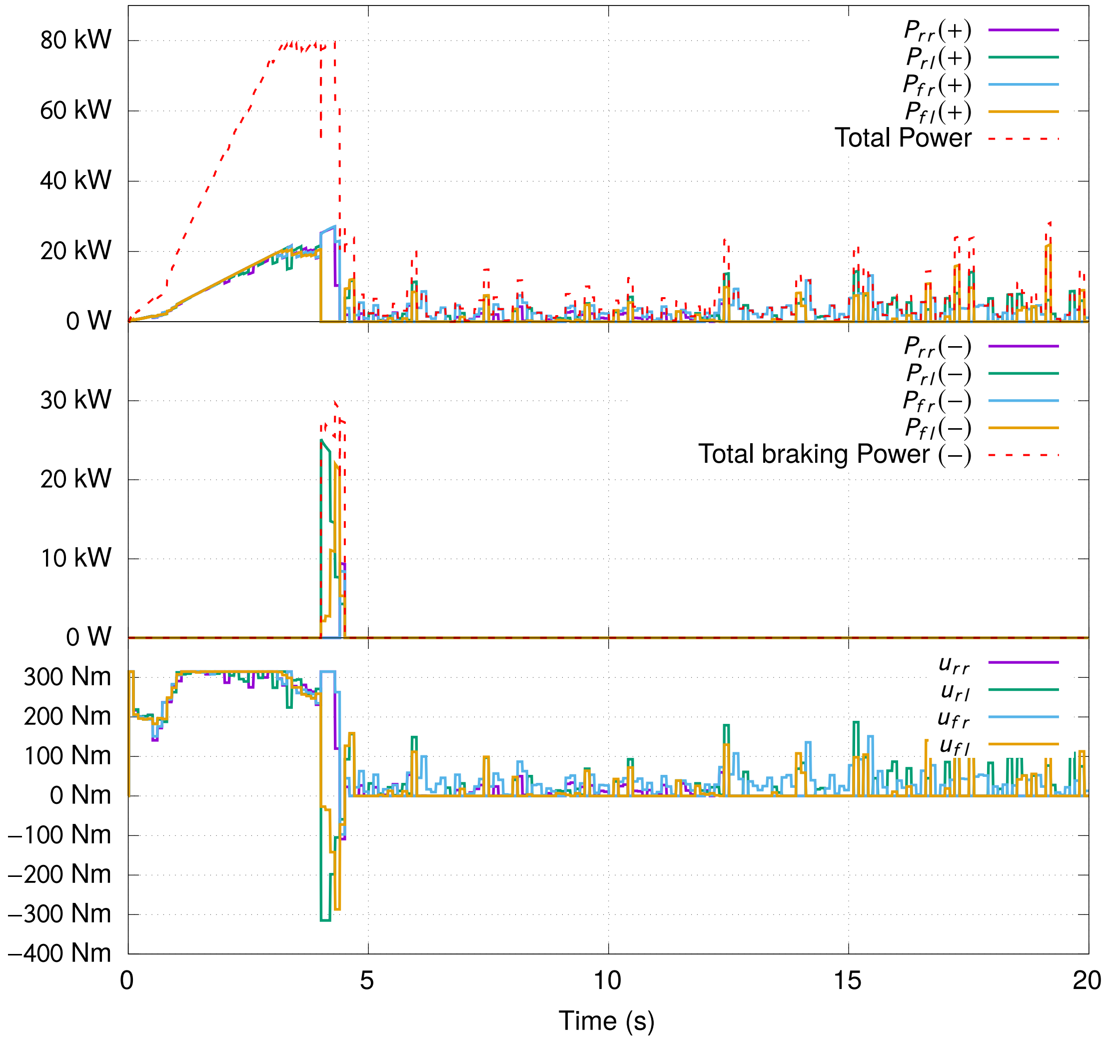

Figure B.8: Total and braking power, as well as the engine torque for a simulation of an acceleration followed by turning with expected radius of 35m, with four wheel traction configuration on wet terrain.

B.2 FST09e 2w

B.2.1 Turning

Turning Dry FST09e 2w

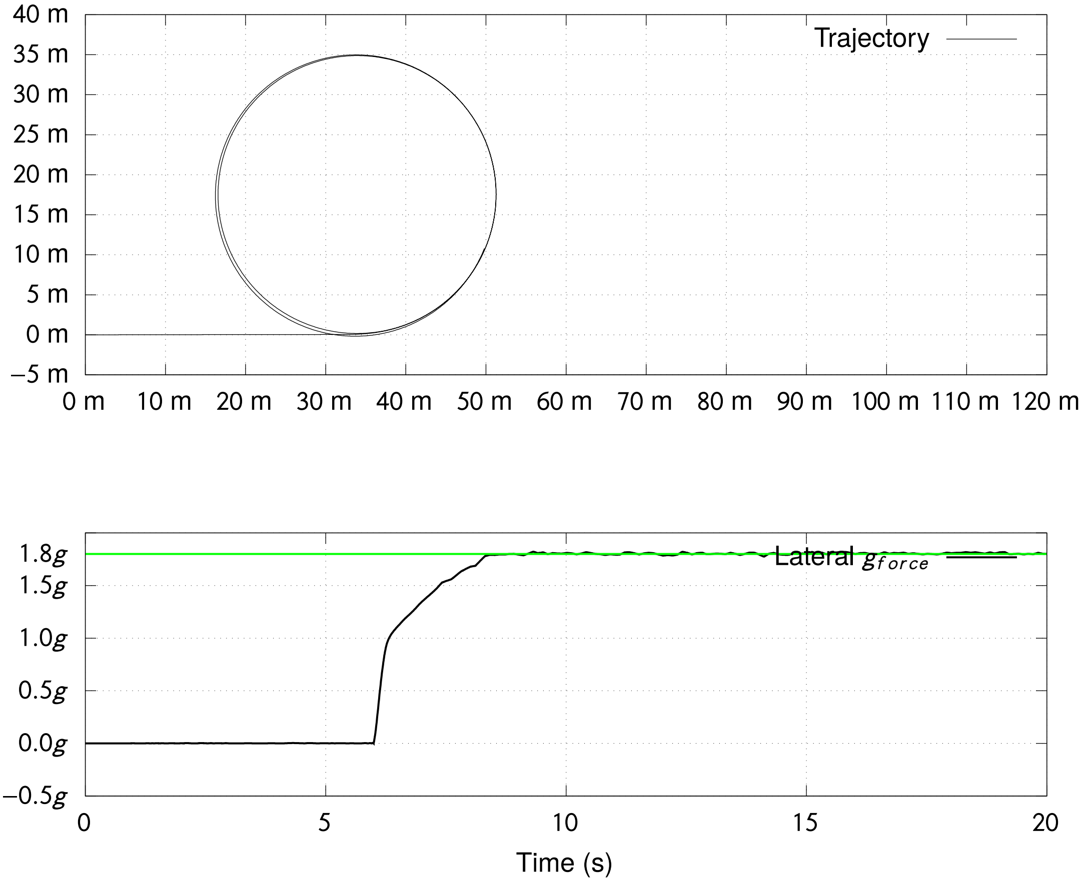

Figure B.9: Vehicle trajectory and lateral g force for a simulation of an acceleration followed by turning with expected radius of 35m, with rear wheel traction configuration on dry terrain.

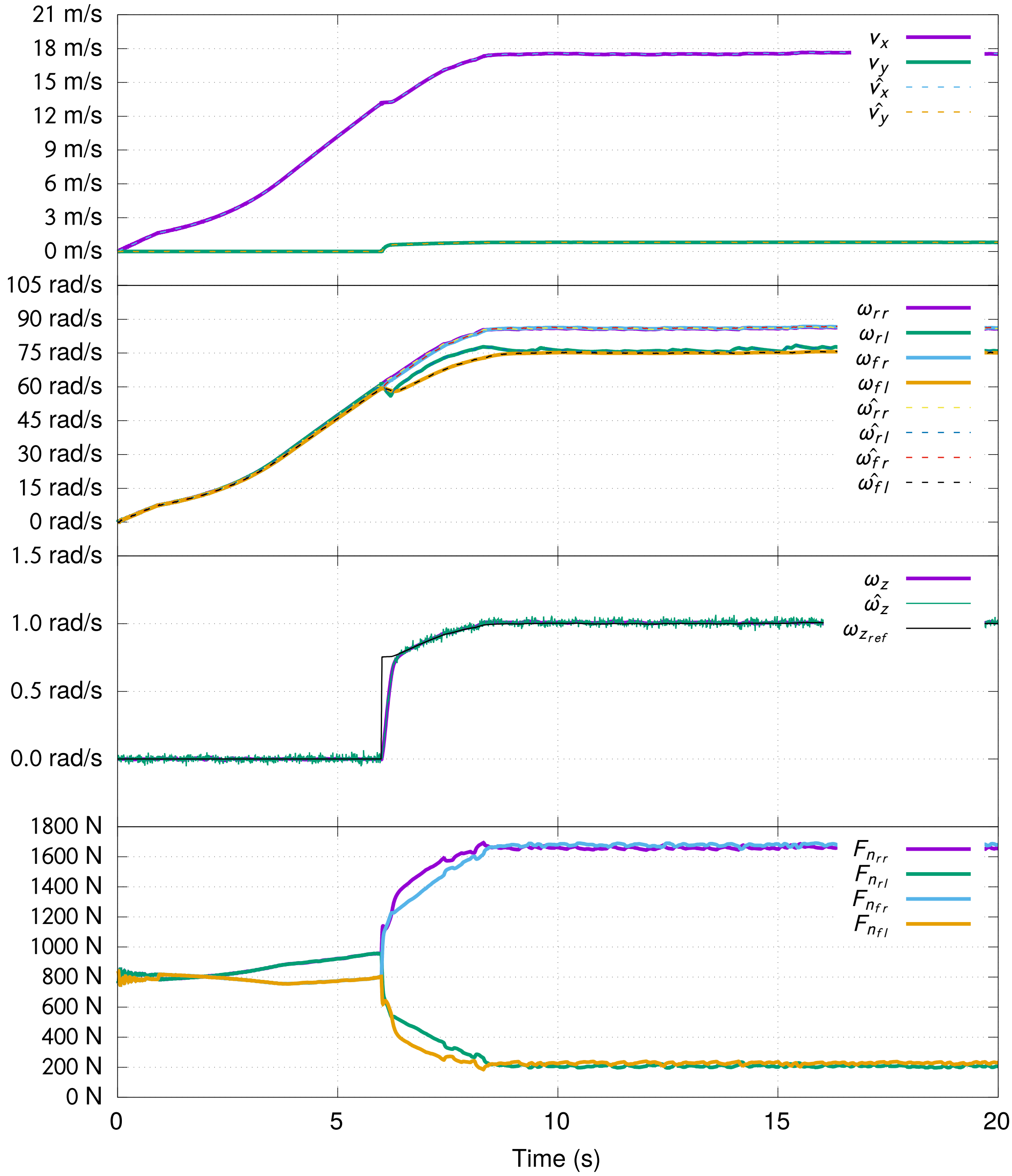

Figure B.10: Vehicle velocity, wheel angular velocity and yaw rate estimation, ground truth and reference yaw rate, for a simulation of an acceleration followed by turning with expected radius of 35m, with rear wheel traction configuration on dry terrain.

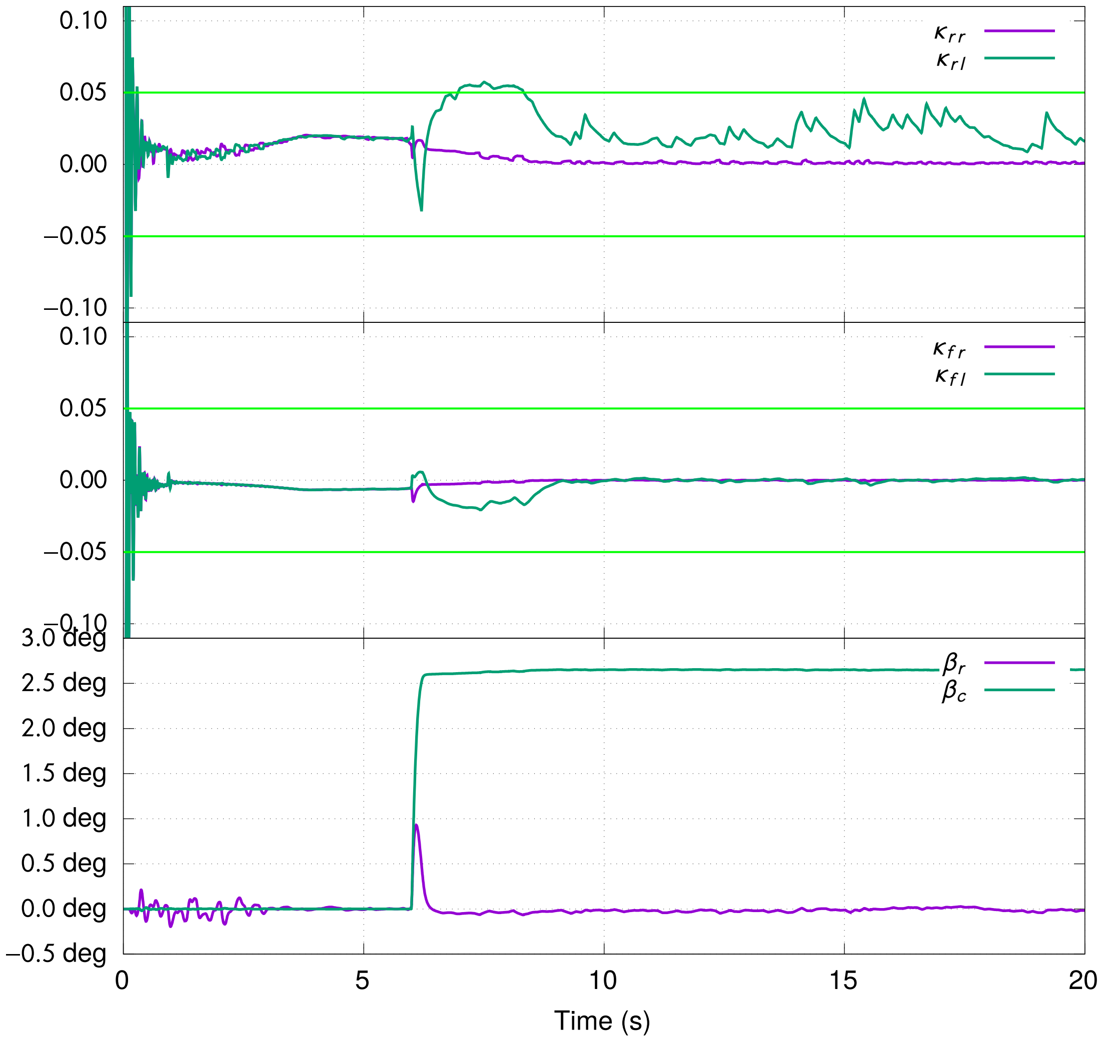

Figure B.11: Front, rear slip ratios and sideslip angles for a simulation of an acceleration followed by turning with expected radius of 35m, with two wheel rear traction configuration on dry terrain.

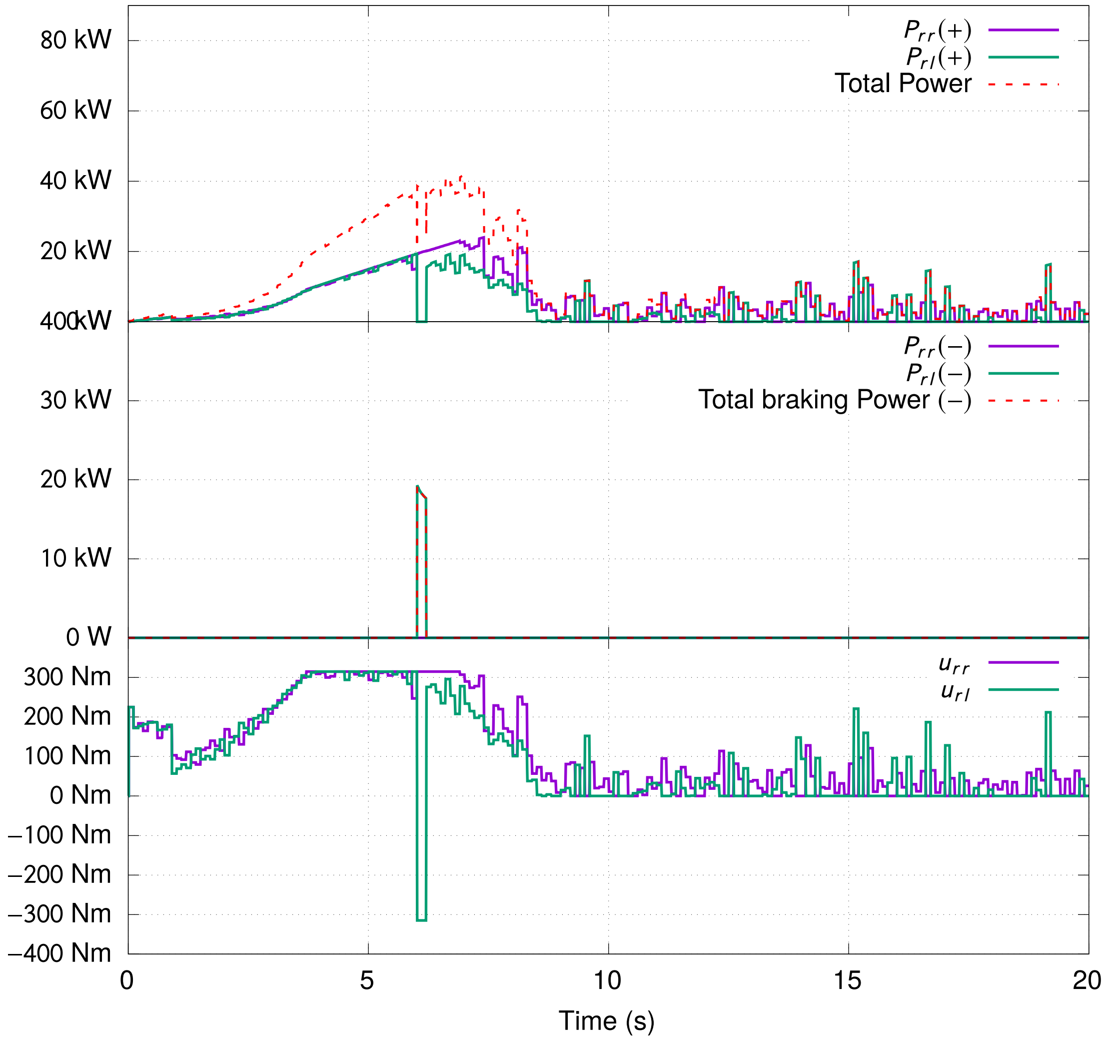

Figure B.12: Total and braking power, as well as the engine torque for a simulation of an acceleration followed by turning with expected radius of 35m, with a two wheel rear traction configuration on dry terrain.

Turning Wet FST09e 2w

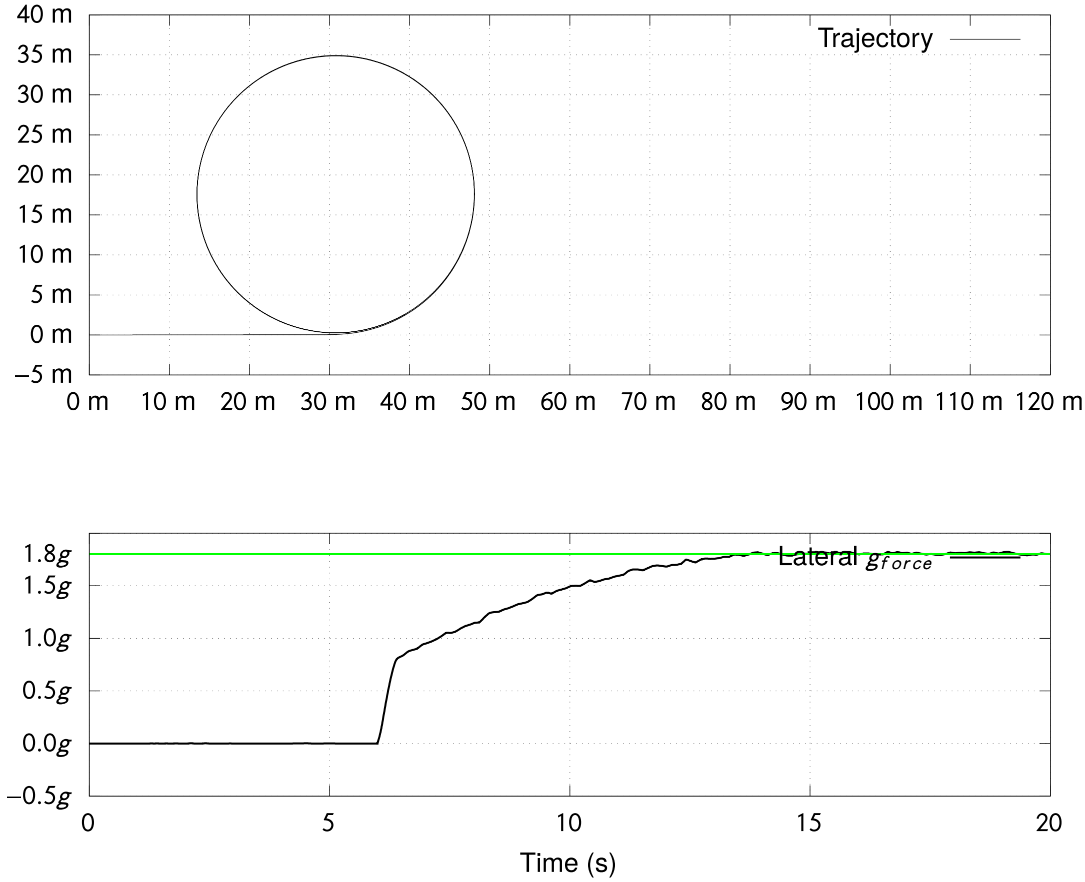

Figure B.13: Vehicle trajectory and lateral g force for a simulation of an acceleration followed by turning with expected radius of 35m, with rear wheel traction configuration on wet terrain.

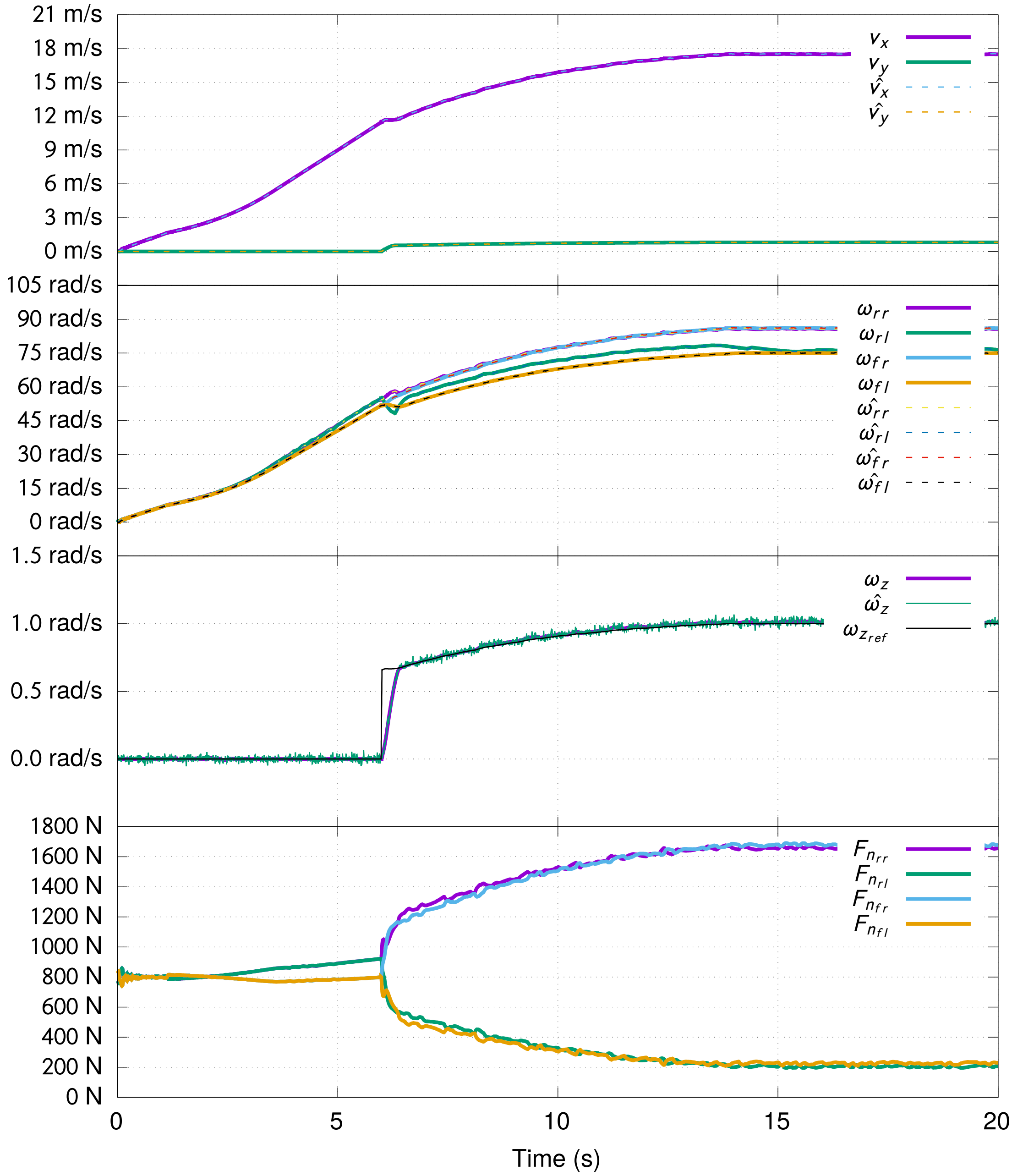

Figure B.14: Vehicle velocity, wheel angular velocity and yaw rate estimation, ground truth and reference yaw rate, for a simulation of an acceleration followed by turning with expected radius of 35m, with rear wheel traction configuration on wet terrain.

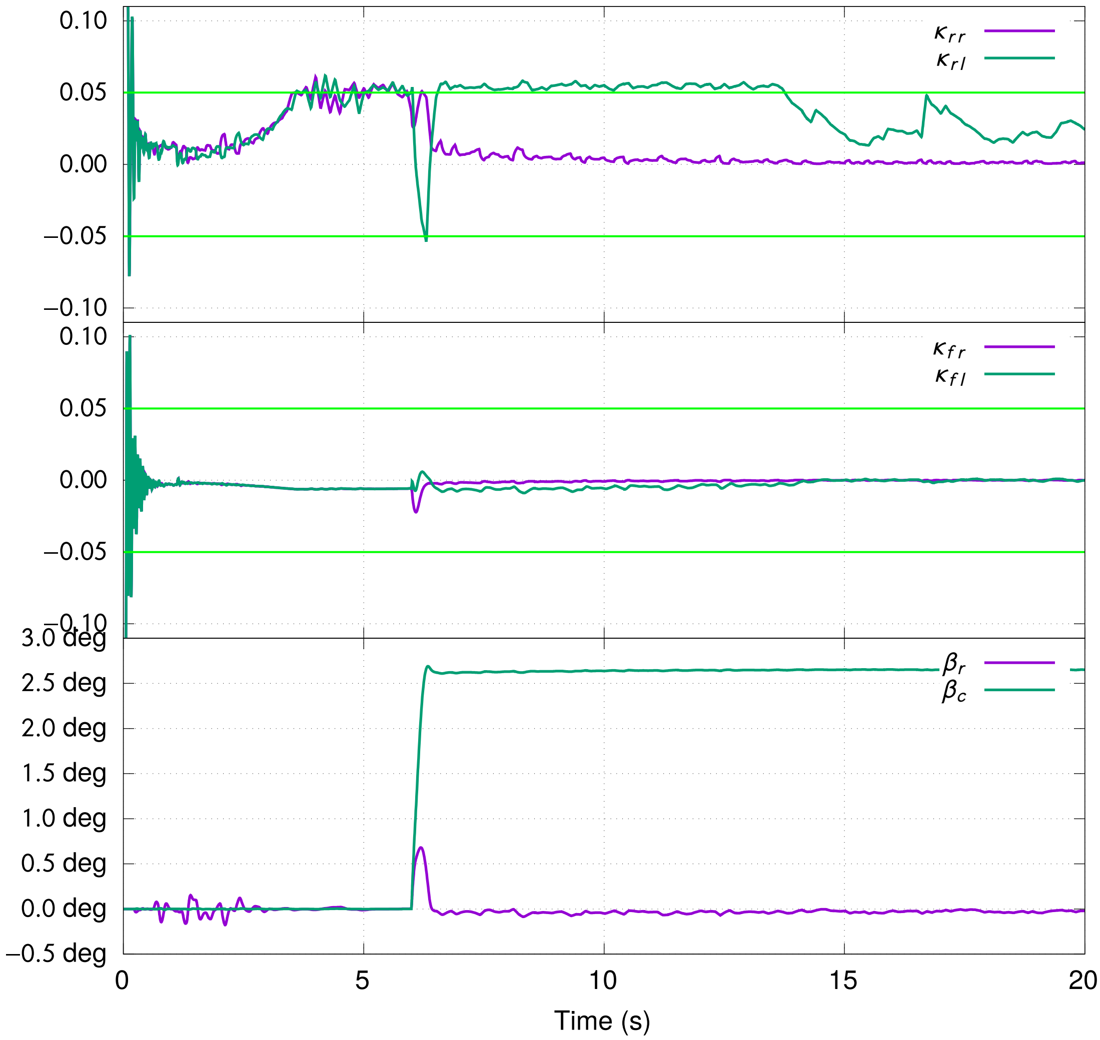

Figure B.15: Front, rear slip ratios and sideslip angles for a simulation of an acceleration followed by turning with expected radius of 35m, with two wheel rear traction configuration on wet terrain.

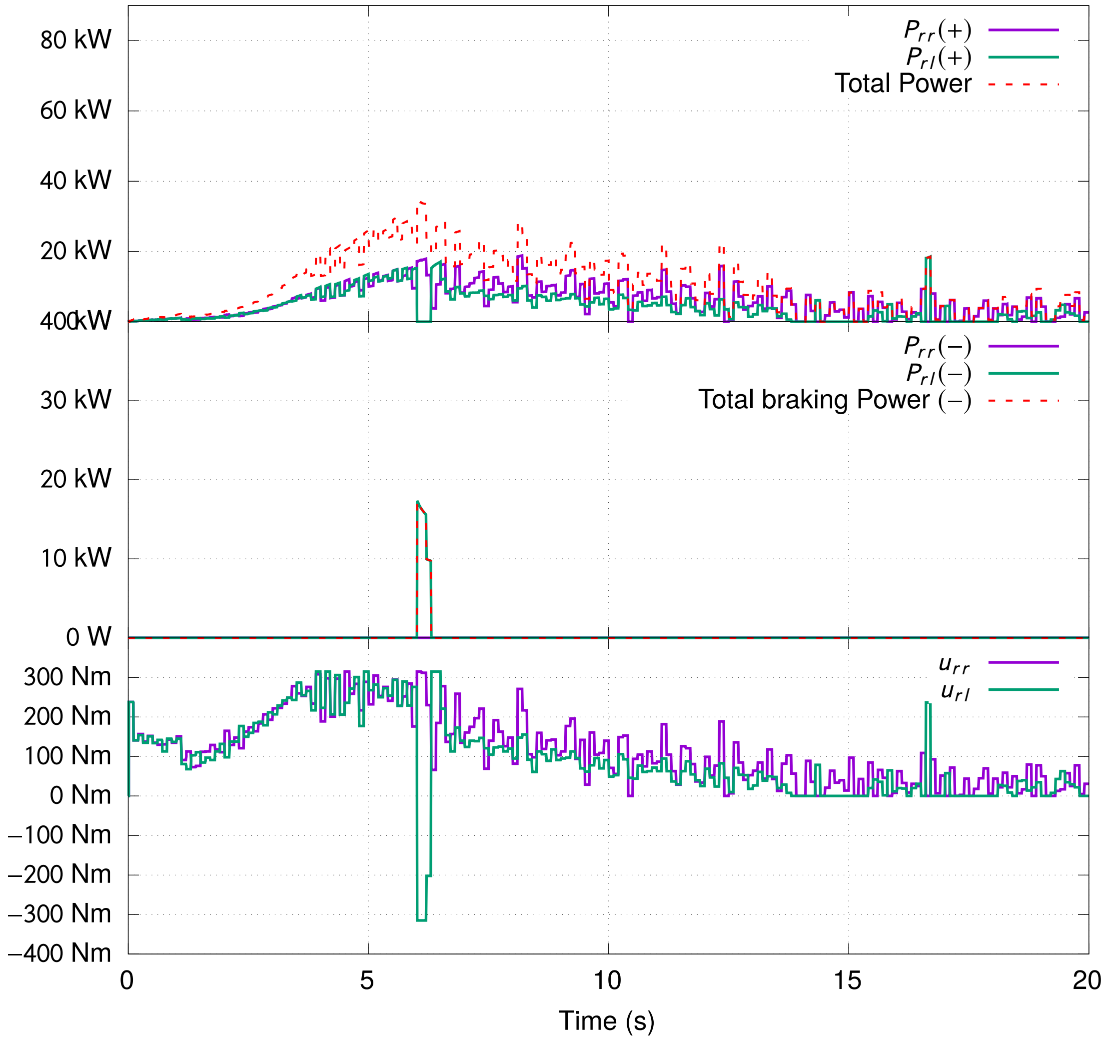

Figure B.16: Total and braking power, as well as the engine torque for a simulation of an acceleration followed by turning with expected radius of 35m, with a two wheel rear traction configuration on wet terrain.

B.2.2 Accelerating

Accelaration Dry FST09e 2w

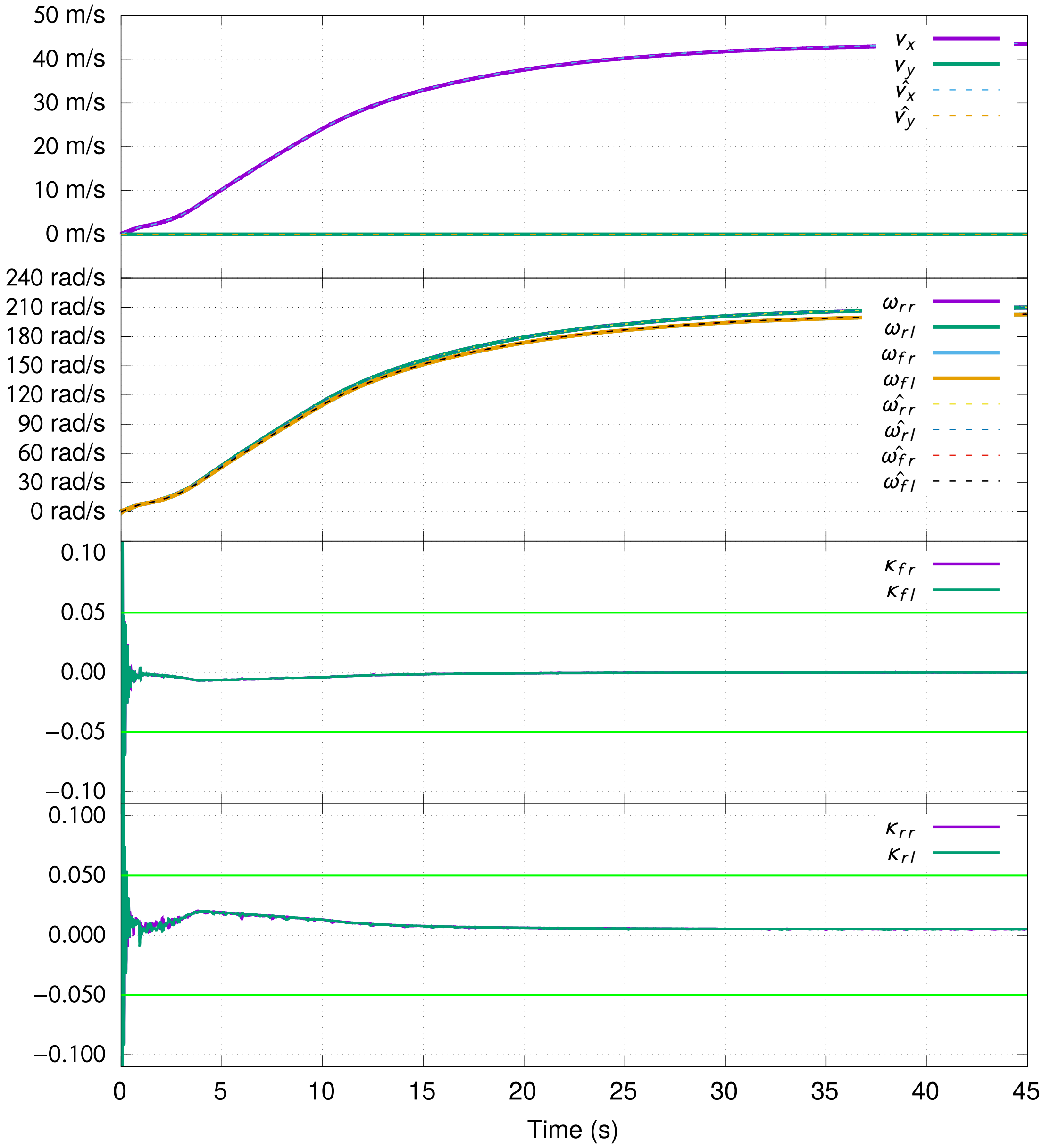

Figure B.17: Vehicle velocity, wheel angular velocity and slip ratio estimation, for a simulation of an acceleration with rear wheel traction configuration on dry terrain.

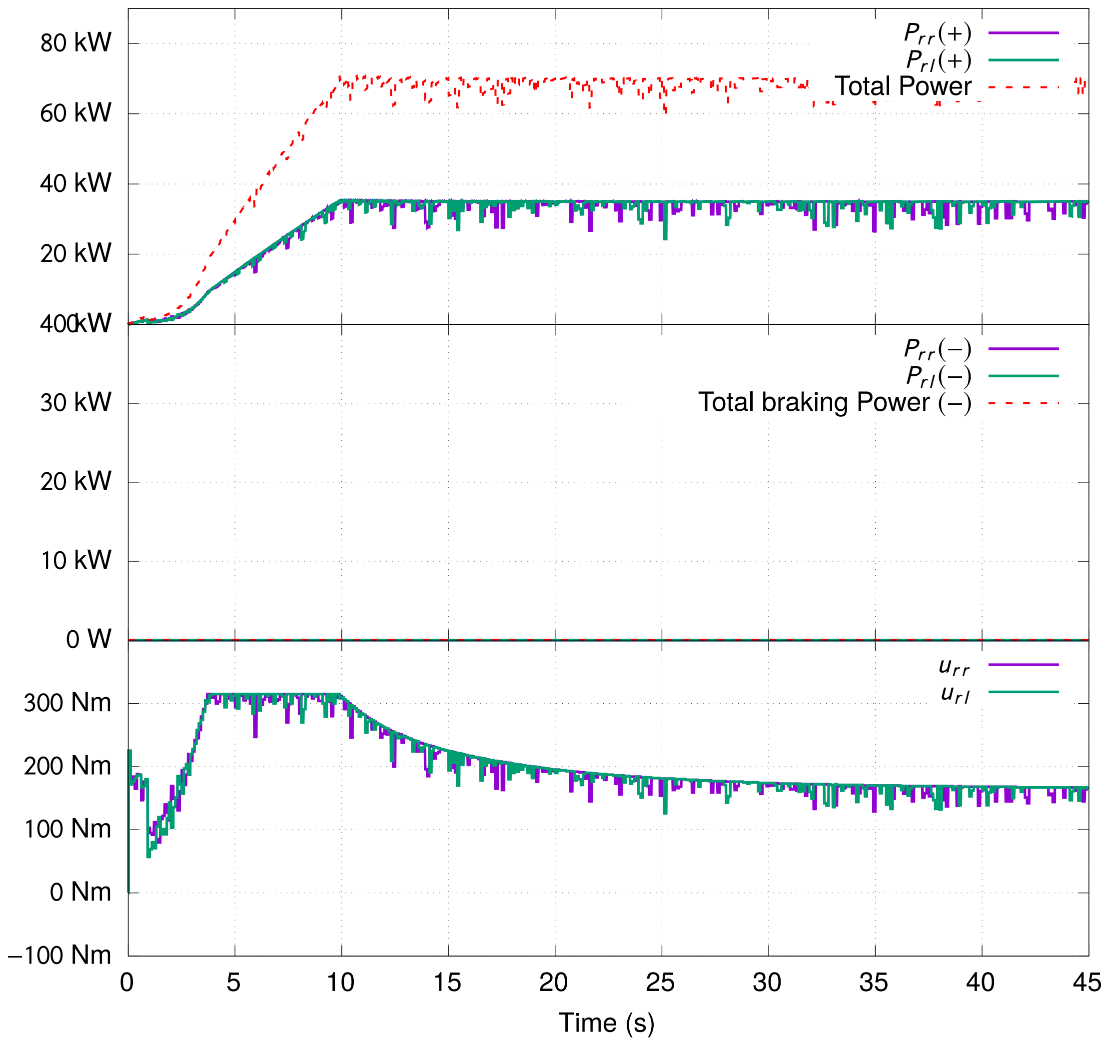

Figure B.18: Power and torque for a simulation of an acceleration with rear wheel traction configuration on dry terrain.

Accelaration Wet FST09e 2w

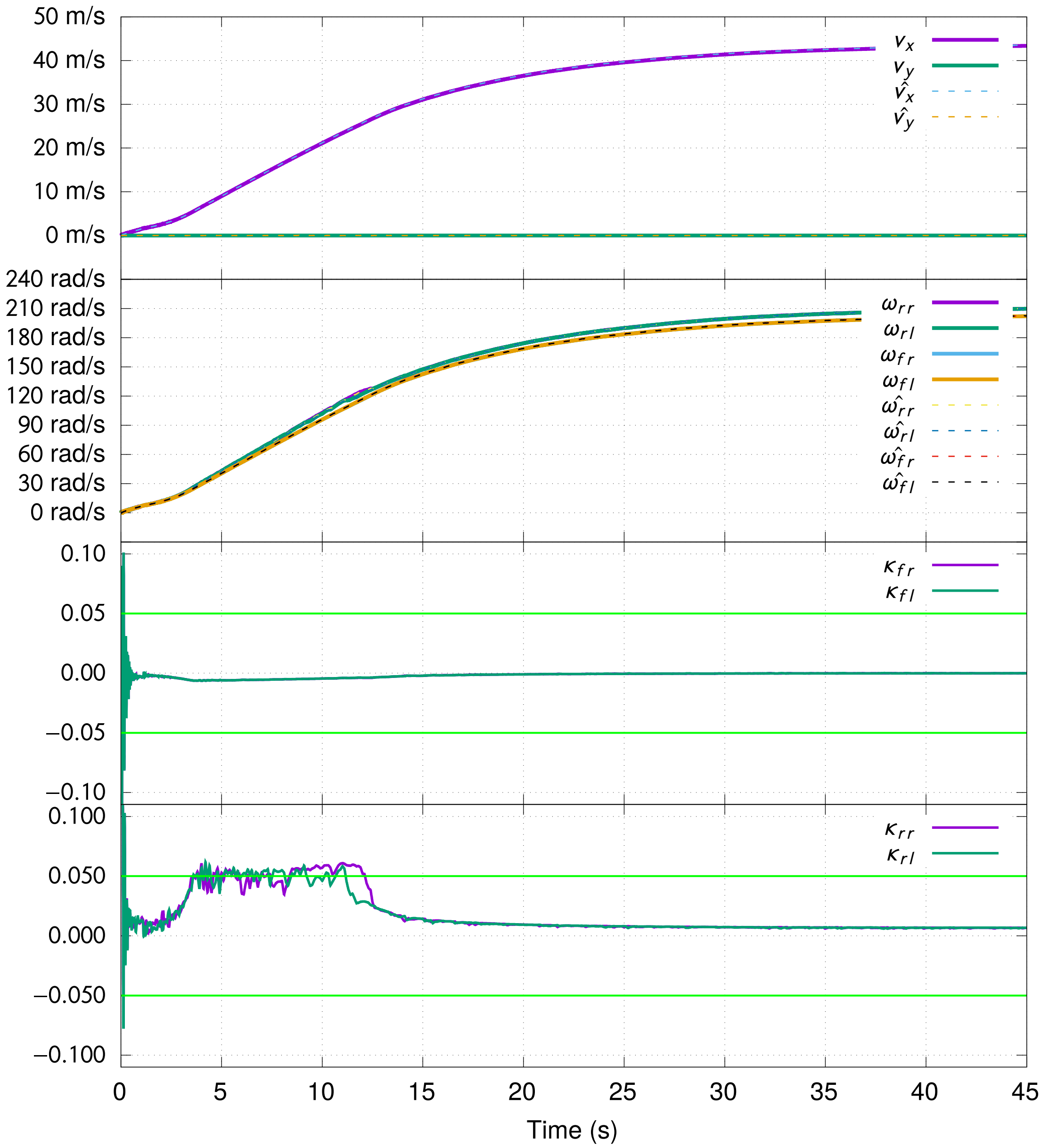

Figure B.19: Vehicle velocity, wheel angular velocity and slip ratio estimation, for a simulation of an acceleration with rear wheel traction configuration on wet terrain.

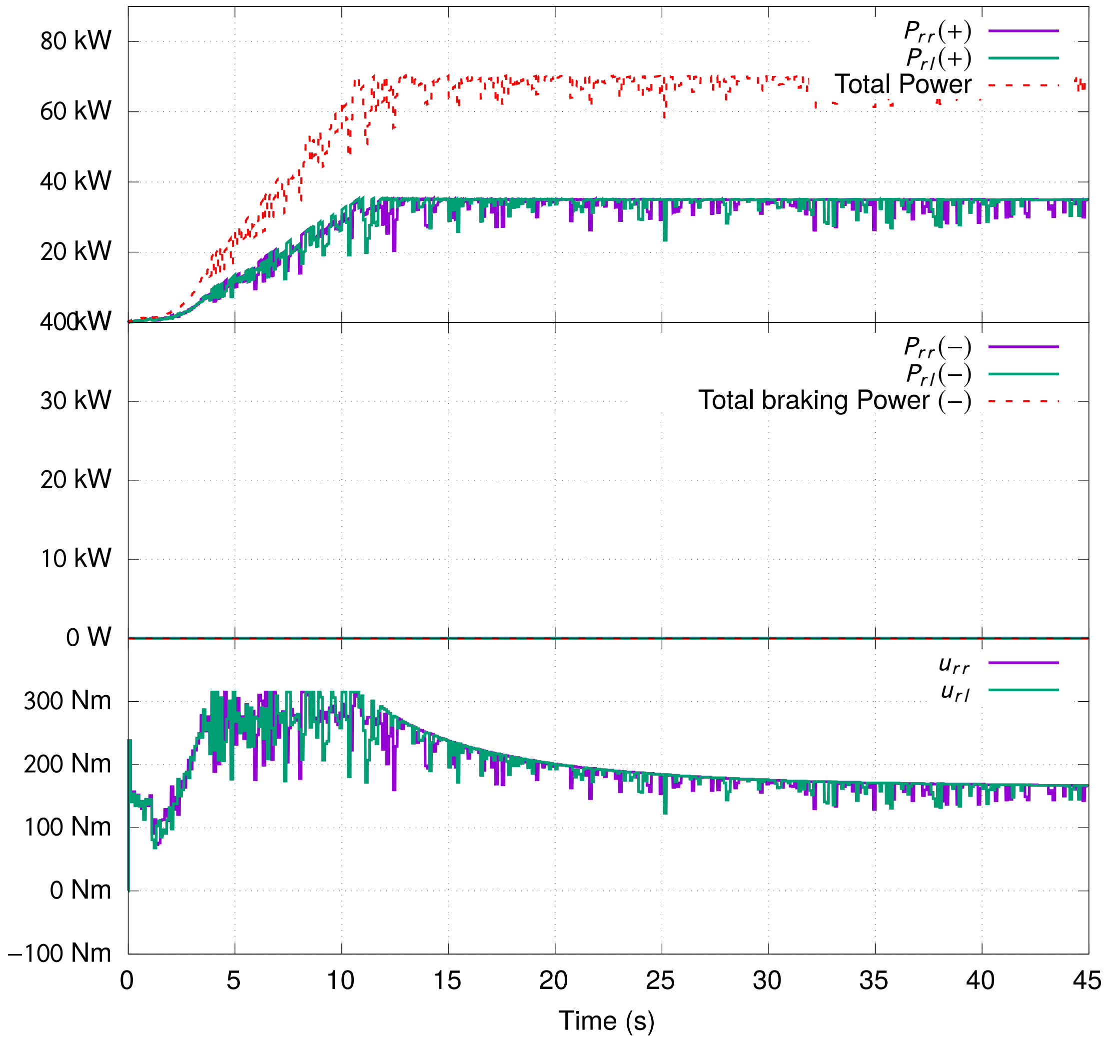

Figure B.20: Power and torque for a simulation of an acceleration with rear wheel traction configuration on wet terrain.

B.2.3 Braking

Braking Dry FST09e 2w

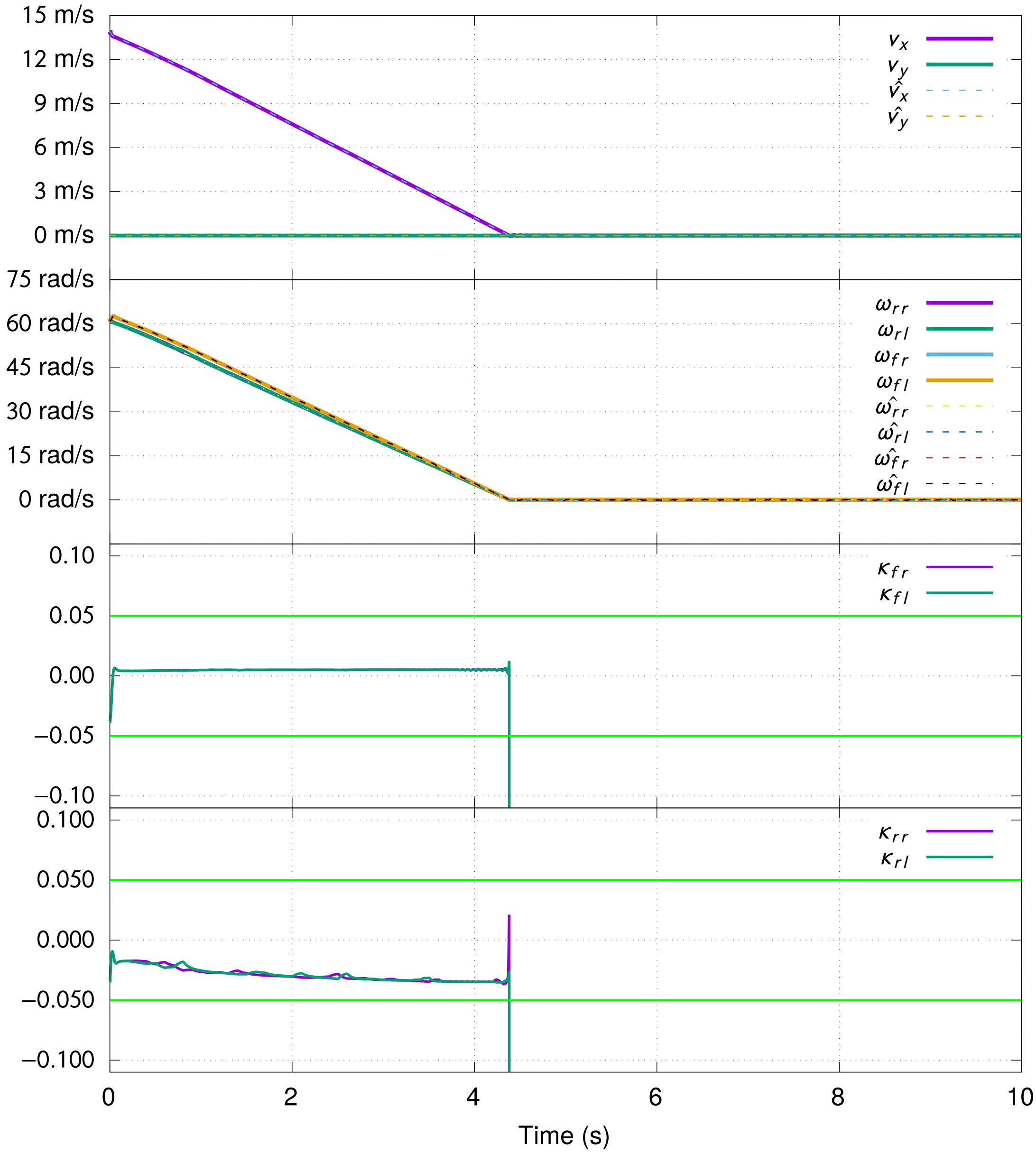

Figure B.21: Vehicle velocity, wheel angular velocity and slip ratio estimation, for a simulation of a braking manouver with rear wheel traction configuration on dry terrain.

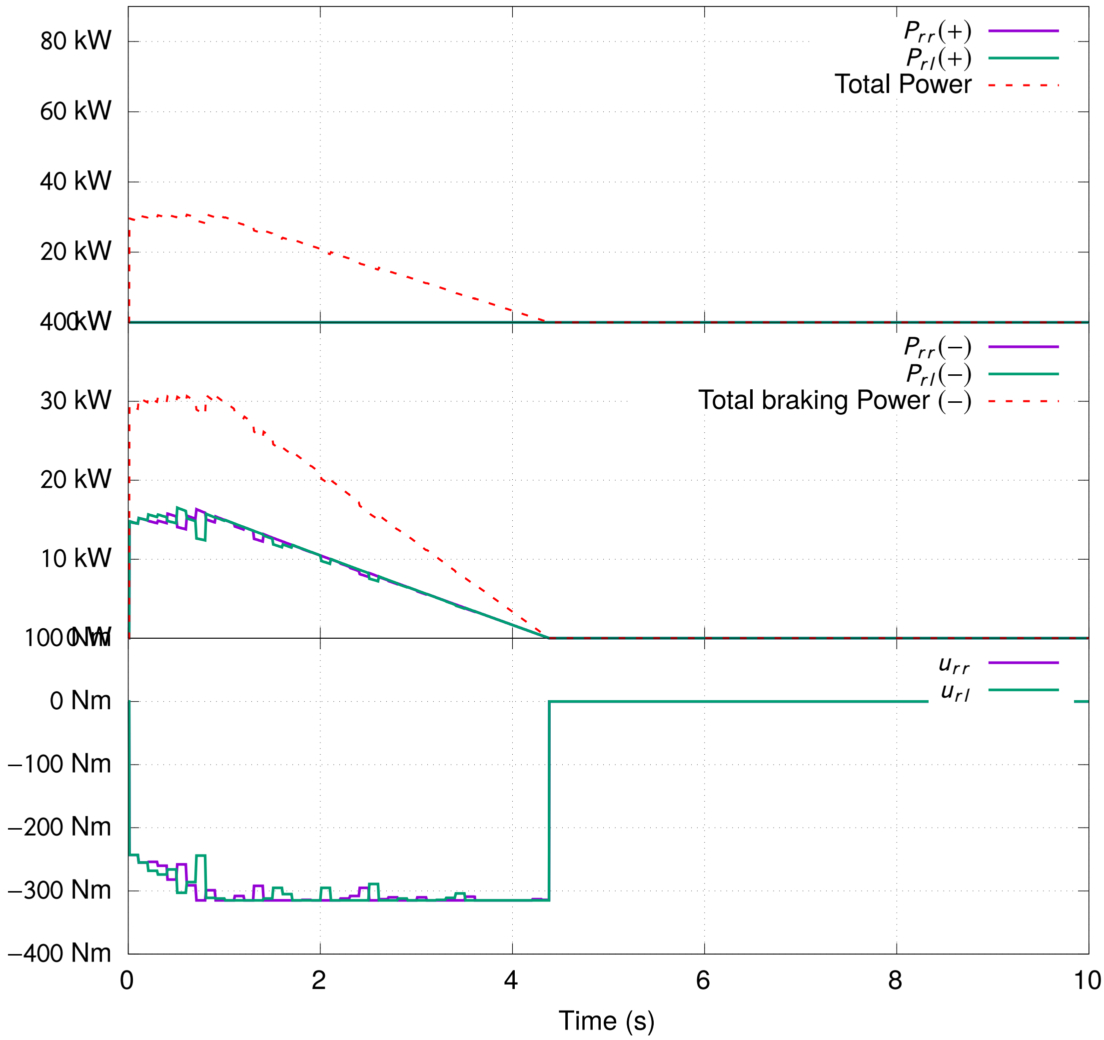

Figure B.22: Power and torque for a simulation of braking manouver with rear wheel traction configuration on dry terrain.

Braking Wet FST09e 2w

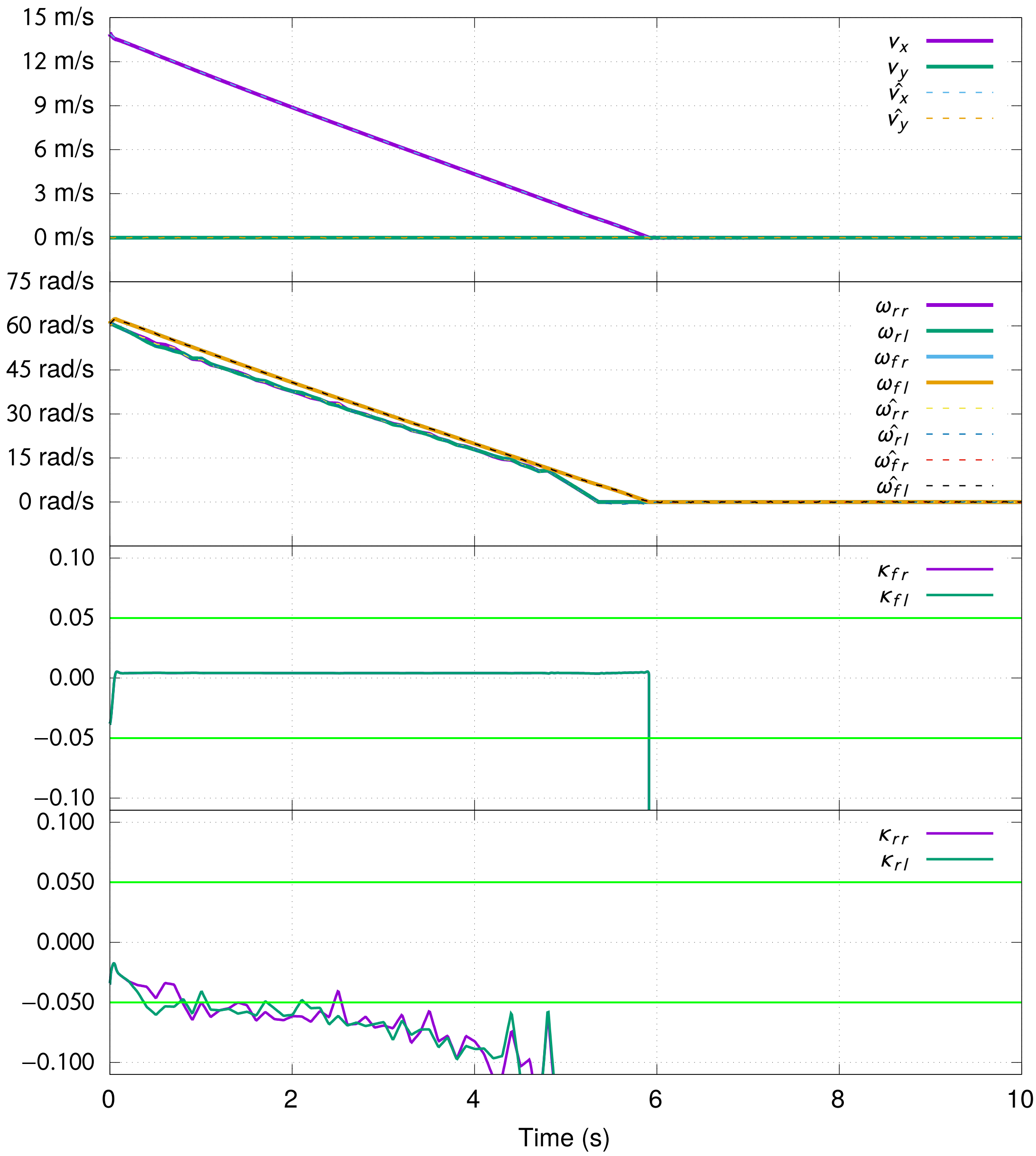

Figure B.23: Vehicle velocity, wheel angular velocity and slip ratio estimation, for a simulation of a braking manouver with rear wheel traction configuration on wet terrain.

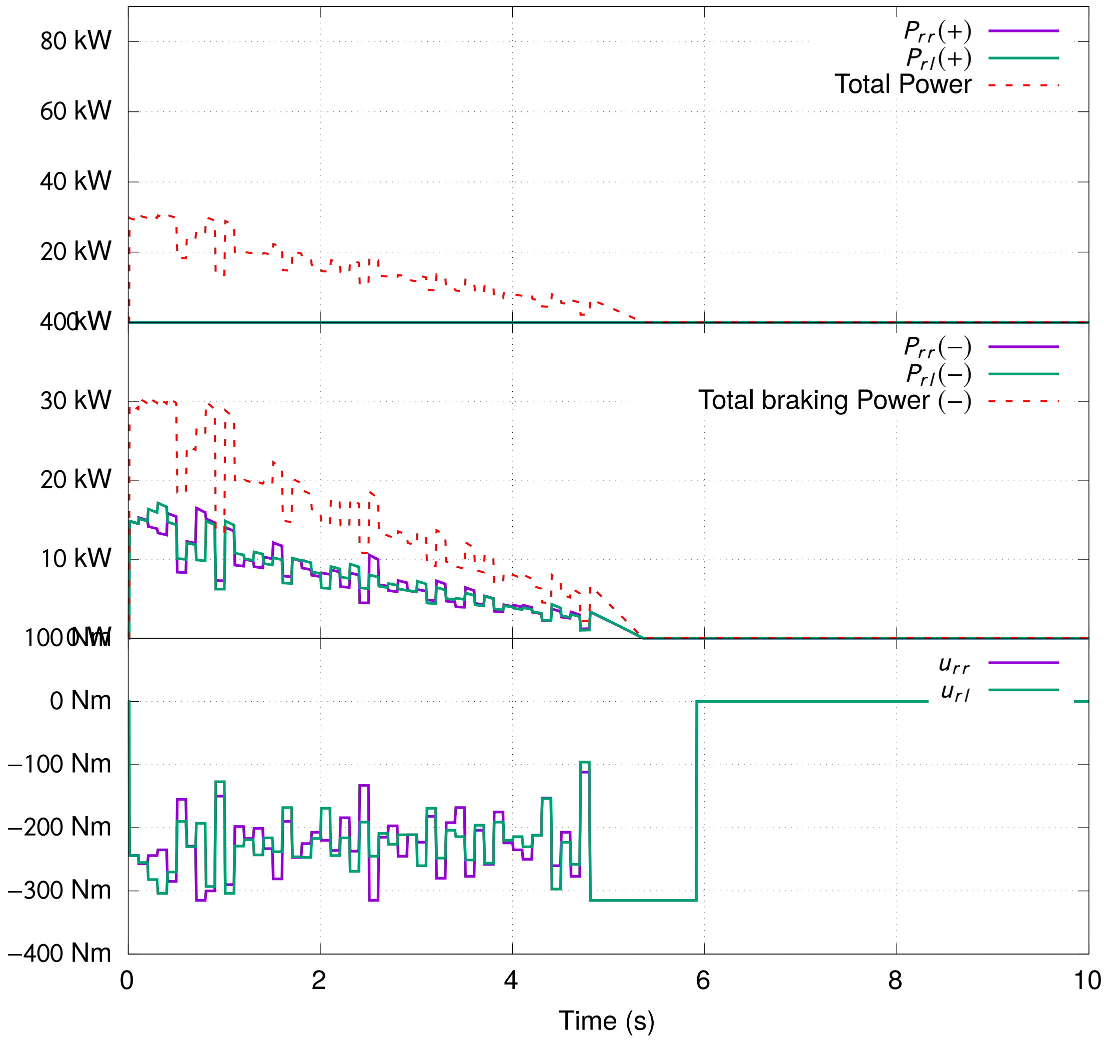

Figure B.24: Power and torque for a simulation of a braking manouver with rear wheel traction configuration on wet terrain.

TÉCNICO
LISBOA

Torque vectoring control of an electric vehicle with in-wheel motors

Nuno Alexandre de Almeida Salgueiro